PhD degree in Systems Medicine (curriculum in Molecular Oncology)

European School of Molecular Medicine (SEMM),

University of Milan and University of Naples "Federico II"

Settore disciplinare: Bio/10

IDENTIFICATION AND CHARACTERIZATIONOF STRESSED REPLICATION FORK INTERMEDIATES

Giorgio Baldi

IFOM, Milan

Matricola n. R11134

Supervisor: Prof. Vincenzo Costanzo

IFOM

IFOM, Milan

Anno accademico 2017-2018

Table of Contents

List of Abbreviations 4

Figure Index 6

Abstract 9

1 Introduction 11

1.1 Eukaryotic DNA replication 11

1.1.1 The DNA replication mechanism 11

1.1.2 DNA replication stress and genome stability 17

1.2 Mechanisms of DNA damage response 20

1.2.1 DNA damage and checkpoint activation 20

1.2.2 Double strand breaks and homologous recombination 23

1.2.3 PAR signalling contributes to DNA damage response 30

1.2.4 Fork maintenance and DNA dynamics at the stalled fork 31

1.3 Role of HR proteins during DNA replication 32

1.3.1 Effect of Rad51 deficiency during DNA replication 33

1.3.2 BRCA2 function during DNA replication 34

1.4 Replication Fork Reversal as DNA damage response intermediate 36

1.4.1 Smarcal1 and replication fork remodelling 38

1.5 *Xenopus laevis* egg extract: an *ex vivo* system 40

1.5.1 Physiological features of *Xenopus laevis* eggs: advantages in biochemistry and molecular biology 40

1.6 Single molecule imaging techniques 43

1.6.1 Atomic force microscopy (AFM) to study DNA structures, and DNA-protein interactions 43

1.6.2 Electron microscopy (EM) to study DNA molecules structures 44

2 Materials and methods 46

2.1 Preparation of interphase *Xenopus laevis* egg extracts 46

2.2 Preparation of demembranated sperm nuclei 47

2.3 Antibodies 47

2.4 PCR 48

2.5 Western blotting 49

2.5.1 Dot blot 49

2.6 Mobility shift assay 50

2.7 Nascent ssDNA detection 50

2.8 Chromatin binding experiment 51

2.9 Nuclease protection 52

2.10 Immunoprecipitation 53

2.10.1 Immunoprecipitation in chromatin context 53

2.11 Immunodepletion 54

2.11.1 Rad51 54

2.11.2 Smarcal1 54

2.12 Neutral agarose gel electrophoresis 55

2.13 RIs purification from *Xenopus* egg extract for microscopy visualizations 55

2.13.1 EM sample preparation and imaging analysis 57

2.13.2 AFM sample preparation and imaging analysis 58

3 Results 59

3.1 Visualization of DNA replication intermediates by AFM 59

3.1.1 Recognition of newly synthetized DNA strands by biotin-dUTP incorporation 61

3.2 Visualization of DNA replication intermediates by EM 69

3.2.1 Analysis of ssDNA gaps at the level of the fork structures in the context of DNA replication stalling 69
3.2.2 Detection and analysis of RVFs 77
3.3 Smarcal1-mediated RVFs accumulation triggers Mre11-mediated degradation in absence of Rad51 nucleofilament 81
3.3.1 Rad51 and Smarcal1 role in RVFs metabolism 81
3.3.2 Rad51 protects DNA from MRE11 mediated degradation 86
3.3.3 Rad51 protects RFVs from Mre11-dependent degradation 90
3.3.4 Smarcal1 role in RVFs metabolism 92
3.3.5 Rad51 overload does not impact on RVFs number 95
3.3.6 Rad51 interacts with Pol-α and Smarcal1 in a chromatin context 100
3.3.7 ATR inhibition leads to RVFs accumulation 102
4 Discussion 105
4.1 Advantages and limits of AFM and EM in RIs visualization 105
4.2 DNA lesion and significant for genome stability 108
4.3 Smarcal1 and Rad51 as players of the replication fork remodelling process . 109
5 References 114

List of Abbreviations

AFM: Atomic Force Microscopy

APH: APHidicolin

bp: base pare

BPB: BromoPhenol Blue

DDR: DNA Damage Response

dNTP: deoxyriboNucleotide TriPhosphate

DSB: Double-Strand Break

dsDNA: double stranded DNA

EM: Electron Microscopy

HDR: Homologue Directed Repair

HR: Homologous Recombination

HU: HydroxyUrea

IR: Ionizing Radiation

NHEJ: Non-Homologous End-Joining

nt: nucleotide

NTP: riboNucleotide TriPhosphate

PAR: Poly-ADP-Ribose

RI: Replication Intermediate

RVF: ReVerse Fork

SDS: Sodium Dodecyl Dulfate

SSB: Single-Strand Break

ssDNA: single stranded DNA

TCA: TriChloroAcetic acid

TMP: 4,5',8-TriMethylPsoralen

v/v: volume / volume

w/v: weight / volume

BER: Base Excision Repair

Figure Index

Figure 1.1 Origin placement, pre-IC assembly and DNA replication initiation 14

Figure 1.2 DNA replication termination process..... 17

Figure 1.3 Possible causes of replication stress..... 18

Figure 1.4 A generic cell-cycle checkpoint signalling pathway..... 21

Figure 1.5 SSB conversion into a DSB during DNA replication 24

Figure 1.6 Model for DNA repair of DNA double-strand breaks 28

Figure 1.7 Model of BIR process 29

Figure 1.8 General model for HR protein function in DNA replication..... 35

Figure 1.9 Reverse fork formation process 37

Figure 3.1 EM allows ssDNA visualization..... 60

Figure 3.2 AFM is suitable for RIs visualization 61

Figure 3.3 Agarose gel analysis of the Biotin-dUTP PCR products 62

Figure 3.4 Streptavidin staining is suitable for newly synthetized DNA recognition 63

Figure 3.5 AFM discriminates different DNA biotin-dUTP contents by streptavidin staining..... 64

Figure 3.6 Biotin-dUTP does not inhibit DNA replication in Xenopus egg extract 65

Figure 3.7 Biotin-dUTP incorporation in Xenopus genomic DNA..... 66

Figure 3.8 Streptavidin staining causes biotinylated-DNA fibres cross-links 67

Figure 3.9 Streptavidin specific daughter DNA staining in RI structure..... 68

Figure 3.10 DNA polymerase inhibitors effect on bulk DNA replication..... 70

Figure 3.11 DNA polymerases inhibition causes Polα chromatin binding accumulation 71

Figure 3.12 ssDNA gaps structure arising in different DNA replication stalling conditions 72

Figure 3.13 APH fork stalling causes ssDNA gaps accumulation at the fork 73

Figure 3.14 ssDNA gaps within the same RIs DNA structure are similar in length 74
Figure 3.15 DNA lesion regions is usually 1.5 knt in lenght 75
Figure 3.16 Polα inhibition causes ssDNA gaps accumulation at the fork. 75
Figure 3.17 MSi1 induces multiple ssDNA gaps accumulation. 76
Figure 3.18 Polα inhibition causes multiple ssDNA gaps accumulation 77
Figure 3.19 DNA polymerase stalling induces RVFs formation 78
Figure 3.20 RVFs number is time and dose-dependent 79
Figure 3.21 Regressed arm length does not change with variations in drug concentration 80
Figure 3.22 APH treatment induces DNA replication polymerases and DDR-related factors accumulation onto chromatin 82
Figure 3.23 EM analysis quantification of Smarcal1/Rad51 contribution to RVFs accumulation 83
Figure 3.24 ELISA detection of BrdU in nascent ssDNA 84
Figure 3.25 Smarcal1 and Rad51 depletion does not impact on ssDNA gaps length at the fork 85
Figure 3.26 Smarcal1-depletion influences the length of regressed branches 86
Figure 3.27 $Rad51^{wt}$, $Rad51^{T131P}$ and RPA binding on gapped DNA template 87
Figure 3.28 Rad51-mediated DNA protection from Mre11 degradation 88
Figure 3.29 Mre11 effect on 3' or 5' overhang DNA templates 89
Figure 3.30 Rad51 protection on 3' or 5' overhang DNA from Mre11 nuclease activity 90
Figure 3.31 Rad51 nucleofilament protects RVFs from Mre11-dediated degradation .. 91
Figure 3.32 Chromatin binding experiment of Smarcal1 overloading onto chromatin.. 92
Figure 3.33 EM analysis quantification of the impact of recombinant Smarcal1 addition on to RVFs formation 93

Figure 3.34 Smarcal1 hyper-loading induces the formation of double RVFs in a single replication bubble 94
Figure 3.35 Analysis of regressed arm length in egg extract treated with H-APH and supplemented with an excess of Smarcal1 94
Figure 3.36 Smarcal1 over loading reduces ssDNA gap at the fork junction 95
Figure 3.37 Chromatin binding experiment of recombinant Rad51 hyper-loading onto chromatin 96
Figure 3.38 EM quantification of RVFs frequency in Rad51 supplemented extract 97
Figure 3.39 Rad51 chromatin hyper-loading induces HJs formation 98
Figure 3.40 EM analysis of HJs frequency upon Rad51 addition 99
Figure 3.41 EM quantification ssDNA gaps length in Rad51 hyper-loading conditions 99
Figure 3.42 Polα and not Polδ co-immunoprecipitates in Rad51 IP 101
Figure 3.43 DNA replication stress affects Polα and Rad51 interaction 101
Figure 3.44 ATR inhibition affects Rad51 Chromatin binding 103
Figure 3.45 ATRi induces accumulation of RVFs 104
Figure 3.46 ATRi leads to the reduction of ssDNA gaps length at the fork junction 104
Figure 4.1 Model showing the effect of DNA polymerase inhibition and Rad51 depletion 113

Abstract

The DNA replication machinery encounters a number of obstacles while duplicating the genome, which put the replicative apparatus under stress. Cells have developed a number of mechanisms to overcome replication stress sources. However, in the presence of chronic stress, or after loss of key factors that help to deal with this stress, a range of deleterious events can occur. One of the main pathways implicated in DNA damage sensing and response is DNA damage checkpoint. When DNA replication fork progression is blocked, checkpoint activation ensures structural stability of the replisome components avoiding fork collapse and promoting, when possible, fast resumption of DNA replication. One of the hallmarks of replication stress is the accumulation single-stranded DNA at the replication forks. Here we used Atomic Force microscopy (AFM) and Electron Microscopy (EM)-based approaches to provide a detailed characterization of DNA lesions arising in the presence of replication stress imposed by interference with DNA polymerase activity in *Xenopus laevis* egg extract. We identified a number of intermediates induced by DNA polymerase inhibition, including replication forks containing ssDNA gaps and reversed forks (RVFs). Importantly, we directly correlated the presence and the length of ssDNA gaps at the replication fork junctions with the onset RVFs. Significantly, we identified one possible source of ssDNA gap accumulation at forks by showing that homologous recombination protein Rad51 is required for optimal function of Polymerase alpha at stressed replication forks. To fulfil this function, Rad5-Polα interaction is likely to be important for stalled fork resumption. We also provided evidence that replication fork intermediates with persistent ssDNA gaps are converted into RVFs by Smarcal1 translocase, showing that this enzyme is among the most important fork remodelers that can trigger fork reversal upon fork stalling. We also showed that RVFs can trigger extensive Mre11 dependent DNA degradation upon replication stress in the absence of functional Rad51. Finally, we provided mechanistic

insights into checkpoint regulation of RVFs levels through ATR, Smarcal1 and Rad51 regulation. Overall this provides structural and molecular insights into the metabolisms of replication forks under stressful conditions.

1 Introduction

1.1 Eukaryotic DNA replication

1.1.1 The DNA replication mechanism

DNA replication is a fundamental biological process for the propagation of life. Indeed, an accurate duplication of the DNA molecules is required to pass the correct genetic information to the next generation. The maintenance of genome integrity requires a precise and coordinated replication of the entire genome once and only once per cell cycle. As a consequence, DNA replication is temporally and spatially regulated by a series of control mechanisms[1].

Genomic DNA replication can be divided in three main steps: DNA replication initiation, during which DNA replication starting sites are established and the unwinding of the DNA molecule is started; the elongation step, during which bulk genomic DNA replication takes place in a semi-conservative way and, DNA replication termination, when DNA synthesis is terminated, the molecular machinery that worked to replicate DNA is disassembled and the daughter DNA molecules are decatenated[1-4].

The sites where DNA replication starts are called replication origins. In *Saccharomyces cerevisiae,* these regions have been identified and they are characterized by a conserved consensus sequence. Although it was not possible to recognize a specific consensus sequence in *Schizosaccharomyces pombe*, AT-rich sequences of 20-50 bp were found to be proficient for DNA replication initiation. In metazoans unique common features for DNA replication origin sites have not been identified yet. It has been proposed that DNA replication origins are preferentially situated in CpG islands and AT-rich regions, although these two elements cannot be considered as predictive for a replication origin site[4]. Pioneer works have been trying to describe specific DNA replication origin sites for the human genome but the lack of follow-up work did not strengthen those observations[5,6].

Eukaryotic genomes contain approximately from 10^7 to 10^{11} DNA base pairs[7]. DNA must be duplicated rapidly and precisely before entering mitosis and proceeding cytokinesis. For this reason, DNA replication initiates at multiple origins sites that are distributed along each chromosome[8]. Their activation must be tightly regulated to ensure that the whole chromosome is completely replicated. Two distinct steps are required for origin activation. During late mitosis and early G1 phase, the pre-Replication Complex (pre-RC), a hetero-multimeric complex essential for DNA replication initiation, is assembled at the replication origin site. The first pre-RC component that binds the DNA is the ORC (Origin Recognition Complex) protein complex, that is able to specifically bind the replication origin sites[9]. This complex is constituted of six subunits (ORC1 to ORC6), and it retains both dsDNA and ssDNA binding activities. It also contains ATP binding and ATPase activities, which are required for ORC-DNA binding regulation[1].

Subsequently to ORC chromatin binding, other two proteins bind to the replication origin site: CDC6 and CDT1[10]. Both these proteins are required for replication origins regulation; indeed, they are loaded onto chromatin during the G1 phase of the cell cycle and then are exported from the nucleus and degraded during the subsequent cell cycle phases, in order to prevent DNA re-replication. Their binding is essential for the MCM (Mini Chromosome Maintenance) complex recruitment. The MCM complex is a hetero-hexamer constituted by six paralogs proteins (MCM2 to MCM7). The six proteins create a toroidal structure with a central hole that constitute the engine of the replicative helicase[11]. Recent structural analysis of the helicase complex suggests that MCM can harbour a ssDNA filament inside the central hole displacing the complementary while it is translocating along the DNA[12,13]. MCM associates to the replication origin as a face-to-face double hexamer: thus, from a single replication origin, two replication machineries will start the DNA synthesis going in opposite direction[14]. The loading of the MCM complex onto the replication origin is referred to as DNA replication "origin licensing"[3] and with it the first step for origin activation is accomplished.

The association of the MCM complex onto the chromatin stimulates the ATPase activity and the dissociation of CDC6 and CTD1[3], and the unloading of these two proteins results in a greater stability of the MCM hexamer association with DNA. To start replication the MCM double hexamer has to dissociate into two hexamers, and this transition is promoted through MCM proteins phosphorylation by the transient DDK (Dbf4-Dependent Kinase) that temporarily associates with the pre-RC[12,15]. Moreover, MCM4 phosphorylation by CDKs (Cyclin Dependent Kinases) triggers the association of CDC45 and the hetero-tetrameric GINS complex with the MCM proteins. Altogether CDC45, MCM and the GINS proteins are known as CMG complex, and they constitute the actual replicative DNA helicase. The GINS complex defines the "origin firing" and with it the second big step of replication origin activation is accomplished. The multi-protein complex assembled on the replication origin so far is referred as the pre-IC (pre-Initiation Complex)[10]. Now the CMG complex can unwind the DNA allowing the DNA polymerases to access the parental DNA strands and to initiate the DNA synthesis[16] (***Figure 1.1***). Some of the origins assembled in G1 are ultimately not fired in S phase. These are known as dormant origins. This results in an excess of origins that are licensed compared to number required to duplicate the whole genome. It has been demonstrated that dormant origins can work as "rescue" replication origins upon replication fork stalling due to DNA replication stress events[17,18]. Moreover, not all active origins are fired at the same time, but they have to respect a specific timing program. As a consequence, replication origins are divided into "early" and "late" according to the time of firing[3,19]. In metazoans, the program that regulates replication timing remains elusive. However, it has been proposed that the nuclear envelope can influence this mechanism[3].

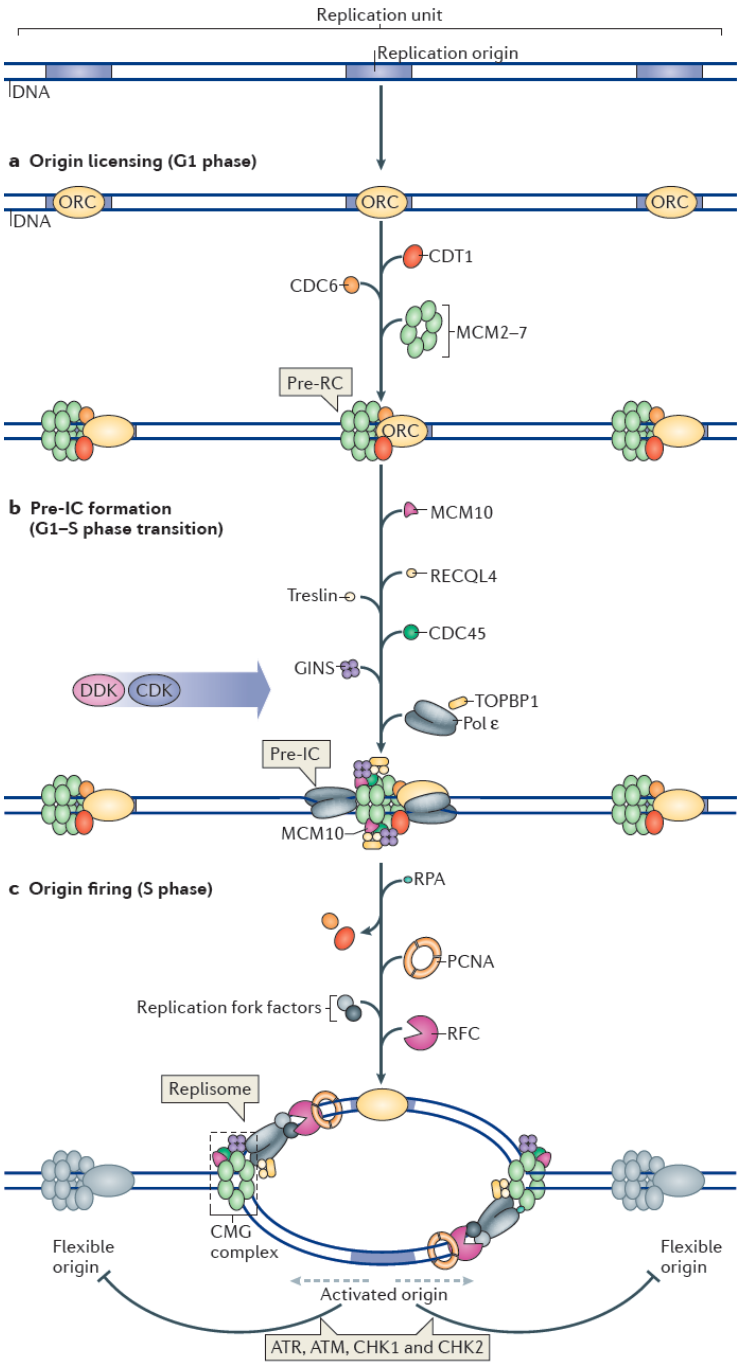

Figure 1.1 Origin placement, pre-IC assembly and DNA replication initiation

This figure shows an example of three replication origins. Pre-replication complex assembly or licensing is restricted to late M – G1 phase of the cell cycle. Sequential loading of ORC, CDT1, CDC6 and finally MCM2-7 hetero hexamer completes the licensing reaction or Pre-replication complex assembly. Replication fork assembly occurs when pre-initiation complex is formed by the activation MCM2-7 helicase. DDK and CDKs phosphorylate several proteins to provide origin firing. In co-ordination with RPA, PCNA and with the action of replicative polymerases α, ε and δ replication fork assembly is established (Picture taken from Fragkos M.; 2015. Ref[10])

Genomic DNA replication during S phase is manly carried out by three DNA polymerases: Polα, Polδ and Polε. All of these DNA polymerases are enzymes that synthesize a new DNA strand extending it from the 3' end of an existing nucleotide chain; they add new nucleotides complementary to the ones present in the template DNA molecule via the creation of phosphodiester bonds. In general, DNA polymerases cannot initiate de-novo DNA synthesis and they can only extend an existing DNA or RNA chain. To begin synthesis, a short fragment of RNA, called primer, must be created. The Polα/Primase pair complex using its primase activity, is able to synthetize a short RNA-primer of 7-14 NTPs and to extend it with a maximum of twenty dNTPs[20,21]. This primer can then be elongated by either Polδ or Polε.

The DNA molecule is constituted by the pairing of two antiparallel DNA strands. The DNA polymerases can only synthesize in the 5'→3' direction and therefore the mechanism of DNA synthesis must be different for the two strands. One strand is continuously extended with high processivity by the replicative DNA polymerase Polε, while the other strand is discontinuously synthesized by the Polδ molecule continue extension of short RNA primers generated by the Polα/Primase complex, thus forming strands of about 200 nucleotides in length known as Okazaki fragments[21,22]. This strand is named lagging strand, while the filament synthetized by Polε is called leading strand.

Thus, while only one RNA primer will be polymerized on the leading strand several primers are created on the lagging strand. Then, the RNA primers must then be removed and replaced by DNA, and the different fragments must become a continuous filament before DNA replication is completed. The main mechanism by which the RNA primers are removed relies on the concerted activity of Polδ, PCNA/RFC (Proliferating Cell Nuclear Antigen / Replicating Factor C) and FEN1 (Flap-Endonuclease 1). Briefly, Polδ supported by PCNA/RFC can displace the RNA primer synthetized by the Polα/Primase

complex, creating a 5'-flap that is cleaved by FEN1; while the RNA primer is displaced the polymerase activity of Polδ replaces the RNA with DNA. FEN1 cuts at the ssDNA-dsDNA junction, and the final nicked DNA molecule is eventually sealed by the DNA ligase 1[21,23].

DNA replication termination is the less studied step of the genomic DNA replication reaction. During this phase important and unique processes have to take place in order to avoid DNA breaks formation and to allow the correct daughter strands resolution. First, DNA unwinding promotes the formation of positive supercoils ahead of the fork; the topological stress accumulated during the elongation phase, has to be resolved during the termination process. When two converging replisomes meet, the replisomes have to be disassembled. It is still debated if all the replisome components are removed or if the replisome is only partially disassembled. Indeed, the subsequent step likely requires the filling of the last ssDNA gap left on the parental DNA. At replisome encounter, a single-stranded gap exists between the 3' end of the leading strand and the downstream Okazaki fragment of the opposing fork (***Figure 1.2***). Currently, it is unclear whether gap filling requires replisome disassembly or whether the maturation of the last Okazaki fragment occurs via the same mechanisms that intervene during replication elongation. Because of the helical structure of DNA, the synthesis of the last stretch of DNA will create a new turn of catenae between the two daughter strands. Eventually this new catena turn has to be resolved in order to allow a correct segregation of the replicated DNA molecules[24-26] (***Figure 1.2***).

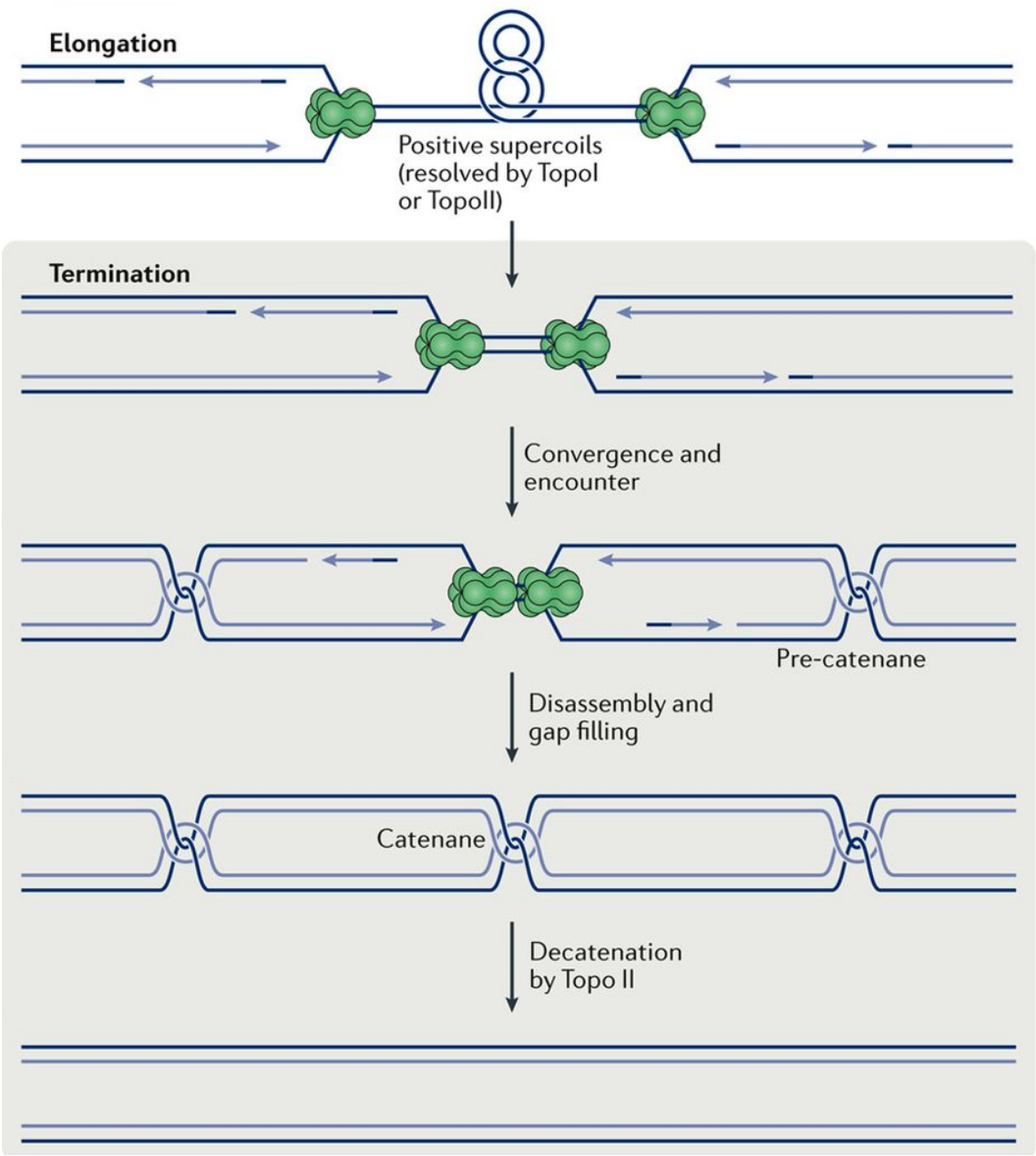

Figure 1.2 DNA replication termination process

Schematic illustration of replication elongation and the five events that are characteristic of replication termination. In order, the resolution of topological stress accumulated during DNA replication; the encounter of the converging replication fork; the disassembly of the replication machinery and the 'final' gap filing step. Eventually, the decatenation of the residual catenane structures. RNA primers are shown in dark blue. (Picture taken from Dewar J. M.; 2017. Ref[26]).

1.1.2 DNA replication stress and genome stability

Replication fork progression is often threatened by different challenges. All the chemical, biochemical or physical conditions that cause the replication fork slowing or

stalling are collectively defined as replication stress sources[18] (***Figure 1.3***). These can include, for example endogenous by-products of cellular metabolism, such as reactive oxygen species or formaldehyde. Peculiar DNA structures such as repetitive sequences, fragile sites or G-quadruples forming sequences can also represent intrinsic obstacles to replication fork progression. The alteration of replication dynamics is one of the main causes of genome instability and it has been demonstrated to be a major source of genomic instability in pre-neoplastic lesions, contributing to cancer development[27-29].

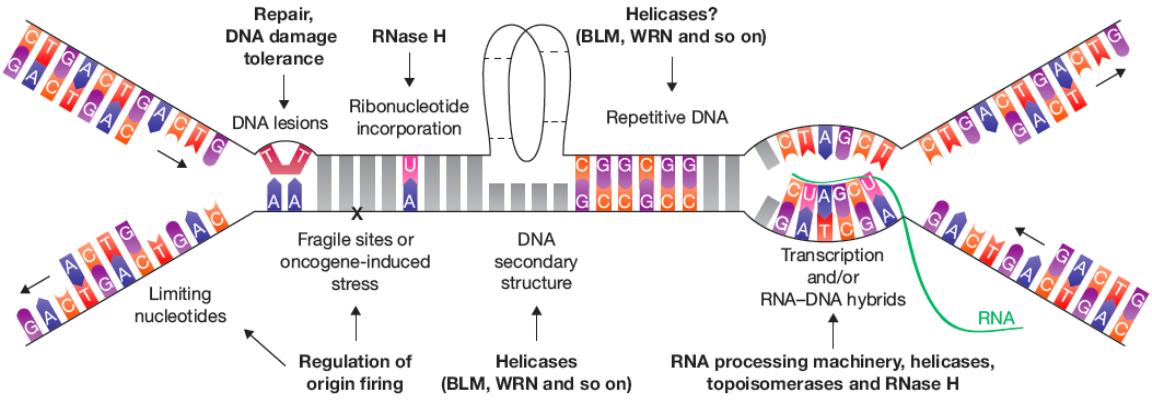

Figure 1.3 Possible causes of replication stress

There are numerous possible sources of DNA replication stress. In this illustration some of them are reported, including pyrimidine dimer, fragile site, ribonucleotide incorporation or DNA/RNA hybrid, DNA secondary structures, limiting nucleotides pool, repetitive DNA sequences and replication-trasctiption collision. Some of the protein or pathways involved in the resolution of the replication stress are reported in bold. (Picture taken from Zeman M. K.; 2014. Ref[18]).

Replication stress sources can be both endogenous or exogenous with respect to the cellular environment and they can impact globally or only locally on DNA replication dynamics.

One source of DNA replication stress can be represented by the mis-regulation of replication origin activation[30]. It is essential that a sufficient number of origins fire each cell cycle to cover the entire genome for an accurate DNA replication. Also, the time-program of origin firing has to be respected in order to avoid over usage of limiting replication factors and dNTPs. DNA replication initiation and elongation rate are

harmonized with the availability of the dNTPs pool. Indeed, if the dNTPs levels are low, replication forks are slowed down and new origins are fired to ensure complete genome duplication. This has been shown to be a checkpoint-dependent mechanism: when nucleotides stocks are too low, ssDNA is accumulated behind the replication fork and, as a consequence, the S phase checkpoint is activated[31,32]. Altered levels of dNTPs are often associated with genome instability and cancer development[33]. Moreover, each replication origin must be fired only once per cell cycle to avoid re-replication of the DNA sequences. An excess of origins is licensed compared to the number required to duplicate the whole genome. As mentioned before, those dormant origins are required as backup in case neighbour replication forks slow down or block[17,18,34,35].

Some genomic regions are intrinsically source of replication stress. These regions are referred to as "difficult to replicate sites". They are often associated with repetitive sequences which can induce DNA polymerases to stumble. In other cases, difficult to replicate site have relative low origin density. As a consequence, after a fork stalling event in these regions, replication resumption can only relay on the ability of those replication forks to restart their activity. Commonly, difficult to replicate sites can overlap with fragile sites, which are defined as the chromosome regions that tends to form a gaps or constrictions. As a consequence, they easily tend to break when the cell is subjected to replication stress conditions[36,37].

Moreover, some sequences are prone to form DNA secondary structures, which, together with DNA-protein adducts, abasic sites, damaged bases and inter- and intra-strand DNA cross links, are referred to as replication fork barriers.

Interference of the transcriptional machinery with the DNA replication fork is also a major source of replication stress[38]. The exact mechanism by which DNA replication is affected by transcription is still unclear. However, interference between the two processes is inevitable because they compete for the same template molecules. RNA/DNA hybrids could directly act as obstacles for the replisome progression. Moreover, like DNA

replication, also transcription causes positive and negative supercoiling, which can make DNA unwinding more difficult because of topological stress. Replication–transcription conflicts significantly contribute to cause genetic and epigenetic instability associated with replication stress. In humans, increasing evidence links the lack of factors that limit replication–transcription interference with cancer development[39].

1.2 Mechanisms of DNA damage response

1.2.1 DNA damage and checkpoint activation

Unresolved DNA damage can lead to mutations, translocations and abnormal recombination events during S phase. Also, chromosome breakage and aneuploidy can occur if the damage is not fixed before mitosis. In order to preserve the genetic information cells have developed control mechanisms called checkpoints that are able to sense and respond to DNA damage and other kind of abnormalities. When a DNA lesion is sensed, cells activate checkpoint and, as a consequence, cell-cycle progression is interrupted giving to DNA repair apparatus the appropriate time to resolve the lesion[40]. Physiologically, when replication fork progression is blocked, the so called "S phase checkpoint" is activated to ensure structural stability of the replisome components avoiding what some authors refer to as "fork collapse" (i.e. the dissociation of the main replication factors from the replication fork)[17,40]. This first response is particularly important because it can help a fast restart of the stalled replication fork.

The S phase checkpoint can be schematically divided in two main pathways: the ATM-CHK2 pathway which is more dedicated to the response to DNA double strand breaks, and the ATR-CHK1 pathway, which is mainly activated by replication fork stalling[41]. The two pathways follow a similar signal cascade: sensor proteins are recruited at the DNA damage site and activate the apical kinases (ATM and ATR); then, those kinases will phosphorylate other signal-related proteins, such as Chk1 and Chk2, which

eventually activate the effector proteins[41]. Effector proteins can be responsible for cell-cycle arrest, activation of the DNA repair program or even activation of the apoptotic program in case the damage is too severe and cannot be resolved (***Figure 1.4***).

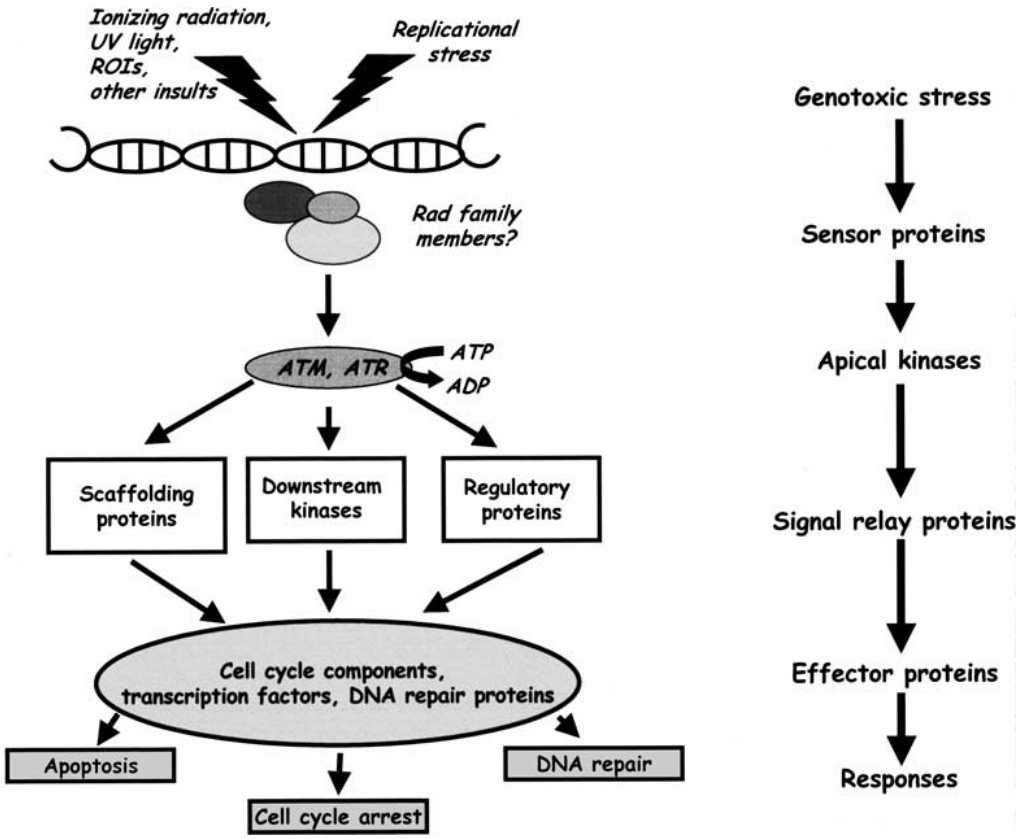

Figure 1.4 A generic cell-cycle checkpoint signalling pathway

Schematic representation of DDR pathway. The replication stress event is identified by the sensor proteins which activate the apical kinases (ATM and ATR). A series of other protein are then phosphorylated by the apical kinases, the signaling cascade will then results in the activation of the DNA repair pathway and cell-cycle arrest or in the activation of the apoptosis program. (Picture taken from Abraham R. T.; 2001. Ref[41]).

An early function of the DDR at replication stress sites is the phosphorylation of the histone H2AX (γ-H2AX). H2AX is the substrate of three main kinases: ATM, ATR and DNA-PK. Thus, γ-H2AX is frequently used as a replication stress marker, together with the formation of 53BP1 foci, another consequence of the DDR. However, both γ-H2AX and 53BP1 foci also occur at DNA damage sites, in particular DSBs, in a replication-independent manner[42-44].

According to the most accepted model of checkpoint activation after fork stalling, when a lesion on the DNA template is encountered, DNA polymerases progression is stopped while the rest of the replisome machinery continues to unwind the parental DNA[45]. The functional uncoupling between the polymerase and the helicase activities generates an abnormal amount of ssDNA which is rapidly coated by RPA. RPA accumulation is one of the prerequisites for ATR recruitment together with its partner protein ATRIP, that is required to stabilize ATR. However, ATR-RPA interaction is not sufficient to activate ATR. Other proteins required to this purpose are TopBP1 and Rad9-Rad1-Hus1 (also referred to as 9-1-1 complex)[46]. Recently, an alternative ATR activation pathway has been discovered, which is mediated by ETAA1, an RPA interacting protein possessing an ATR activating domain similar to the one of TopBP1[47,48].

It is still unclear which DNA structure can activate the ATR signalling cascade, since different damaging agents, generating different aberrant DNA structures, result in the same signal activation. Some evidences indicate that the RNA primase activity of the Polα/Primase complex is likely necessary to boost the checkpoint signal[49,50]. Indeed, Polα/Primase activity increases the number of primer-template junctions, which have been shown to be required for the loading of the 9-1-1 complex *via* Rad17-RFC[51]. Once activated, ATR phosphorylates several of the replisome components and the effector kinase Chk1[40,52].

As mentioned before, polymerase-helicase uncoupling generates ssDNA. An excess of ssDNA can be deleterious because it can expose the DNA to degradation leading to the generation of DSBs. A specialized protein complex, the replication protection complex (RPC) couples the CMG helicase and the polymerase activity and it is composed by four factors, Tim1, Tipin, Claspin and And1[40]. Noteworthy, Claspin has been shown to work also as a checkpoint signalling mediator, being essential for Chk1 activation.[53] Tim1/Tipin, which form a stable complex *in vitro*, are required to prevent helicase/polymerase uncoupling even in unchallenged DNA replication conditions;

moreover, they are important for Claspin chromatin binding[13,54]. Recent studies suggest that And1 forms a bridge connecting the CMG complex with Polα[54,55]. Very intriguingly recent data show that And1 deficiency in DT40 chicken cells results in Mre11-dependent ssDNA accumulation even in absence of exogenous sources of DNA replication stress[56]. Defects in the S phase checkpoint proteins or in the RPC components have been linked with severe DNA replication and repair defects leading to ssDNA accumulation, fork reversal and inefficient DNA replication restart[54,57-64].

1.2.2 Double strand breaks and homologous recombination

Genome stability relies on the ability of cell to repair DNA lesions. Each cell in the human body faces tens of thousands of DNA lesion per day[65]. These lesions can be an obstacle for DNA replication and, transcription and if not repaired or they are incorrectly repaired, they can be cause of mutations or chromosome aberrations that can threaten cell viability[66]. DNA lesions can involve aberrant modifications of nucleotide bases such as oxidation, pyrimidine dimers, methylation and the formation of abasic sites or else they can be induced by the disruption of the phosphate-deoxyribose backbone. Aberrations that alter the phosphodiester chain, can interest either one strand or both of the strands of the DNA molecules. In the first case they are called single-strand breaks (SSBs); while, in the other one, they are called double-strand breaks (DSBs).

The DNA breaks either single- or double-stranded can be generated by ionizing radiation (IR) via direct or indirect generation of reactive oxygen species, and also by the failure of the topoisomerases activity that can cause a physical break in the DNA backbone[67-69]. If an SSB is left un-repaired it could be converted in DSBs during the DNA replication. Indeed, if the helicase machinery will encounter a single nick in the template DNA, it will fuse the two strands generating a so called one-ended DSB[66] (***Figure 1.5***).

Cells exploit two main pathways to repair DSBs: the homologous recombination (HR) and the non-homologues end-joining (NHEJ) pathway. The NHEJ can only process double-ended DSBs and represents a fast but potentially mutagenic way to repair DNA damage; in contrast, HR is based on the redundancy of the genetic information, and it uses the information present in the sister chromatid to reconstitute the full and correct information on the damaged molecules. Thus, this pathway is only suitable during the S- or G2-phase of the cell cycle[70] when the sister chromatid is present.

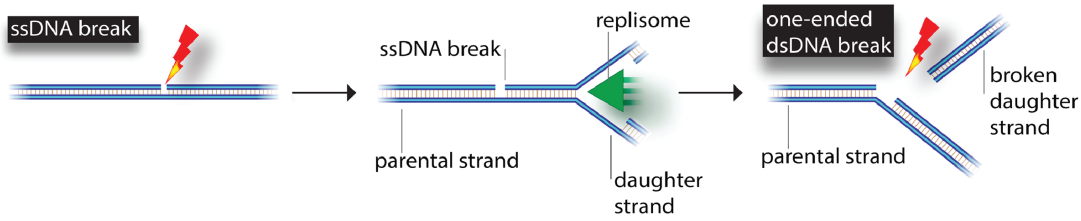

Figure 1.5 SSB conversion into a DSB during DNA replication

A single strand break is an interruption of one of the two phosphodiester chain. SSB can be converted in one-ended dsDNA break when the replication helicase unwinds a portion of DNA containing a ssDNA break. (Picture taken from Ranjha L.; 2018. Ref[70]).

NHEJ does not required any or very little (2 nt), homology between the two ends of the broken DNA molecules. The broken sites are encircled by the heterodimer Ku70-80, then the DNA-dependent protein kinase catalytic subunit (DNA-PKcs) stabilises this complex and eventually XRCC4-XLS complex and the DNA ligase IV ligates the two DNA ends together[71]. In this pathway DNA ends are not, or very little, processed prior the ligation step. Only in the presence of chemical or protein adducts, at the DNA extremity, the action of endogenous nucleases is required to "clean the ends" and to make the DNA suitable for the ligation reaction[70]. In contrast, for all the majority of other pathways, the first step that precede the DSBs resolution is the DNA-end resection by endogenous nucleases that digest the DNA leaving a 3' protruding end[72].

Another alternative way to repair DSBs is represented by the microhomology-mediated end-joining (MMEJ), also called single-strand annealing (SSA). In this case, both DNA ends are resected leaving a 3' protruding ends. The DNA extremitys are then used to search for a small homologous sequence in a range from 2 to 20 nt within the resected ends. Once the two ends are paired together, any protruding flaps generated by the 3' tail flanking the homologous sequence, are removed and the remaining DNA gaps are filled by a specialized DNA polymerase named PolQ or Polθ[73]. Eventually, the remaining nicks into the DNA strands are ligated together by Lig3/Lig1[74]. This pathway is certainly error-prone since a piece of information is lost during the annealing and the flap resection steps.

In contrast, with HR-mediated repair, a large homologous sequence is used to restore the correct genetic information in the proximity of the broken site; usually the sister chromatid is used as template to replace the missing information. Like for MMEJ, both DNA ends have to be resected and this process can be divided in two steps: the short-range resection and the long-range resection. The short-range resection is carried out by the MRN complex and CtIP. The MRN is a hetero trimeric complex constituted by Mre11, Rad50 and Nibrin (or NBS1). In vertebrates both Rad50 and NBS1 are needed for the *in vivo* function and regulation of the complex. Mre11 is the core enzyme of the hetero-trimer; indeed, this protein shows both an endonuclease activity and a 3' to 5' exonuclease activity[72]. The most accepted model mechanism proposes that the MRN complex creates a single-nick in proximity of the DNA ends through its endonuclease activity. The complex proceeds then backward until the extremity of DNA exploiting the 3' to 5' exonuclease activity. As final result, a 3' overhang DNA strand is left[70,72,75]. This strategy of DNA digestion is required to bypass possible chemical or protein adducts that could impede the DNA end processing. The MRN activity is promoted by the phosphorylation of CtIP by CDK1 and CDK2[76]. This is one of the controls that allow specific resection, and thus recombination, to happen only during the S- and G2-phase

when the sister chromatid is available as template. The initial resection step stimulates the long-range resection process which is carried out by EXO1 or DNA2. EXO1 is a 5' to 3' exonuclease and it is able to process the dsDNA template extending the first 3'overhang produced by the MRN complex. Also, DNA2 harbours the same exonuclease activity but it requires the interaction with either BLM or WRN helicase in order to elongate the ssDNA overhangs[70,72].

After the ssDNA is exposed, as a consequence of the ends resection process, it is covered by RPA. RPA prevents the DNA digestion by other nuclease activity and impedes secondary structure formation that can arise from self-annealing sequences. Moreover, RPA helps the checkpoint kinases activation, that induces cell-cycle arrest allowing sufficient time for DNA repair[77-79]. In order to promote DNA strands invasion and to search for sequence homology, RPA has to be substituted with the HR key factor Rad51. This protein is highly conserved through evolution, it has a ssDNA binding activity and it forms right-handed helical protein filaments on the resected DNA ends that acts as nucleoprotein scaffolds, known as pre-synaptic complex, for the following steps. RPA has higher affinity for ssDNA than Rad51, and the presence of RPA on ssDNA prevents Rad51 binding *in vitro*[80]. However, to proceed with recombination is critical that RPA is replaced by Rad51. To this purpose Rad51 is loaded onto DNA with the help of other proteins known as mediators[81-87]. Since its critical role, Rad51 has to be tightly regulated and a first level of regulation is represented by Rad51 ATP binding and ATPase activities. The ATP binding activity increases Rad51-ssDNA affinity favouring nucleofilament stability and growth. Conversely, ATP hydrolysis reduces Rad51 affinity for the DNA. This is a mechanism to control the nucleofilament elongation[81,88]. Moreover, Rad51-ADP binding is required for the subsequent steps of DNA invasion[70].

In vertebrates, the Breast cancer type 2 susceptibility protein (BRCA2) is one of the most important Rad51 mediators. BRCA2 is a multidomain protein that can interact with Rad51 via its C-terminal region and through the eight BRC repeats domains situated in

the central portion of the protein. The BRC repeats can independently bind free Rad51 protein but normally only few of them can associate with Rad51 at a given time. BRC repeats 1 to 4 show a high affinity for soluble Rad51 and promote the nucleation reaction of the presynaptic complex; moreover, they inhibit Rad51 ATPase activity promoting the nucleofilament stabilization. BRC repeats 5 to 8 are less avid for Rad51 compared to the first set and they are supposed to help the Rad51 nucleofilament growth. On the contrary, BRCA2 C-terminal binding domain for Rad51 seems to be important and more involved in Rad51-nuclofilament stabilization in a DNA replication context[42,89-91].

Similarly to BRCA2, Rad51 paralogs contribute to Rad51 loading onto the chromatin and Rad51-nucleofilament stabilization[92]. In mammalian cells, Rad51 paralogs family consists of five proteins: Rad51B, Rad51C, Rad51D, Xrcc2 and Xrcc3. Rad51 paralogs can form 2 different complexes, the CX3 complex made by Xrcc3 and Rad51C and the BCDX2 complex formed by Rad51B, Rad51C, Rad51D and Xrcc2. However, the functional role of these proteins and their mutated forms in DNA replication and DNA repair is largely unknown[81-83,85,93].

Once the pre-synaptic complex is established, the research for the homology donor starts in order to initiate DNA synthesis. In human cells additional proteins which play an important role in Rad51 homologous sequence pairing[75] have been identified, such as Rad51AP1 and BRCA1-BARD1. However, the mechanism that carries out this process is poorly understood. The direct interaction between Rad51-nucleofilament and the donor DNA template is known as synaptic complex. The subsequent DNA strand invasion leads to the formation of the so-called D-loop intermediate, which is the key structure of the HR pathway. The 3'-end of the invading strand is used as primer to initiate the DNA synthesis. Even if trans-lesion polymerases have been implicated in the HR process, it has been proposed that most of the DNA polymerization is due to Polδ activity[94,95]. Subsequently, the second DNA-end goes for the so-called second capture, and it is annealed with the ssDNA left unpaired from the D-loop structure formation. It is still

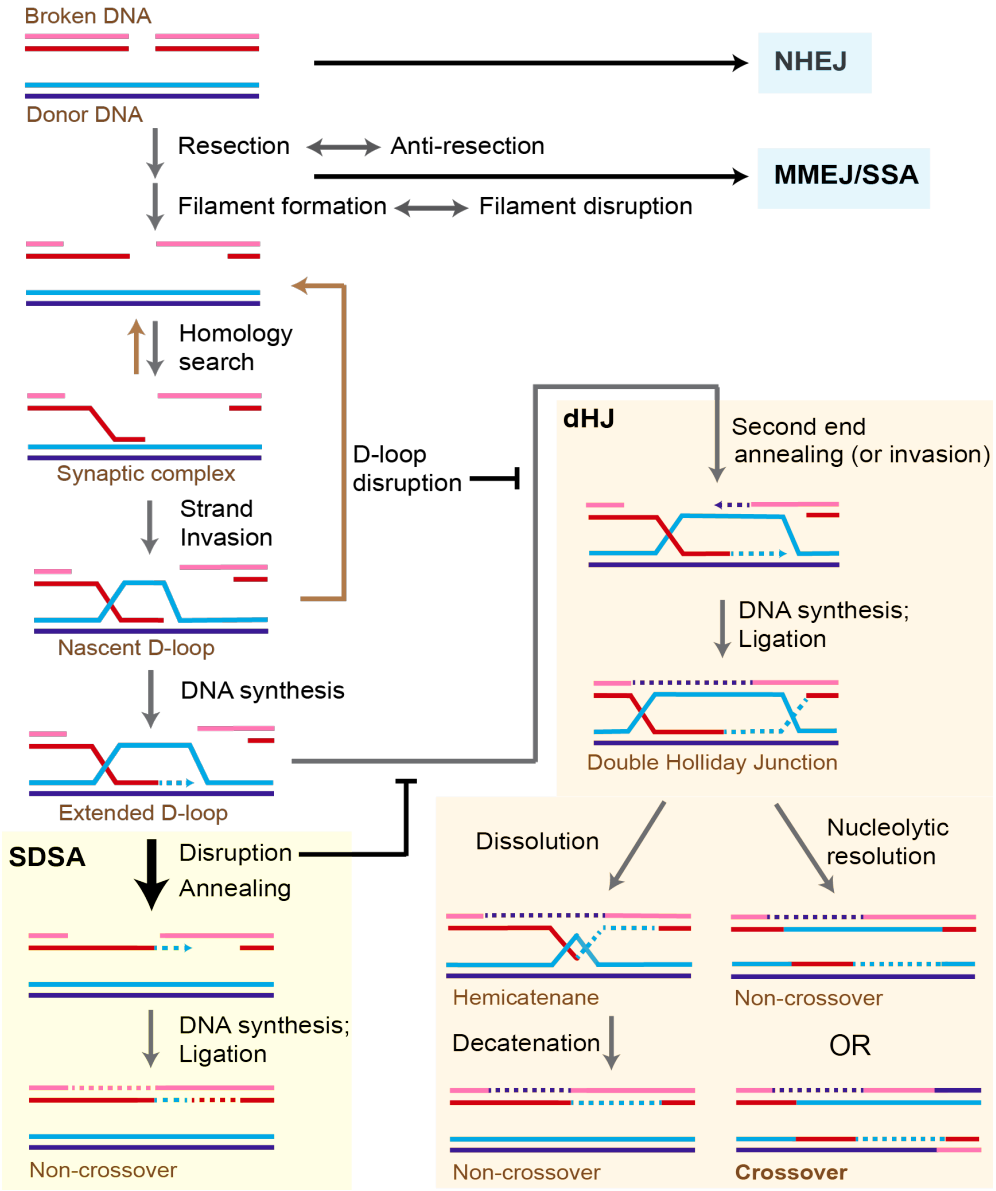

Figure 1.6 Model for DNA repair of DNA double-strand breaks

DSB can be repaired by multiple pathways such as NHEJ in which two unresected DNA ends are directly ligated. MMEJ and SSA rely on different extents of homology between the two DSB ends for repair the DNA lesion. HR exploits the redundancy of the genetic information to repair the DSB. DNA ends are resected by endogenous nucleases giving 3' protruding overhang. The 3' tail are used to search for homologous sequence and to invade the donor DNA. DNA invasion results in the D-loop formation giving the start for DNA synthesis. The newly synthetized DNA can be used to pair the two DNA ends in a process referred to as SDSA, resulting in D-loop disruption and in a non-crossover product. Otherwise, a second invasion process can take place resulting in a dHJ structure which can be resolved by endogenous nucleases. According with the nucleolytic cut direction, the resulting product can be either crossover or non-crossover product. (Picture taken from Wright W. D.; 2019. Ref[75]).

debated whether the second capture process is actually a second strand invasion process similar to the first one[70,75,92]. As a result of the second capture and DNA synthesis the D-loop is converted in a double Holliday junction structure (dHJ). The dHJ is eventually cut by specialized endogenous nucleases such as MUS81-EME1, SLX1-SLX4 and GEN1. Depending on the cut direction, the final product can give raise to a reciprocal crossover or non-crossover product (***Figure 1.6***).

The HR is not a straight forward pathway but it can be considered as a multi-branched process; the repair pathway choice also depends on substrate complexity and other factors such as the D-loop stability. For example, the DNA end that was extended during the DNA synthesis could dissociate from the D-loop structure and reanneal to the other ssDNA end of the DNA damage site; this process is known as synthesis-dependent strand annealing[70,75,92] (***Figure 1.6***). In this case, the resulting product can only be a non-crossover product.

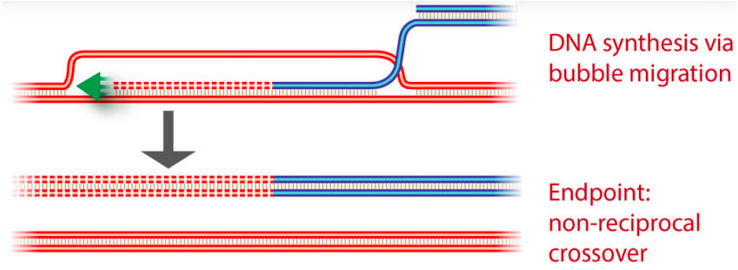

Figure 1.7 Model of BIR process

In BIR, the invaded DNA molecule is stabilized, and DNA synthesis proceeds along the whole length of the template DNA via a bubble-like structure to the chromosome end. BIR is a unique pathway for repair of one-ended DSBs resulting from collapsed DNA replication forks. The genetic result of BIR is a non-crossover. (Picture taken from Ranjha L.; 2018. Ref[70]).

As mentioned before, if SSBs are left unrepaired they can be converted during the S phase in a single-ended DSB, those peculiar DNA lesions are processed via a specific pathway called break-induced replication (BIR). The initial steps resemble the one of a canonical HR process but, in this case, the invading strands are stabilized and the DNA

synthesis proceeds until the end of the chromosome via a bubble-like structure (***Figure 1.7***). The DNA synthesis is dependent from Polδ enzymatic activity assisted by the Pif1 helicase[95], but it is still largely unknown how the complementary strands is synthetized. However, BIR is highly mutagenic, so this pathway is only used when it is impossible to proceed with other repair patways[70].

1.2.3 PAR signalling contributes to DNA damage response

Poly-ADP-ribosylation (also known as PARylation) is an important post-translational modification that is implicated in the regulation of a wide range of biological processes including DNA repair, transcription, chromatin remodeling and cell division[96]. More recent studies have suggested an involvement of Poly-ADP-Ribose (PAR) signal in Okazaki fragment maturation[97]. In vertebrates, PAR molecules are synthetized by the PARP protein family. PARPs are enzymes that use NAD^+ as substrate to transfer two or more ADP-ribose motifs to acceptor proteins[98].

In humans, the PARP family is composed of 17 members. Among these, PARP1 was the first member of the PARP family to be identified; it has poly-ADP-ribosylation DNA-dependent activity and it plays a key role in DNA damage repair, particularly in base excision repair (BER). PARP1 is activated by DNA strand breaks, it undergoes auto-poly-ADP-ribosylation and PARylates the Ku70/80 complex, PCNA and histones. This results in the recruitment of PAR-binding DNA repair factors, such as XRCC1 and MSH6 to the site of damage[96,99]. Recent *in vitro* studies have shown direct DNA PARylation at DSBs sites[100].

A number of PARP1 inhibitors have been developed to block repair of chemotherapeutic agent-induced genotoxic damage and, thereby, potentiate the cytotoxic effect of chemotherapeutics in cancer patients[99]. Inhibition of PARP1 appears to be particularly effective in conjunction with chemotherapeutics on cancer cells harboring mutations in components of homologous recombination DNA repair pathway, primarily

BRCA1, and BRCA2[101]. Tumors BRCA-deficient that are PARP-inhibitor resistant show a sensitivity to checkpoint inhibitors[102] underling the close correlation of these signaling pathways.

PAR catabolism is primarily mediated by PARG, an enzyme having both endo- and exo-glycosidase activity[96,98]. PARG protein is mainly confined in the cytoplasm compartment and only after DNA-damage induced PARP1 activation it is transported into the nucleus. This mechanism ensures a coordinate activity between the two proteins allowing a rapid and transient increase of PAR signal at the damage site[96,98]. Different studies have reported that PARG deficiency results in SSBs and DSBs, suggesting a fundamental role for PARG in DNA repair regulation.

1.2.4 Fork maintenance and DNA dynamics at the stalled fork

DNA replication represents one of the most dangerous moment on the cell cycle since endogenous and exogenous events can challenge genome integrity by interfering with the progression, stability and restart of the replication fork. In order to overcame potential deleterious block events, cells are able to protect the stalled fork structure and to favor fork resumption processes. Failure to protect stalled forks or to process the replication fork appropriately for replication restart results in the accumulation of mutations and genomic aberrations.

Fork pausing can be the consequence DNA damage, occurring during the S-phase of the cell cycle, through several mechanisms: by causing uncoupling between the replisome and the helicase at the fork; by uncoupling the leading and lagging strand synthesis; or by blocking the replicative helicase progression and therefore inhibiting template unwinding. In most cases, the replisome remains stably associated with the stalled fork[103] and then resumption of replication can occur once the block is relieved.

However, in peculiar region of the genome such as telomers or if the DNA damage is too severe, replication forks may experience replisome dissociation and collapse. Fork collapse may be caused by protein–DNA complexes that cannot be efficiently removed, templates that have been exposed to the action of cross-linking agents, DNA breaks or by the run off of the replisome at telomeres. In most cases, fork collapse should not represent a problem in eukaryotes using multiple replicons, as forks converging from adjacent

replicons can complete replication. Furthermore, considering that only a fraction of replication origins are fired at each round of DNA synthesis, it is reasonable to assume that the excess origins represent a reserve of replicons for cells experiencing extensive fork collapse.

One of the most studied mechanisms controlling for genomic integrity during S phase is the replication checkpoints. In checkpoint mutants, stalled forks rapidly degenerate, accumulating gapped and hemireplicated molecules. These long ssDNA regions seem to result from lagging strand defects, probably due to the unscheduled dissociation of the lagging strand polymerases and to the erosion of nascent chains mediated by the Exo1 exonuclease. Stabilization of stalled replication forks by replication checkpoints is thought to occur through stabilizing the association of the replisome with the fork and through restraining the activity of recombination enzymes at stalled forks. In both cases, physical interaction with the checkpoint or checkpoint-dependent phosphorylation of replication or recombination/repair enzymes has been invoked. The Polα/primase complex, RPA and Claspin[104] phosphorylation are thought to be implicated in stabilizing the replisome–fork association.

Recombination-mediated replication-restart and damage-bypass mechanisms are frequently used to replicate damaged DNA or to resume replication after fork collapse. Recombination mechanisms assist completion of replication when forks collapse in regions where there are no converging forks that could complete replication, or when the DNA lesions or the stalled replication forks are processed to double-strand breaks. Damage bypass replication mechanisms are assisted by specialized translesion synthesis DNA polymerases that use the genetic information present on the undamaged sister chromatid to overcome the damaged site. The recombination-mediated damage bypass might be assisted by joint structures resembling hemicatenanes, in which one newly synthesized strand is coiled around the other newly synthesized strand, and which were shown to form after origin firing and to migrate chasing the forks.es

1.3 Role of HR proteins during DNA replication

The role of HR factors during DNA replication has been elusive for years, in part because they often are the product of essential genes. Beyond their importance for DSBs resolution, it is likely that these genes are involved in other DNA metabolism functions.

In fact, Rad51 knockout B-lymphocyte cell lines undergo apoptosis even if cultured in absence of DNA replication stressing agents or DNA damage inducing agents and accumulate different kinds of chromosome aberrations and breakage[105]. Similar results were obtained for BRCA1- or BRCA2-deficent embryonic cells. Even in these cases, cell death was preceded by severe chromosome aberration during mitosis[106]. Genetic ablation of the MRN complex components results in cell lethality in chicken and mouse cells[107-110]. These results demonstrate that Mre11, Rad50 and Nbs1 are essential in vertebrates in the absence of external sources of DNA damage.

The fact that homology directed repair (HDR) related genes are essential, even in absence of DNA damage inducing agents, suggests that they might have a role in other fundamental cellular pathways beside their role in DSBs resolution.

Several studies have demonstrated that Rad51, BRCA2, RPA and PCNA co-localize forming nuclear foci during S phase as a consequence of replication inhibition and DNA damage[111-114]. These results may suggest a coordinated role of HR factors and DNA replication related proteins during S phase. In accordance with this hypothesis, it was shown that HR-factors deficient cells, lacking BRCA2, Rad51 or Xrcc2, have reduced rates of replication fork progression and an increased density of replication origin firing[115]. Altogether these results suggest that HR protein activities are of considerable significance for genome stability during both DSBs repair and DNA replication.

1.3.1 Effect of Rad51 deficiency during DNA replication

In addition to DSBs repair, recombination proteins have critical functions in other pathways of the DNA metabolism. Thus, recombination proteins in multiple ways promote the stability of replicating DNA[60,116]. However, Rad51-depletion performed in different systems does not affect bulk DNA replication[117,118]. On the other hand, Rad51 absence causes ssDNA gaps accumulation[118,119], which causes G2 phase arrest and an

increased post replicative RPA foci formation and eventually chromosome breaks during mitosis.

Indeed, EM experiment conducted in the *Xenopus* and yeast system have shown how Rad51 depletion results in aberrant ssDNA gaps accumulation at the fork junction and behind it also in unchallenged DNA replication condition[118,120]. More in detail, the ssDNA gaps observed in Rad51-depleted *Xenopus* extract showed a different sensitivity to mirin, a specific Mre11 chemical inhibitor[121]. The gaps located at the fork junction are not abolished by mirin while the gaps situated behind the fork front were reduced upon Mre11 inhibition. This suggests a fundamental role for Rad51 in preventing an excess of Mre11-mediated degradation of the newly synthetized DNA molecules[118] (***Figure 1.8***). The Rad51 protection role is even more important during replication fork stalling as it has been reported in studies conducted with different experimental systems[40,118,122-124]. However, a coordinated Rad51 and Mre11 activity is critical at the stalled replication fork. Indeed, the two proteins are crucial for collapsed fork reassembly and DNA replication resumption [120].

1.3.2 BRCA2 function during DNA replication

The first insights about a role for HR proteins in DNA replication were suggested by data showing the requirement of these protein to prevent fork collapse or protect stalled replication forks. BRCA2-deficent mouse embryonic fibroblasts have an increased sensitivity to replication fork stalling agents as shown in the 2003 by Lomonosove and collogues[125]. In their study, these authors showed that BRCA2 deficiency results in accumulation of DSBs when replication fork stalling is induced by HU treatment. This suggested a function for BRCA2 in preventing stalled replication forks from collapse.

EM based DNA single molecules analyses have shown that *S. cerevisiae* strains deficient for Rad52 (which in yeast perform a similar function of human BRCA2)

accumulates aberrant DNA structures similar to the ones found in Rad51-deficient cells. In both *rad51Δ* and *rad52Δ* strains ssDNA gaps were accumulated at the replication fork junction and behind it[118]. These data suggested a correlated role for these two factors in replication fork protection that is independent from their function in the DSBs repair pathway.

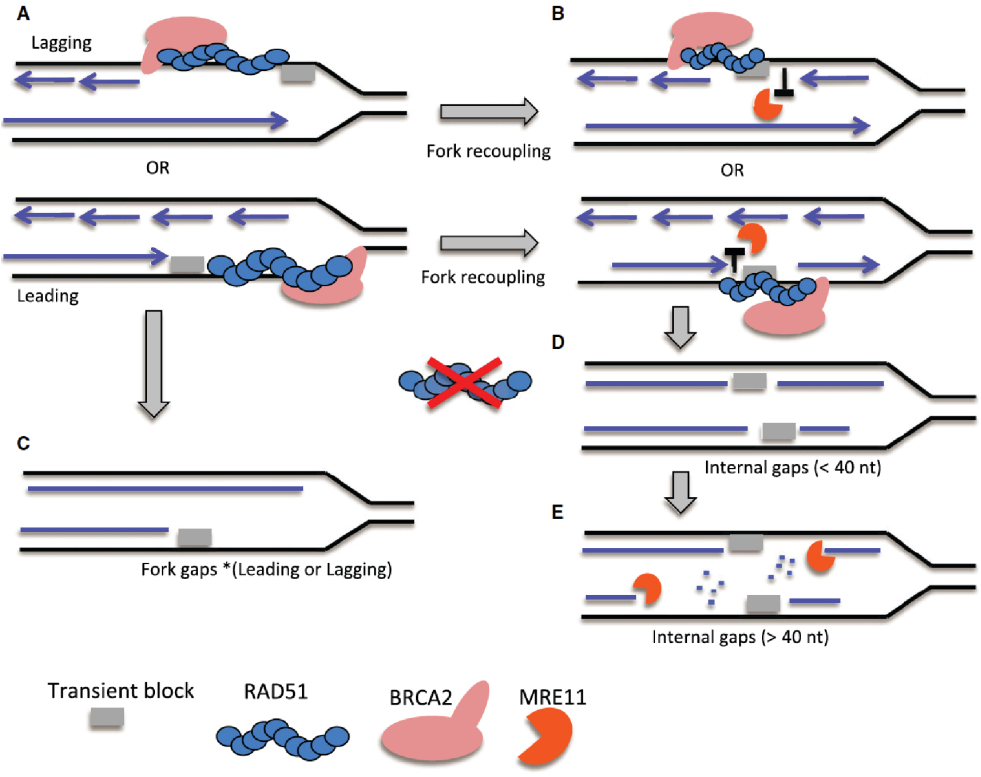

Figure 1.8 General model for HR protein function in DNA replication

(A) BRCA2 helps and stabilizes Rad51 to bind ssDNA. (B) Rad51 bound to fork junctions might ensure recoupling of leading and lagging strand synthesis. Rad51 bound to internal gaps behind forks might promote their repair and protect them from Mre11-mediated degradation. (C) In the absence of Rad51 bound to replication forks, ssDNA gaps at forks would persist. (D) Small internal gaps that arise in the absence of Rad51 might further extend. (E) Mre11 is likely to be the major nuclease-extending internal gaps. (Picture taken from Kolinjivadi, A. M.; 2017. Ref[127]).

Moreover, analogously to Rad51-deficient *Xenopus* extract, BRCA2-depleted cells suffers from extended DNA degradation mediated by Mre11 activity[89,121,126].

Furthermore, similarly to what happens for the HDR pathway, BRCA2 is required for Rad51 nucleofilament formation and stabilization also in a DNA replication context. Thus, the BRCA2 fork protection role is exerted through Rad51 nucleofilament formation and stabilization[89].

Intriguingly, it has been reported that, differently from the HR pathway, the BRC repeats are dispensable for the BRCA2-mediated fork protection activity, but BRCA2 C-terminal region, containing Rad51 binding site, is essential to mediate Rad51 nucleofilament stabilization and to prevent Mre11-mediated degradation of the newly synthesized DNA[89].

These studies bring strong evidence that HR factors play a major role in preventing chromosome breaks by counteracting endogenous nuclease activity during DNA replication and through HDR of DSBs in late S – G2 phase. Rad51 and BRCA2 are probably promoting HR-coupled DNA synthesis after the bulk replication is completed leaving no segment of DNA un-replicated (***Figure 1.8***).

1.4 Replication Fork Reversal as DNA damage response intermediate

A reversed replication fork (RVF) is a four-way junction DNA structure resulting by the annealing of the two newly synthesized DNA strands and as a consequence the re-annealing of the parental DNA strands (***Figure 1.9***). By a structural point of view, an RVF represents a DNA structure containing a Holliday junction (HJ) which, on one end, the so-called regressed arm, resemble a molecule containing a DSB.

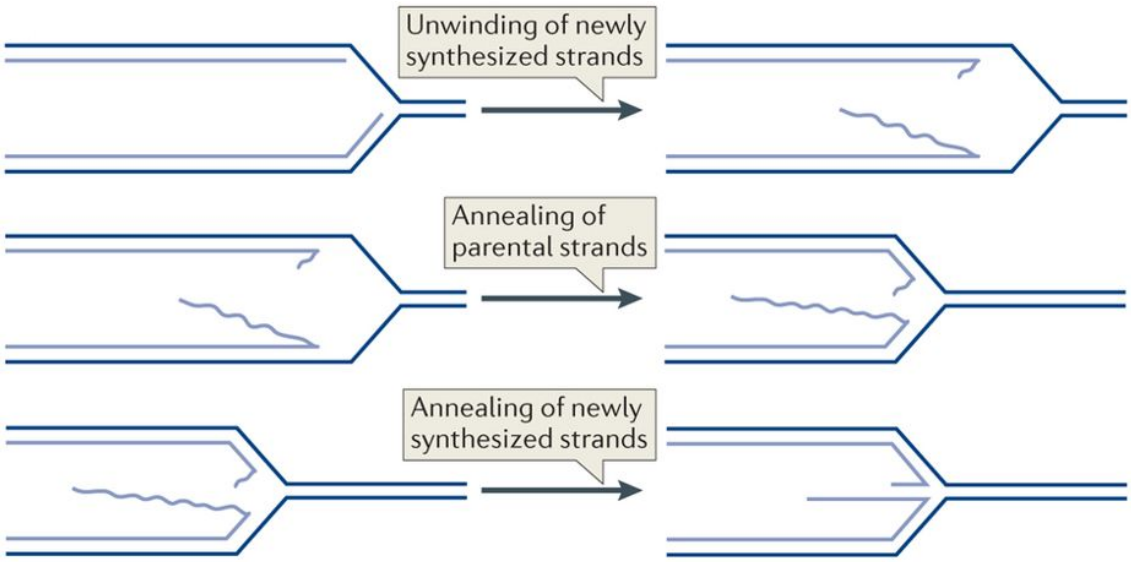

Figure 1.9 Reverse fork formation process

In the most accepted model, RVFs are the consequence of three main steps: the unwinding of the newly synthetized strands (upper part of the panel), the reannealing of the parental DNA behind the replication fork (middle of the panel) and the annealing of the newly synthetized strand (bottom panel). (Picture taken from Neelsen K. J.; 2015. Ref[128]).

Since fork reversal could be triggered by a number of replication fork stalling agents or checkpoint-deficient conditions[61,62,128], these structures were initially hypothesized to be the result of a pathological process[59,129]. More recently emerged the idea that fork reversal could represent a way to stabilize the stalled replication fork in order to protect the DNA structure and avoid DNA breakage[128,130]. In recent years the implication of recombination proteins in the replication fork reversal metabolism has become more and more evident. As mentioned before, RVFs are a single HJ containing structures. During HR mediated DSBs repair, Rad51 promotes strand invasion and the D-loop formation and, as a consequence, the creation of a double HJ intermediate at the end of the repair process. Thus, one of the proteins proposed to be involved in the fork reversal process was Rad51[130]. However, it is unlikely that Rad51 is the only protein involved in RVF formation. Moreover, taking into account that regressed arm can have a size of more than 1 kbp, other proteins with helicase and translocase activity have been proposed to participate in the fork reversal process. Among these proteins are listed Rad54[131],

Smarcal1[132], ZRANB3[133], HLTF[134], FBH1[135], RECQ5[136], and FANCM[137]. However, the interplay between these factors and RAD51 is not well defined, and it is not clear to which extent these proteins can function redundantly.

When a replication fork encounters a DNA lesion (i.e. DNA nicks or gaps), any kind of fork barrier (i.e. chemical or protein adducts, intra- and inter-strand DNA crosslink) or any structural impediment to fork progression (i.e. DNA secondary structures, difficult to replicate sequences, transcriptional machinery collisions) and fork reversal formation could be triggered as a mechanism to protect the replication DNA molecule. At the same moment cells gain time to resolve the replication block ahead of the replisome. Once the stalling source is removed DNA replication can be resumed.

Different alternative mechanisms of fork re-start have been proposed. Some of them involve the activity of proteins such as RECQ1[138], RAD54[131]. Other hypothesized mechanisms of fork restart include the activity of endogenous nucleases such as Mre11, Exo1, Dna2-WRN or MUS81 to degrade RVFs before restart[121,131,138-142].

However, it is still debated whether fork reversal is a pathological event for DNA replication or not. It has been shown that inhibition of this process is deleterious for genomic DNA stability[128,132,143]. Thus, the understanding of the mechanisms involved in RFVs metabolism has become of primary interest for the DNA cancer biology field[144].

1.4.1 Smarcal1 and replication fork remodelling

One of the most described DNA damage response proteins involved in RVFs metabolism is Smarcal1[145]. Bi-allelic loss of function mutations for Smarcal1 in humans cause the Schimke Immunoosseus Dysplasia (SIOD)[146], a pleiotropic syndrome characterized by skeletal dysplasia, renal failure, T-cell immunodeficiency and micro-cephaly. Smarcal1 (SWI/SNF-related, matrix associated, actin-dependent regulator of

chromatin, subfamily a-like1), also known as HARP (HepA-related protein), is an annealing-helicase belonging to the SNF2 family.

Smarcal1 is a multi-domain protein, with a highly conserved RPA-interacting domain at the N-terminal region and two subsequent HARP domains situated in the first half of the protein. The C-terminal protein portion harbour the ATPase domain which is divided in two sub-domains, known as ATPaseN and ATPaseC[132]. Indeed, it has been reported that Smarcal1 is able to promote fork regression, in an RPA- and ATP-dependent manner, *in vitro*[147].

Smarcal1 has been identified as a replisome component and it travels with active replication forks also in unchallenged conditions[148]. Smarcal1-deficent cells show an increased sensitivity to DNA replication stressing agents[148], resulting in a higher frequency of fork collapse mediated by endogenous nucleases clevage[132,148]. Thus, it is likely that Smarcal1 has a surveillance role with regard to stalled forks. It has been shown that in fork stalling conditions, when DNA helicase and DNA polymerase uncoupling leads to ssDNA accumulation, RPA-Smarcal1 interaction is required to activate the Smarcal1 annealing-helicase activity[145,147]. Furthermore, it has been reported that Smarcal1-RPA-dependent foci are formed also during DSBs repair even though it is not clear what is the role of Smarcal1 in this context[148].

Intriguingly, both Smarcal1 and RPA are substrates of the checkpoint apical kinase ATR[123,143,145,149,150], which is the main factor activated upon replication fork stalling. ATR-mediated phosphorylation is required for RPA-Rad51 exchange. ATR can also phosphorylate Smarcal1 with an inhibitory effect on its enzymatic activity[143,151]. Even though Smarcal1 harbours four S/Q-T/Q motifs which are possible ATR-phosphorylation target sites, only one of these seems to be the targeted for ATR-mediated regulation of Smarcal1[143,145]. ATR-dependent Smarcal1 inhibition could be essential to prevent a massive formation of RVFs which are then substrate for SLX4- and CtIP-dependent resection.

1.5 *Xenopus laevis* egg extract: an *ex vivo* system

Ever since their development and first use almost thirty years ago, cell-free extracts prepared from eggs of the African clawed-frog *Xenopus laevis* contributed to key discoveries in different research fields such as cell cycle regulation, DNA replication, DNA damage response, chromosome condensation and segregation. Indeed, in the absence of an intact cell, these soluble egg extracts can be used to recapitulate the key nuclear processes occurring during the eukaryotic cell cycle *in vitro* under the same controls mechanism that exist in vertebrate cells[77,78]. The development of cell-free system from *Xenopus* eggs extract has provided the first non-viral cell-free system capable of faithfully reproducing nuclear transitions, from the reconstitution of a functional nucleus to the assembly of chromatin and replication of the DNA.

For these reasons *Xenopus laevis* egg extract system is often considered half a way from an *in vivo* an *in vitro* system and it is something indicated as an "*ex vivo*" experimental system.

1.5.1 Physiological features of *Xenopus laevis* eggs: advantages in biochemistry and molecular biology

Certain aspects of oogenesis in *Xenopus* explain why *Xenopus* eggs extracts are a suitable system for the molecular analysis of processes such as DNA replication, chromatin assembly and checkpoint signaling. First, the most voluminous organ in *Xenopus* frogs is the ovary, which harbors several thousands of oocytes. The maturation of the oocyte into eggs can be artificially induced by gonadotropins injection and eggs are laid unfertilized outside the body of the animal. Eggs are ~1.2 mm diameter large and are produced in large quantities providing enough material for biochemical experiments[152,153]. Like mammals, *Xenopus* oocyte are arrested in metaphase of second

meiotic division. Fertilization promotes completion of meiosis, the extrusion of a polar body and progression into interphase of the cell cycle[154]. Second, *Xenopus* eggs contain abundant stockpiles of maternal material (proteins and mRNA) to support twelve synchronous rounds of cell division in the absence of significant transcription[152]. Thus, this system is ideal to study of protein complexes and to biochemically dissect protein-DNA transaction in a temporally controlled manner.

Xenopus egg extracts have been particularly exploited to reveal the fine mechanism of checkpoint signaling and DNA repair pathways[45,49,63,77-79,155]; the signaling cascade and, the consequent repair pathway activation, that take place during DNA replication and must be coordinated with replication fork progression.

Genetically tractable model systems have been instrumental to identify impairing mutations in genes involved in cell cycle checkpoints and DNA damage response. However, these approaches suffer important limitations among which the fact that essential genes cannot be isolated in standard genetic screenings. On the other hand, using highly specific antibodies it is possible to totally immune-deplete any protein of interest from the *Xenopus* extract without impairing the overall system. Hence, the cell-free extract derived from *Xenopus* eggs offers the possibility to overcome the limitation derived from essential gene silencing.

Xenopus eggs extracts support semi-conservative replication of DNA molecules and complete chromosome duplication under the same cell cycle controls of an *in vivo* system[19,156-158]. Moreover, from a DNA replication point of view, this system resembles the embryonic features of fertilized eggs: replication of *Xenopus* sperm DNA initiates from replication origins spaced every 10 to 20 kb during early *Xenopus* development[16,159], while in most dividing somatic cells, the replicon size ranges from 50 to 300 kb[8]. Over 200,000 replication origins are required to replicate the full genome (3.1 Gbp) in 30 minutes explaining why in the *Xenopus* extract 10 times more replication intermediates are created than in a somatic system[19]. Therefore, *Xenopus* egg extract is very useful for

the analysis of DNA replication intermediates given their abundance during a normal DNA replication reaction in this system. Recently, the development of novel techniques for single molecules analyses has been helpful to understand the function of DNA repair and checkpoint proteins during DNA replication[118,130]. In particular, the use of nanometric-scale imaging techniques, such as electron microscopy (EM), allowed the direct visualization of the structure of replicating DNA, giving new details about DNA lesions during perturbed DNA replication and providing insights into the function of proteins involved in DNA replication[23,128]. In parallel, atomic force microscopy (AFM) made possible the study of complex protein-DNA and protein-protein interactions of particular complexity[160-164].

In vertebrates, and so with the *Xenopus* extract, the distribution of replication origins is random and is not sequence specific. This allows the extract to replicate different types of DNA. Indeed, *in vitro* replication assays can be set up using either demembranated sperm nuclei or naked DNA molecules such as plasmids or single strand DNA circular molecules[155,157,165]. Addition of sperm DNA to egg extract is followed by chromatin remodeling and nuclear membrane formation, two processes that are not required for replication origin licensing. However, nuclear formation is critical to concentrate the factors involved in origin firing such as the S phase kinases[159,166-168]. This explains why is also possible to replicate plasmids DNA but with a lower efficiency, i.e. the licensing occurs normally but the formation of a nucleus and thus the replication efficiency depends on the size of the DNA moleule[169]; plasmid DNA usually cannot trigger nuclei formation. More recently large bacterial artificial chromosome (BAC) templates (about 130 – 150 kb in size) have been employed for study of the response of defined chromosome areas to replication stressing condition[155]. These molecules trigger nuclear formation and DNA replication in *Xenopus* extract allowing the use of all the above mentioned biochemical and imaging techniques for detailed structural and molecular analyses.

1.6 Single molecule imaging techniques

1.6.1 Atomic force microscopy (AFM) to study DNA structures, and DNA-protein interactions

Atomic Force Microscopy is a technique that allows to visualize and to measure surface structures with unprecedented resolution and accuracy. AFM great advantage is that almost any kind of sample can be imaged, being hard, such as the surface of a ceramic material, or very soft, like highly flexible polymers (such as individual molecules of DNA). The AFM works by scanning with a probe over the sample surface, building up a map of the height, or topography, of the surface as it goes along. So, AFM generates images which recapitulate the 2D sample projection while providing data about the height of the analyzed samples. As a result of these analyses the volumetric proprieties of the sample can be deduced[170-172].

A simplified optical microscope, known as an inspection scope, is usually used for selecting the region of interest on the sample prior AFM scanning. The AFM image construction starts from a direct physic interaction of the microscope probe with the sample; thus, it is possible to perform measurements virtually in any fluidic medium. For instance, performing sample scanning in physiological buffers, made possible to monitor in real time some biological reactions[173-175].

Furthermore, the direct interaction of the probe with the sample provides, in real-time with the recording of the image, various physical data, such as the sample stiffness or the chemical composition. For all these reasons, since its invention in the 1980s, AFM has been used in all fields of science, such as chemistry, biology, physics, engineering, nanotechnology, medicine, and more[172].

Another key advantage of AFM is that can be coupled with others imaging techniques, giving the opportunity to observe the sample in a broad range of resolution, from millimeters to nanometers.

The AFM is quite often compared with electron beam based instruments such as the Scanning Electron Microscope (SEM) or Transmission Electron Microscope (TEM) in terms of usability and final outcome of the analysis. However, as a starting approach AFM results easier than EM because there is minimal sample preparation required. Indeed, with AFM, acquisition of images from samples can be performed in an atmosphere ambient without prior treatment of the samples. On the other hand, AFM image recording is usually slower than an EM[171,172].

In conclusion, AFM is particularly suited for biological applications: living cells can be imaged, as well as single molecules such as proteins and DNA. The force contrast gives 3D topography information, as well as the possibility to assess other information such as the mechanical properties or adhesion strength. Long molecules such as DNA or glycoproteins can be studied to measure intrinsic properties such as the persistence length or interactions with bound proteins. The molecules do not required coating or staining and they can be imaged in dry, semi-dry or liquid conditions[176-181].

1.6.2 Electron microscopy (EM) to study DNA molecules structures

Electron microscopy is a powerful method to examine in details sizes and shape of biological macromolecules and it is particularly useful to study isolated or reconstituted macromolecular assemblies. Basic procedures involve adsorption of the sample onto a support film, followed by staining or shadowing with chemicals mix or metals.

Sample imaging of the dehydrated samples under high vacuum conditions with electron beam-based instruments can reach a maximal resolution of 1 to 2 nm. The basic procedures can be adapted to obtain information about molecule sites, internal structures and atomic composition of the samples[182].

In the biology field, a wide range of applications are available using EM techniques, including virus identification, mapping of hybridized regions in heteroduplexes, detailing

of macromolecular interactions, and analysis of the organization of molecular components in transcription, splicing, translation and replication complexes[82,183-189]. Moreover single-particle EM allows the reconstruction of proteins 3D structure[190].

One of the most important applications for the genome stability field is using EM to define the details of the DNA replication process thanks to the structural insight obtained after high resolution imaging of replicating DNA molecules. The combination of crosslinking agents and electron microscopy has been extensively exploited to reveal the fine architecture of DNA replication intermediates isolated from replicating cells or *Xenopus* extract. This is a fundamental approach to uncover the basic mechanisms of DNA duplication, as well as the perturbation of this process by genotoxic treatments. The direct visualization of DNA Replication Intermediates (RIs) by EM is suitable in a number of different biological systems like bacteriophages, bacteria, yeast, *Xenopus* eggs extract, and mammalian cells[183,191].

2 Materials and methods

2.1 Preparation of interphase *Xenopus laevis* egg extracts

Xenopus laevis egg extracts were prepared as previously described[153]. Mature *X. laevis* female were primed 1 week in advance with 50 U of pregnant mare serum gonadotropin (PMSG) per animal. To induce ovulation, 400 U of human chorionic gonadotropin per animal were injected 12-16 hours before *Xenopus* extract preparation. *Xenopus* eggs are laid naturally arrested in metaphase of meiosis II. High quality metaphase arrested eggs are crucial for the preparation of the best Interphase extract so eggs with spontaneous necrosis or pigmented variegation were removed using a 1.5 ml Pasteur pipette during all the washing steps and if necessary also later. Initially, *Xenopus* eggs are laid and collected in 90 mM NaCl buffer. The eggs were then incubated for 10-15 minutes in dejellying buffer (20 mM Tris pH 8.5, 110 mM NaCl, 5 mM DTT) until the jellycoat was completely removed, then washed three times with 50 ml of Marc's Modified Ringer (MMR; 5 mM Hepes pH 7.4, 100 M NaCl, 0.5 mM KCl, 0.25 mM $MgSO_4$, 0.5 mM $CaCl_2$, 0.025 mM EDTA). Eggs were then activated with 1 μl/ml calcium ionophore A23187 for about 5 minutes, in order to mimic fertilization thus inducing mitotic exit and entry into S phase. Activated eggs were washed three times with MMR and twice with cold S-Buffer (50 mM Hepes pH 7.4, 50 mM KCl, 2.5 $MgCl_2$, 250 mM Sucrose, 2 mM β-mercaptoethanol, 15 μg/ml leupeptin). The eggs were packed by 1 sec centrifugation at 6000 rpm at 4 °C; the excess of buffer was removed and then they were crushed by a 10 min centrifugation at 13000 rpm at 4 °C. The cytoplasmic fraction between the lipidic cap and the pellet was collected and supplemented with cytochalasin B (40 μg/ml) and then centrifuged at 70000 rpm for 15 min at 4 °C. The cytoplasmic and membrane fractions were collected and supplemented with 40 μl/ml of cycloheximide and 3% v/v glycerol. The egg extract was eventually snap frozen and stored in liquid nitrogen.

2.2 Preparation of demembranated sperm nuclei

It is fundamental to have high quality demenbanated sperm nuclei, low quality material can impact on experiment quality and reproducibility[153]. Demembranated sperm nuclei were prepared from testes of male frogs primed with 50 U Folligon seven days in advance. Testes were rinsed three times in cold MMR buffer, twice in cold NPB buffer (250 mM sucrose, 15 mM Hepes pH 7.4, 1 mM EDTA, 0.5 mM spermidine trichloride, 0.2 mM spermidine tetrachloride, 1 mM DTT) and finally chopped with a razor blade. The obtained material was homogenized in a dounce, filtered through a 25 μm nylon membrane and centrifuged at 3000 rpm for 10 min at 4 °C in HB-4 swing-out rotor. The pellet was resuspended in 1 ml of NPB buffer at room temperature, then 50 μl of 10 mg/ml lysolecithin was added and samples were incubated at room temperature for 5 min. Sperm demembranation was tested by mixing 1 μl of sample with 1 μl of Hoecht staining (1 μl/ml). Once demembranation reaches more than 95%, 10 ml of cold NPB buffer supplemented with 3% w/v BSA (Bovine Serum Albumin) were added to the 1 ml sample and centrifuged at 3000 rpm for 10 min at 4 °C in HB-4 swinging bucket rotor. Obtained pellet was resuspended in 500 μl of cold NPB buffer supplemented with 0.3% w/v BSA and 30% v/v glycerol. The sperm density was then counted, adjusted to 10^7 sperms/ml and aliquots were quickly frozen in liquid nitrogen.

2.3 Antibodies

Protein	**Source**	**Identifier**
BRCA2	Kolinjivadi et al. 2017	N/A
ATR	Aze et al. 2016	N/A
Polα-p180	Kolinjivadi et al. 2017	Abmart: clone 13026-1-3/C199

Msh6	Aze et al. 2016	N/A
Polδ-PolD1	Kolinjivadi et al. 2017	Abmart: clone 19570-1-1/C316
Smarcal1	Kolinjivadi et al. 2017	N/A
ORC1	Aze et al. 2016	N/A
Mre11	Jean Gautier, Columbia University	N/A
MCM7	Santa Cruz	clone sc-9966
RPA70	Jean Gautier, Columbia University	N/A
p-Chk1 (S345)	Cell signalling	#2348
Chk1	Santa Cruz	clone sc-8408
CDC45	Hashimoto et al. 2010	N/A
Fen1	IFOM antibody service (A. De Antoni)	N/A
Rad51	Abcam	clone ab123
Rad51	Kolinjivadi et al. 2017	N/A
PCNA	Bio-rad	MCA1558
H2B	Abmart	ab1790
Anti-Mouse	Bio-rad	1706516
Anti-Rabbit	Bio-rad	1706515

2.4 PCR

The pBluescript II KS (+) was amplified using as forward primer (5' GTTACCCAACTTAATCGCCT) and reverse primer (5' GATACCTGTCCGCCTTTCTC). Polymerase chain reaction (PCR) was carried out using the GoTaq® DNA polymerase kit (Promega), which included 10 mM (2.5mM each) deoxynucleoside triphosphates (dNTPs), 10x GoTaq® buffer, and 5U/μL GoTaq®

DNA polymerase. PCR conditions were 1 cycle of 3 min at 95 °C, followed by 29 cycles of 1 min at 95 °C, 1 min at 56 °C, and 2 min at 72°C, and finishing with 10 min incubation at 72 °C.

2.5 Western blotting

Protein mix were separated through SDS-poly acrylamide gels (Bio-rad). All the gels were run at 100 V until the blue dye front reach the bottom of the gel. Proteins were then transferred on 0.2 µm Nitrocellulose membrane (Bio-rad) using the Trans-Blot® Turbo™ Transfer System (Bio-rad). Nitrocellulose filter were then rinsed with deionized water and stained by Ponceau S in order to check transfer quality. Membranes were then washed three times with TBS-T (50 mM Tris pH 7.5, 150 mM NaCl, 0.1% w/v Tween 20) at room temperature (RT), blocked for 1 hour at RT with shaking in 5% w/v not fat milk dissolved in TBS-T, and subsequently incubated for 2 hours or overnight at 4 °C in agitation with the indicated primary antibodies. After the incubation with the primary antibody membranes were washed thrice 10 min at RT with TBS-T and, incubated with the appropriated secondary antibody for 1 hour in agitation. The secondary antibody excess was washed away by performing three washes of 10 min at RT with TBS-T. Eventually the membranes were incubated for 2 min with WesternBright™ ECL (Advansta) and visualized on Fuji medical X-Ray film.

2.5.1 Dot blot

Few microliters of purified replicated genomic DNA mix or biotin-dUTP sample were spotted and let adsorbed onto the Amersham Hybond-N+ nylon membrane and subsequently crosslinked by UV cross-link at 1200 J/m^2 (Stratalinker UV2400). Membranes were blocked for 1 hour at RT in agitation with 5% w/v BSA dissolved in TBS-T, and subsequently incubated for 2 hours with streptavidin-HRP (ThermoFisher)

in agitation. Protein excess was washed away by performing three washes of 10 min at RT with TBS-T. Eventually, the membranes were incubated for 2 min with WesternBright™ ECL (Advansta) and visualized by ChemiDoc™ Imaging Systems.

2.6 Mobility shift assay

Fluorescently labeled DNA substrate (20 nM) was incubated with the amounts of Rad51^{WT}, Rad51^{T131P} or RPA indicated in figure legend in P-buffer for 5 min at 37 °C. Reactions were resolved on 0.8% agarose gel and scanned using a Fuji FLA 9000 imager. All the experiments related to mobility shift assay were performed in collaboration with Prof. Lumír Krejčí and Karina Zadorozhny.

2.7 Nascent ssDNA detection

Nascent unpaired ssDNA in replicating egg extract was detected as previously shown[132] with some modifications. Briefly, for each sample 40 mM BrdU (Sigma) and 10 mM biotin-16-dUTP (Roche) were added to 200 µl interphase egg extracts 10 min after addition of sperm nuclei (4000 nuclei/µl). Extracts were either mock-treated, Rad51- or Smarcal1- depleted and supplemented with recombinant proteins, APH or mirin as described in Figure legends. To isolate nuclei reactions were stopped by dilution with 900 µl ice cold EB, layered onto 500 µl of EB supplemented with 30% (w/v) sucrose and centrifuged at 3,000 x g for 10 min at 4 °C. To stabilize replication structures and prevent branch migration DNA was psoralen-crosslinked. To this end pellets were resuspended in 100 µl EB and transferred to a 96-well plate (100 µl per well). 4,5,8-Trimethylpsoralen (TMP) was added at 10 mg/ml to each well. Samples were incubated for 5 min at 4 °C in the dark and irradiated with 365 nm UV light for 7 min on a precooled metal block using a Stratalinker UV irradiator equipped with 365 nm light bulbs. The procedure from TMP addition to irradiation with ultraviolet light was repeated three more times. For complete

protein digestion, psoralen-crosslinked chromatin was incubated with proteinase K (1 mg/ml) and RNase A (167 mg/ml) for 2 h at 37 °C in EB. Genomic DNA was extracted with one volume of 1:1 (v/v) phenol–chloroform mixture, precipitated with isopropanol and partially digested with restriction enzyme StuI, which generates genomic fragments with blunt ends in the context of AGG'CCT sequence. DNA was plated into 96 well streptavidin coated plates (ThermoFisher, 15500), which were incubated with mouse monoclonal antibodies against BrdU (1:500) (Anti BrdU B44 BD Bioscience) in PBS-Triton 0.05% for 2 hr at 23 °C to selectively detect nascent-strand ssDNA. Plates were washed three times with PBS-Triton 0.05% and probed with HRP labelled anti mouse IgGs (Dako). After washing chemoluminescence was detected by standard ECL using a plate reader.

2.8 Chromatin binding experiment

Chromatin isolation was performed as previously described[152,153] with little modifications. Thawed *Xenopus* egg extract was supplemented with 40 μl/ml of cycloheximide, 30 mM creatine phosphate, 150 μg/ml creatine phosphokinase and sperm nuclei (4000 nuclei/μl). 30 μl of egg extract for each experimental point were incubated at 23 °C. At the indicate times reactions were stopped by diluting and mixing the extract with 300 μl EB-NP40 (50 mM Hepes pH 7.4, 100 mM KCl, 2.5 mM $MgCl_2$, 0.25% w/v NP40) and layered onto 300 μl of EB-Sucrose (50 mM Hepes pH 7.4, 100 mM KCl, 2.5 mM $MgCl_2$, 0.25% w/v NP40, 30% sucrose). Chromatin was separated from the cytoplasmic fraction by spinning the sample in a swinging bucket rotor at 10000 rpm for 5 min at 4 °C. The resulting chromatin pellet was washed once with 500 μl of EB (50 mM Hepes pH 7.4, 100 mM KCl, 2.5 mM $MgCl_2$) and spun in fixed bucket rotor centrifuge at 10000 rpm for 5 min. Finally, the pellet was resuspended in O'Farrell buffer

(50 mM Tris pH 6.8, 10% v/v Glycerol, 20 mM β-ME, 0.80% w/v SDS, 0.02% w/v BPB) and eventually analysed by western blotting.

2.9 Nuclease protection

Fluorescently-labeled DNA substrates were prepared as already described[193]. Briefly, equimolar amounts of the corresponding oligonucleotides were mixed in hybridizing buffer (50 mM Tris, 100 mM NaCl, and 10 mM $MgCl_2$), heated to 75 °C for 3 min and cooled slowly to room temperature for annealing. The substrates were then purified by HPLC using a 1 ml Mono Q column (GE Healthcare Life Sciences) and a 20 ml gradient in 10 mM Tris buffer containing 1 M NaCl. The purity was checked on native PAGE. The corresponding fractions were then concentrated on a concentrator (Vivaspin) and washed with buffer W (25 mM Tris and 3 mM $MgCl_2$). The concentrations were determined using the absorbance at 260 nm and the corresponding molar extinction coefficients. For the nuclease protection assays, DNA substrate (20 nM) was incubated with $Rad51^{WT}$, $Rad51^{T131P}$ or RPA in the P buffer (80 mM KCl, 10 mM Tris-HCl pH 7.5, 1 mM DTT, 10 mg/ml BSA, 2 mM $MnCl_2$, 2 mM $MgCl_2$ and 2 mM ATP) for 5 min at 37 °C followed by incubation with 30-50 nM recombinant yeast or human Mre11, as indicated in figure legend for 30 min at 30 °C. Reactions were deproteinized by incubation with 0.1% SDS and 500 mg/ml of proteinase K at 37 °C for 5 min, heat-denatured, analysed on 30% denaturing PAGE gels (acrylamide:bisacrylamide, 19:1) and scanned using a Fuji FLA 9000 imager. Where indicated, gels were quantified using Multi Gauge V3.2 software (Fuji). All the experiments related to nuclease protection were performed in collaboration with Prof. Lumír Krejčí and Karina Zadorozhny (Department of Biology, Masaryk University, Brno 625 00, Czech Republic).

2.10 Immunoprecipitation

Clarified extracts were obtained by diluting interphase egg extract five times with IP buffer (40 mM HEPES-KOH pH 7.5, 10% w/v sucrose, 50 mM KCl and protease inhibitor cocktail) and spun in centrifuged at 13000 rpm for 30 min. Clarified extract was incubated with 3 μg of affinity purified anti-BRCA2 or anti-Rad51 antibody or non-specific IgG one hour on ice. The samples were then mixed with 30 μl ProteinA Dynabeads (Invitrogen) and incubated for 2 hours at 4 °C in a gentle rotation mode. Then beads were washed thrice with IP buffer and twice with IP buffer containing 0.1% v/v Triton X-100. The proteins were then eluted from the beads by boiling them with 1X laemmli buffer (62.5 mM Tris pH 6.8, 2% w/v SDS, 25% v/v glycerol, 0.01% w/v bromophenol blue, 715 mM β-mercaptoethanol).

2.10.1 Immunoprecipitation in chromatin context

For each sample 5μg of antibody were incubated 1h at 4 °C with 50μL of slurry Dynabeads-proteinA in a final volume of 500 μL. Beads were washed 3 times with 500 μL PBS. Beads were stored at 4 °C in EB-EDTA-NP40 (50 mM Hepes pH 7.4, 100 mM KCl, 2.5 mM $MgCl_2$, 0.25% w/v NP40, 1 mM EDTA) supplied with protease inhibitor until extract lysate was ready for the incubation.

Extract was thawed and supplemented with 40 μl/ml of cycloheximide, 30 mM creatine phosphate, 150 μg/ml creatine phosphokinase and sperm nuclei (4000 nuclei/μl). 50 μl of egg extract were incubated at 23 °C for each experimental point, at the indicate time reactions were stopped by diluting and mixing the extract with 450μl EB-EDTA-NP40 buffer supplied with protease inhibitor. Samples were homogenized by strong agitation. Samples were then subjected 3 times to a 10' sonication step (30" ON / 40" OFF cycle and Max Power with the Bioruptor device). After the sonication step an aliquot from each sample was kept apart as input to be loaded as control. The rest of the reaction

was incubated for 1h at 4°C with Dynabeads-proteinA conjugated with the indicated antibody. After the incubation Dynabeads were first washed 3 times with 500µL of cold EB-EDTA-NP40 supplied with protease inhibitor and then 3 times with 500µL of cold EB-EDTA. Buffer was carefully removed and Dynabeads were re-suspended in 25µL of 1X O'Farrell and boiled. The entire volume was loaded on gel for SDS-PAGE and subsequent WB analysis.

2.11 Immunodepletion

2.11.1 Rad51

5 µg of affinity-purified anti-Rad51 or equal amount of nonspecific IgG were incubated with 50 µl of protein A dynabeads (ThermoFisher, 10002D) for 1 hour at RT. Unbound antibodies were removed from the beads as described above and 500 µl of extract was added to the antibody-bound beads and one round of immunodepletion was carried out for one hour. The supernatant was considered as immunodepleted extract and 1 µl of extract was immunoblotted to check the efficiency of depletion.

2.11.2 Smarcal1

5 µg of affinity-purified anti-Smarcal1were incubated with 50 µl of protein A dynabeads (ThermoFisher, 10002D) for 1 hour at RT. Dynabeads were then washed to remove the excess of unbound antibody. Subsequently, 500 µl of extract were added to antibody-bound beads and one round of depletion, lasting about 1 hr, was carried out as already described. The supernatant was considered as immunodepleted extract and 1 µl of extract was immunoblotted to check the efficiency of depletion.

In all the cases, to obtain mock-treated extract to be used as a control, a parallel depletion was carried out with the same extract and the same protocol using Dynabeads-ProteinA conjugated with affinity-purified rabbit pre-immune IgGs.

2.12 Neutral agarose gel electrophoresis

In order to assess bulk DNA replication in egg extract neutral agarose gel electrophoresis was performed to separate genomic DNA that has incorporated radioactive-labelled nucleotide[63,194]. *Xenopus* egg extract was supplemented with 40 µl/ml of cycloheximide, 30 mM creatine phosphate, 150 µg/ml creatine phosphokinase, sperm nuclei (3000 nuclei/µl) and 1:1000 α-^{32}P-dATP. For each experimental condition 20 µl of extract were incubated at 23 °C and stopped at the indicated time points by diluting the sample six times with stop buffer (8 mM EDTA, 80 mM Tris pH 8.0, 1% w/v SDS), supplemented with 1 mg/ml protease K and incubated at 37 °C for 1 hour. Samples were treated with RNase (0.6 mg/ml) to degrade any trace of RNA and purified DNA was then separated from unincorporated label by electrophoresis through a 0.8% agarose gel. The DNA was precipitated by incubating the gel in 30% TCA for 20 min, the gel was then dried and exposed for autoradiography. For quantification of DNA replication, gels were exposed to a phosphoscreen (GE Healthcare) for approximately 12 hr, or for a longer time depending on radioactive signal. The recorded radioactive signal was monitored within a phosphoImager (Typhoon) and measured with ImageJ software.

2.13 RIs purification from *Xenopus* egg extract for microscopy visualizations

Genomic DNA isolation and purification was performed as described by Sannino et al.[153] and Lopes[183], with minor modifications. For each experimental point 200 µl of thawed *Xenopus* egg extract were supplemented with 40 µl/ml of cycloheximide, 30 mM creatine phosphate, 150 µg/ml creatine phosphokinase and sperm nuclei (4000 nuclei/µl) and incubated at 23 °C for the indicated time. As internal control, we assessed the incorporation of a fluorescent-labelled nucleotide, Cy3-dCTP, in a separate aliquot of

extract; chromatin decondensation, nuclear assembly and strong Cy3-dCTP incorporation suggest that DNA replication is ongoing. The DNA replication reaction was stopped by three-time dilution of the sample using EB-EDTA (50 mM Hepes pH 7.4, 100 mM KCl, 2.5 mM $MgCl_2$, 1mM EDTA), gentle mixed using a cut p200 tip and layered onto 1200 µl of EB-Sucrose-EDTA (50 mM Hepes pH 7.4, 100 mM KCl, 2.5 mM $MgCl_2$, 1mM EDTA, 30% w/v sucrose). Nuclei were separated from the cytoplasmic fraction by spinning the sample in swinging bucket rotor at 10000 rpm for 5 min at 4 °C. The supernatant was gently removed without disturbing the pellet, and nuclei were resuspended in 100 µl EB-EDTA. To ensure a clear visualization at the microscope, DNA was cross-linked by four cycles of 5 min incubation with 10 µg/ml TMP (4,5',8-trimetilpsoralen) followed by 7 min of irradiation with 366 nm UV light (Stratalinker UV2400). Samples were further diluted to a final volume of 400 µl and supplemented with 250 µg/ml RNase and 0.1% w/v SDS. Samples were then incubated at 37 °C for 1 hour, after which they were supplemented with 130 mg/ml protease K and incubated for 2 hours at 50 °C. Samples were then vigorously mixed with 1 volume of Chloroform:Isoamyl alcohol 24:1 then spun at 13200 rpm for 10 min at 4 °C. The supernatant was carefully recovered and mixed with 1 volume of isopropanol and 1:10 sodium acetic acid. By spinning the samples at 13200 rpm for 5 min at 4 °C DNA pellet was eventually formed, and then it was washed with 500 µl of 70% v/v ethanol. The final DNA pellet was resuspended in 100 µl TE (10 mM Tris pH 8.0, 1 mM EDTA), quantified by NanoDrop and digested 3.5 hours at 37 °C, using 20 U of NdeI each microgram of DNA. After the digestion step the DNA was further purified through the Qiagen Genomic-tip 20/G. Qiagen tips were equilibrated by applying 1 ml Buffer QBT (750 mM NaCl, 50 mM MOPS pH 7.0, 15% v/v isopropanol, 0.15% v/v Triton X-100) and allowing the column to empty by gravity flow; the column was then washed three times with 1 ml 10mM tris pH 8.0, 1 M NaCl, and thrice with 1 ml 10mM tris pH 8.0, 300 mM NaCl.

Samples were then loaded onto the column, and each column was the washed twice with 1 ml 10mM tris pH 8.0, 0.5 M NaCl. The DNA was eventually eluted twice with 1 ml 10mM tris pH 8.0, 1 M NaCl, 1.8% w/v caffeine. Sample were then moved to Amicon Ultra-0.5 mL 100K devices and washed with 400 µl TE and finally concentrated to a final volume of 30 µl. The quality of the final samples was checked using agarose gel electrophoresis.

2.13.1 EM sample preparation and imaging analysis

Preparation of genomic DNA samples for EM analysis was carried out as previously described[153,183,195]. Carbon-coated EM grids were produced by deposition of 4 nm of vaporised carbon onto 4 cm^2 freshly cleaved mica sheet using a MED 020 apparatus (Leica). Carbon layer was then transfer on EM-grade water surface and deposited onto EM copper grids pre-activated with scotch solution (25 cm of Scotch tape, 100 ml chloroform). In order to obtain a better resolution and more precise image analysis, the RIs samples were spread using the Native BAC-spreading method. Briefly, according with sample concentration, from 0.5 to 5 µl of genomic DNA solution were mixed with 1 µl formamide, 0.4 µl BAC 1:10 in TE, 0.2 µl glyoxal, and TE in order to reach 10 µl final volume. The BAC-containing mix was slid down on a freshly cleaved mica ramp on in a water bath and, fished using pre-activated carbon-coated EM grids. Carbon-coated grids were activated by 30 min incubation in Ethidium bromide solution (33.33 µg/ml in water). Carbon grids were then stained by 15 sec incubation in uranyl acetate solution (0.5 mM, 0.5 HCl, 90% v/v ethanol), and subsequently rinsed three times in pure ethanol. The EM grids were let dry and subjected to platinum/carbon (Pl/C) shadowing, both to made them suitable for EM visualization and to improve DNA/back ground contrast. Images were obtained and analysed by Digital Micrograph and FIJI.

2.13.2 AFM sample preparation and imaging analysis

A 1 cm radius mica disc was attached on a microscope slide with glue and a fresh mica layer was stripped off with scotch tape before each experiment to get a flat and clean surface suitable for DNA samples absorption. 0.5 to 1 ng/µl of DNA was spotted on freshly cleaved mica in an appropriate adsorption buffer (10 mM Hepes, 1 mM $ZnCl_2$, 0.2% w/v SDS) and incubated for 5 min at RT. The sample was washed 3 times with 500 µl of milli-Q water and dried first with tissue paper, without touching the mica, and then by nitrogen air flow.

To stain biotinylated DNA with streptavidin 20 µl of 10 mM Hepes, 1 mM $ZnCl_2$ and increasing concentration of streptavidin (from 2.5 to 250 nM) were drooped onto the mica, were the DNA sample was previously attached. The slides were then washed 3 times with 500 µl of milli-Q water and then dried as described above.

Tapping AFM was performed in dry conditions using a JPK NanoWizard® 3 AFM. To limit the environmental vibration, we used an active vibration isolation system (Accurion i4 series JPK base); moreover, we used also an acoustic enclosure to limit the vibration coming from the environment noise. Images were saved in topography data and phase shift data. The AFM probe used in all the measurements was a silica AFM probe designed for both non-contact or tapping mode (ACTA from AppNano, reflect side coated in aluminium).

Images were analysed either by JPK DP Data Processing Software version 4.2.62 or ImageJ 1.47.

3 Results

3.1 Visualization of DNA replication intermediates by AFM

In this thesis we tried to identify and to characterize the RIs structures arising upon replication stress, resulting from DNA polymerase inhibition, in order to better understand the contribution of fork protection proteins Rad51 and Smarcal1 and their regulation by the ATR dependent checkpoint.

To this end, we set up a number of EM- and AFM-based protocols to uncover the nanometric features of different DNA RIs isolated under unchallenged and stressful conditions. While EM does not allow an easy visualization proteins bounded onto long DNA molecules, AFM imaging technique can be used to study DNA-protein interactions. We adapted the EM protocol, already established in our lab[153], to isolate RIs from genomic DNA replicated in *Xenopus* egg extract and to visualize them by AFM. Briefly, sperm nuclei were incubated in *Xenopus* egg extract, genomic DNA was crosslinked by TMP to stabilize RIs and to avoid DNA branch migration. The genomic DNA was then purified and subsequently digested with a restriction enzyme (NdeI). Ongoing replication forks generate peculiar Y-shaped structures consisting of one parental DNA arm and two daughter arms of equal length (***Figure 3.1*** and ***Figure 3.2***). DNA replication intermediates were finally concentrated on size-exclusion columns (See section 2.13).

EM visualization confirmed the good quality of our RIs purification (***Figure 3.1***). Thereafter, RIs were adsorbed on fresh cleaved mica stage for AFM visualization (See section 2.13.2). Canonical RIs were observed with two arms of identical length (nascent DNA) and a tail behind them (parental DNA), confirming the ability of AFM, as of EM, to enable the visualization of the typical Y-shape structure of RIs.

In both the cases, RIs structure recognition by EM and AFM is based on morphological analysis of the peculiar 'Y' shape that replicating molecules display after the digestion step, in which at least two of the three DNA branches are of equal length.

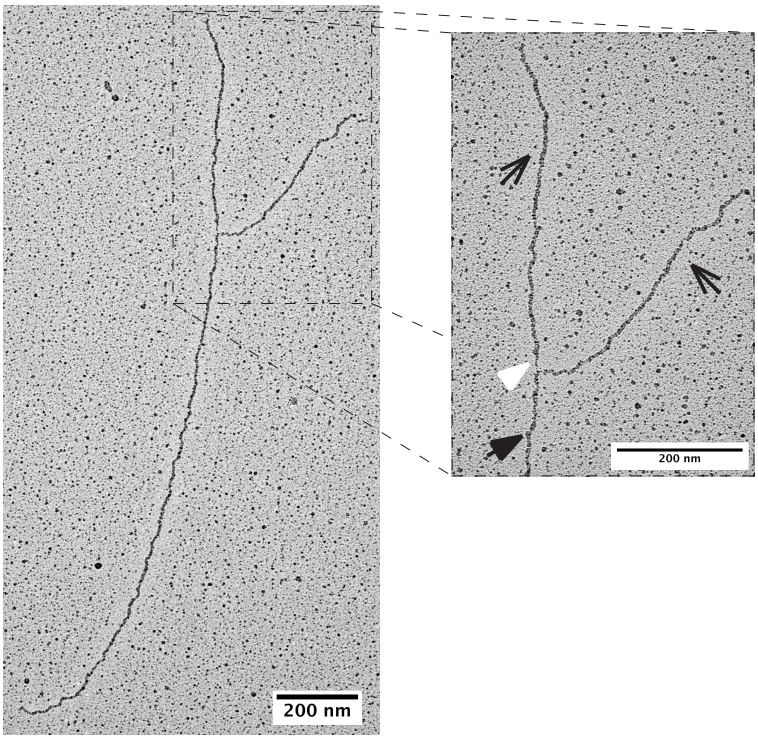

Figure 3.1 EM allows ssDNA visualization

EM micrograph showing an example of RIs, it is evident from the peculiar 'Y' shape molecule. Empty black arrowheads point towards the DNA daughter strands which are of similar length (to be considered as equals, if the length differences do not exceed the 10%), full black arrow points to the parental DNA stand. The white arrow points the ssDNA gap which is generally present at the replication fork junction.

EM mediated RIs visualization also allows the identification of other peculiar RIs features. At higher magnifications, ssDNA region is usually detectable at one or two sides of the fork junction, facilitating the identification of the daughter strands (***Figure 3.1***). AFM-mediated analysis instead does not allow clear visualization of the thin ssDNA usually present at the fork junction. The visualization of DNA molecules by AFM is done in semi-dry conditions, so the mica surface is always subjected to the environmental humidity. In such conditions, ssDNA gaps tend to form small secondary structures that can be confused with the dsDNA.

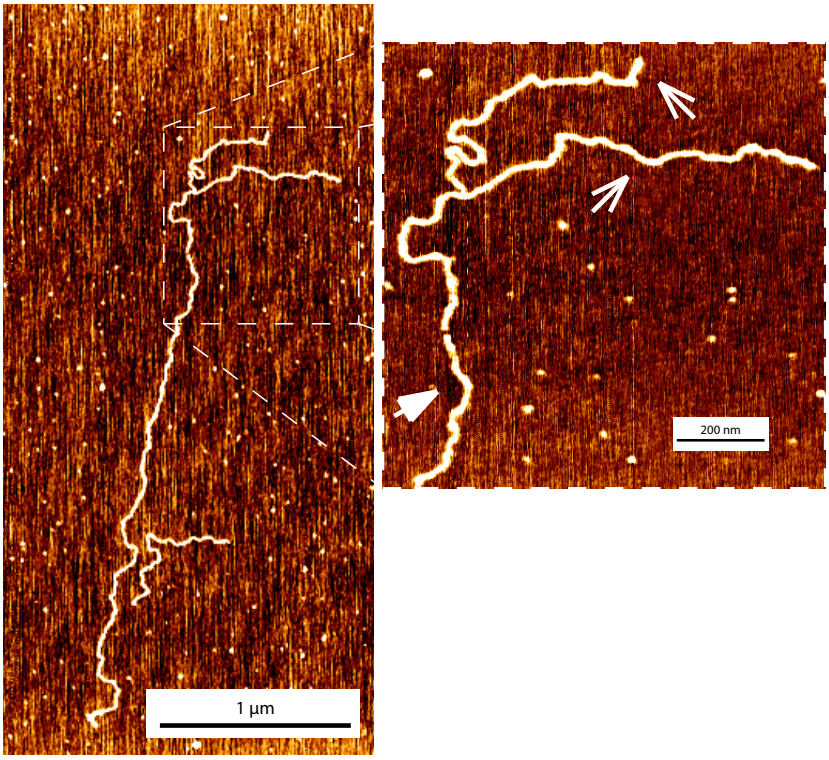

Figure 3.2 AFM is suitable for RIs visualization

AFM scan showing an example of RIs, it is evident from the peculiar 'Y' shape of the molecule. Empty white arrowheads point toward DNA daughter strands which have similar length (to be considered as equals, if the length differences do not exceed 10%), full white arrow points to the parental DNA stand.

In order to overcome the AFM inability to visualize ssDNA strands, we tried to implement the recognition of the newly synthetized DNA strands by incorporation of modified nucleotides.

3.1.1 Recognition of newly synthetized DNA strands by biotin-dUTP incorporation

During DNA replication, the unwinding of parental DNA allows polymerases to synthesize the nascent strands by deoxyribonucleotides incorporation. In order to visualize nascent DNA, we designed an experiment in which biotin-labelled nucleotides get incorporated during DNA synthesis. Biotin incorporation into newly-synthetized DNA can be detected by visualizing streptavidin molecules bound to biotin[196,197].

In order to setup this methodology in a controlled way, we generated different samples by performing PCR reactions using pBluescript plasmid as a template and increasing amounts of biotin-dUTP were added to the reaction mix. In particular, three different concentration of biotin-dUTP were used, i.e. 50%, 25% and 12.5%, in order to obtain different amounts of biotin-dUTP incorporated in newly synthetized DNA[198-200]. Here after, L (as linear), 50-B, 25-B and 12.5-B refer to the PCR products synthetized with no biotin 50%, 25%, and 12.5% of biotin-dUTP, respectively. PCR reactions were analysed by agarose gel electrophoresis. Increasing percentage of biotin-dUTP into the reaction mix led to a progressive decrease in DNA mobility; hence it showed progressive increase in molecular weight as a consequence of biotin-dUTP incorporation (***Figure 3.3***).

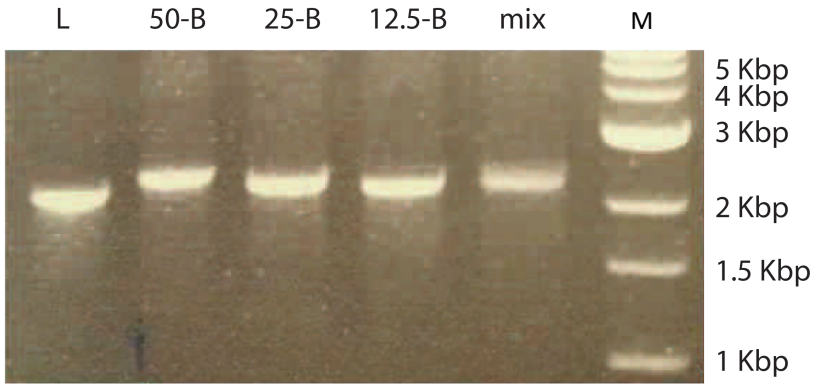

Figure 3.3 Agarose gel analysis of the Biotin-dUTP PCR products

1% agarose gel was used for the qualitative visualization of the PCR reactions products. L is the molecule amplified without biotin-dUTP, 50-B was amplified with 50% of biotin-dUTP vs dTTP, 25-B with 25% of biotin-dUTP and 12.5-B with 12,5% of biotin-dUTP. Sample mix is a mix of products coming from the first three reactions. M indicates the ladder.

The four different DNA samples described above were adsorbed on freshly cleaved mica sheet, incubated with streptavidin and then visualized by AFM (***Figure 3.4A***).

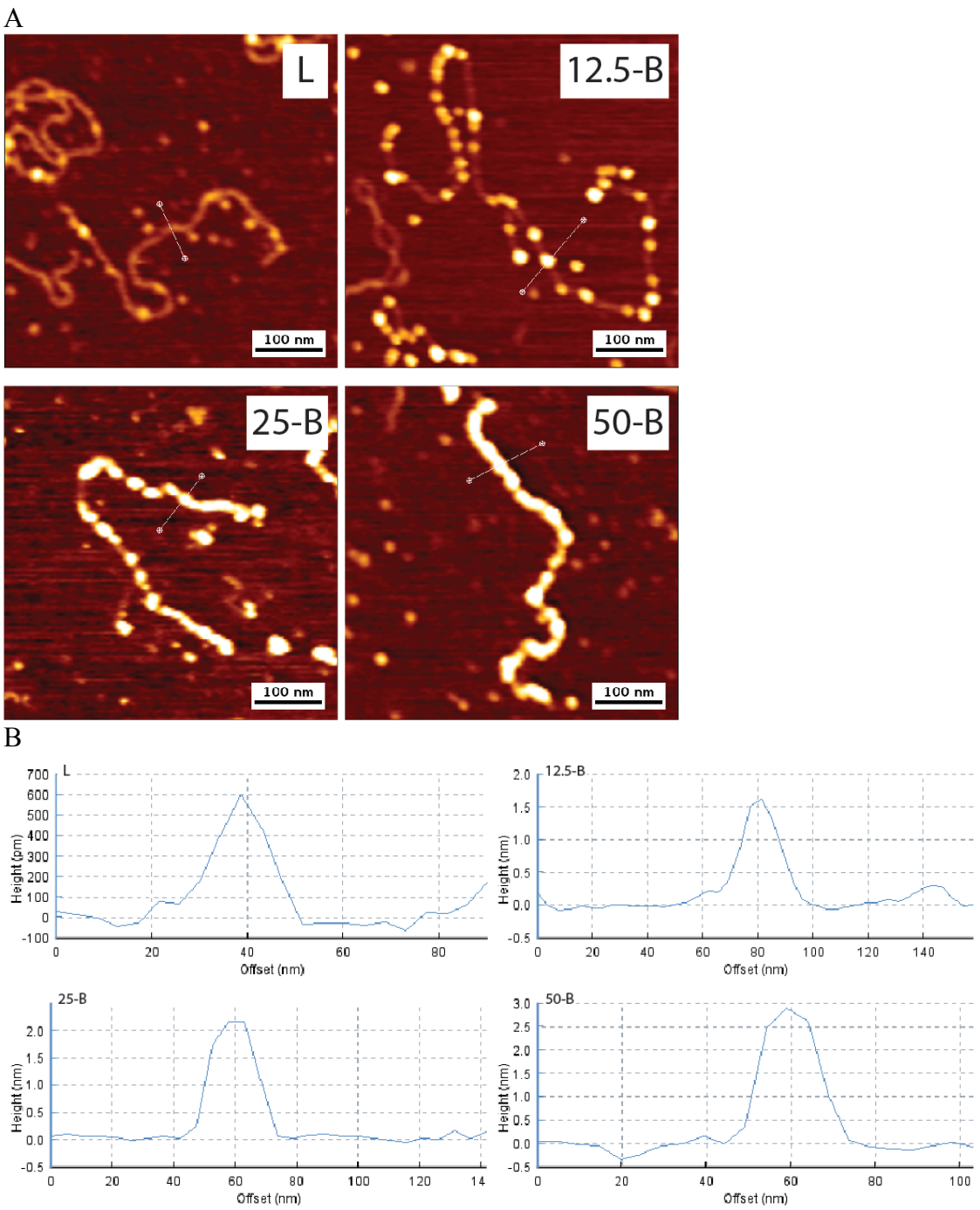

Figure 3.4 Streptavidin staining is suitable for newly synthetized DNA recognition

Different biotin content in DNA molecules lead to different patterns of streptavidin staining (A). These differences are also evident in cross-section graphs (B). The white line crossing each molecule indicates the line used to visualize the height (nm) the cross-section of the DNA-protein complex. (A) and (B) L is the molecule amplified without biotin-dUTP, 50-B was amplified with 50% of biotin-dUTP vs dTTP, 25-B with 25% of biotin-dUTP and 12.5-B with 12,5% of biotin-dUTP

The molecule height values of the biotinylated-DNA samples treated with streptavidin detected by AFM were incremented, when compared with the control, in a biotin content-

dependent manner as it is also shown by the cross-section profiles of the molecules (***Figure 3.4B***). The height data in the streptavidin covered molecules are the direct sum of the DNA and streptavidin molecules. Similarly, also the thickness of the complexes was increased according to the amount of streptavidin bound to DNA. Thus, we measured the average volume of single streptavidin-DNA complexes. The volume data demonstrated a statistically significant linear correlation between volumetric hindrance of the streptavidin-DNA complex and the biotin content into DNA molecules (***Figure 3.5***).

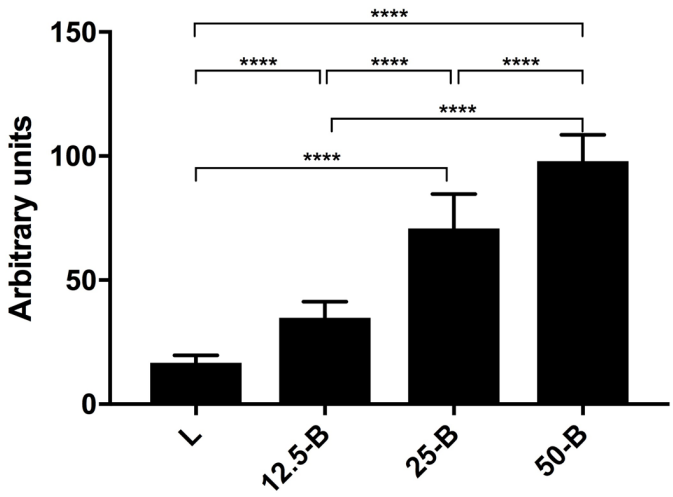

Figure 3.5 AFM discriminates different DNA biotin-dUTP contents by streptavidin staining

Graph of grey mean value in function of biotin incorporation. Mean values ± SD of three independent experiments (n=3). More than 100 complexes were measured for each sample, **** $p<0.0001$ obtained by multiple comparison Kruskal/Wallis test. Linear regression calculated equation $Y = 1.671*X + 18.5$, $R^2 = 96.16\%$.

Taken together, our experiments reveal that we can visualize the biotin-dUTP incorporated into the DNA produced by PCR reaction. Thus, the visualisation of streptavidin bound to the biotin-incorporated into DNA potentially represents a new methodology to detect newly-synthesized DNA at the level of RIs by AFM. To test this hypothesis, we performed an experiment in which the *Xenopus* egg extract was

supplemented with 40 μM of biotin-dUTP, which is similar to the endogenous dTTP concentration[152]. Because of its steric hindrance, the biotin-linker modification of the nucleotide used in our assay could potentially exert an inhibitory effect on DNA polymerases activity[198]. Thus, DNA replication efficiency of the *X. laevis* egg extracts supplemented with biotin-dUTP was monitored by replication assay using two different DNA templates as explained below. Nuclear membrane formation is essential for sperm DNA replication, however nuclear membrane could affect biotin-dUTP intake. Hence, to assess directly the DNA polymerase inhibitor effect of biotin-dUTP we used the M13 ssDNA template. M13 is a circular ssDNA template which does not required nuclear assembly to be replicated in the *Xenopus* egg extract. Both DNA replication assays confirmed that the biotin-dUTP concentration we used did not affect DNA replication reaction in *Xenopus* eggs extracts (***Figure 3.6***).

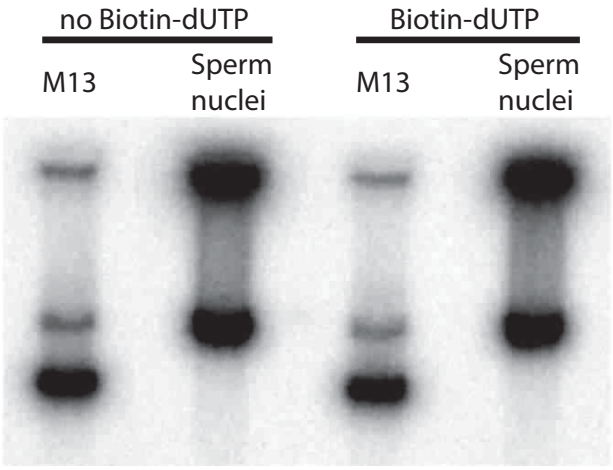

Figure 3.6 Biotin-dUTP does not inhibit DNA replication in *Xenopus* egg extract

Agarose gel autoradiography showing replicated M13 or sperm nuclei replicated in *Xenopus* egg extracts supplemented with (lane 3 and 4) or without 40 μM of biotin-dUTP (lane 1 and 2).

To confirm that *X. laevis* DNA polymerases were able to incorporate the modified nucleotide into genomic DNA, we performed a dot-blot analysis to assess the actual biotin content of our samples (***Figure 3.7***). Streptavidin-HRP conjugated protein were used as probe to detect the presence of biotin in our samples. Specific signals were detected onto

the spots corresponding to the DNA that had been replicated in the presence of 40 µM of biotin-dUTP and input biotin-dUTP controls.

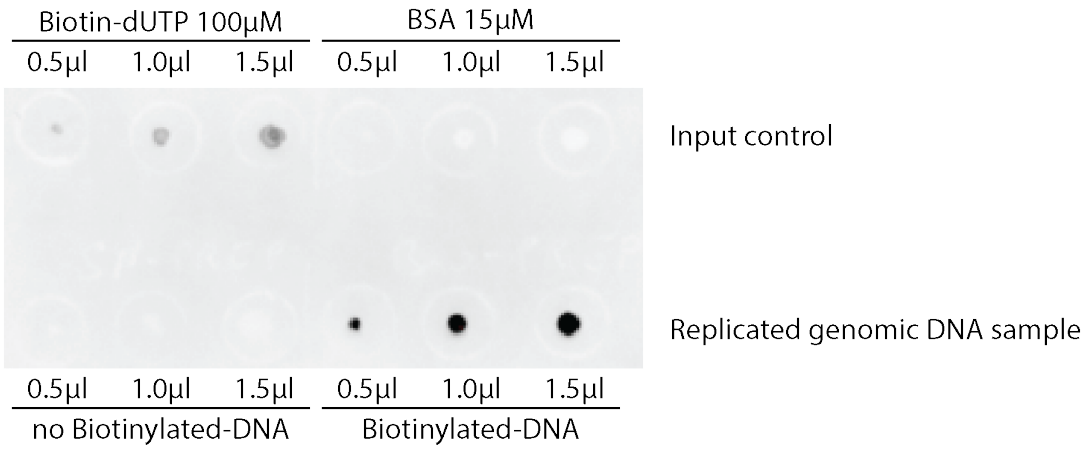

Figure 3.7 Biotin-dUTP incorporation in *Xenopus* genomic DNA

Dot-blot showing the actual biotin dUTP incorporation in *Xenopus* sperm replicated DNA. Specific signals correspond to biotin-dUTP and biotinylated-DNA drops.

Then, we proceeded to visualize RIs obtained from sperm DNA replicated in *X. laevis* egg extract in the presence of biotin-dUTP. To further confirm that the structures observed were genuine RIs, we aimed to discriminate the nascent DNA strands from the parental DNA. As previously described, the biotin-dUTP incorporation at the level of RIs was visualized using the streptavidin detection method. After streptavidin labelling, most of the DNA molecules were found folded together and aggregated, making it difficult to identify the DNA strands and interpret the shape of the structures observed (***Figure 3.8***). A possible interpretation of this result is that the biotinylated-DNA molecule could be bridged by streptavidin molecules, creating aggregates and net-like structures. Indeed, each single streptavidin can bind four biotin molecules, bringing in a close contact two or more biotin motif that were initially distant.

Nonetheless, some rare molecules were clearly showing the peculiar RIs structure (***Figure 3.9***). Altogether these results suggest that by detecting streptavidin bound to biotinylated-DNA products we could formally discriminate between parental strand and

nascent strands. However, formation of large complexes of DNA molecules linked together by streptavidin bridges did not allow clear discrimination of single DNA molecules[196]. Although our results are promising, we need to further improve our experimental conditions to reach an optimal situation in which newly-synthesized DNA can be stained without altering the structure of RIs.

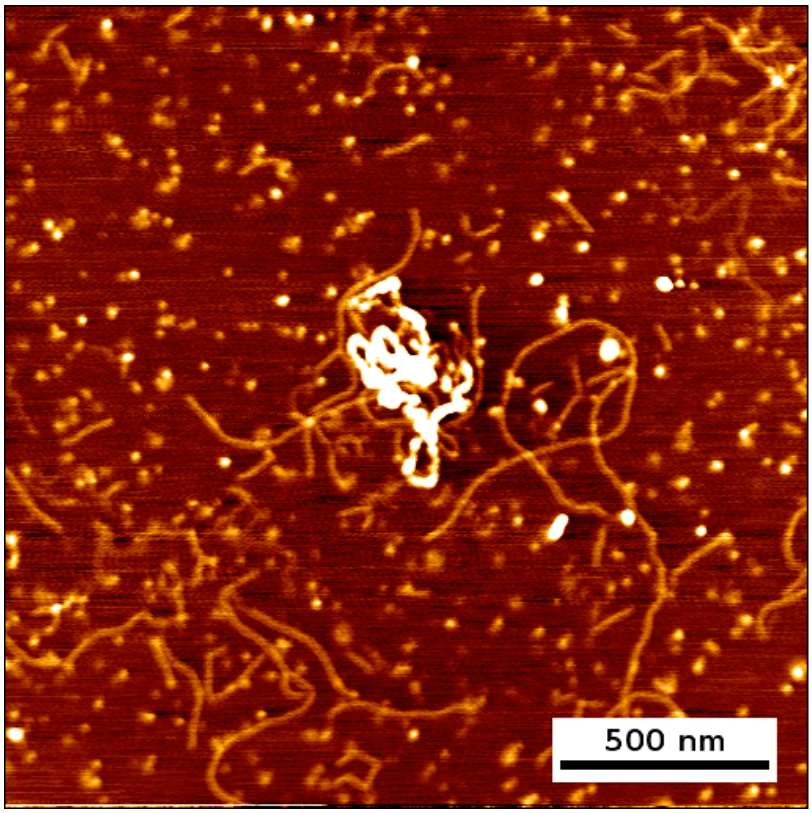

Figure 3.8 Streptavidin staining causes biotinylated-DNA fibres cross-links

AFM scan showing an example of biotinylated-RI stained with streptavidin. Scale bars indicates the colour code associated to the height data of the picture.

Altogether the results here described here are provide a proof-of-principle that the methodology could be applied to monitor nascent DNA, but further investigations are required to establish a robust protocol. Streptavidin-mediated aggregation could be potentially solved by using monomeric streptavidin or monovalent streptavidin, which binds one molecule of biotin at time, thus avoiding inter- and intra-strand bridges[201]. In addition, reducing biotin-dUTP concentration in the *Xenopus* egg extract would favour a

better visualization of the DNA strands which in our hands had the tendency to be completely covered by streptavidin in our current experimental settings.

Applying these adjustments, it would be possible to design experiments aiming to investigate, *ex vivo,* the DNA polymerases activity. In this context, it would be possible to use this new methodology to measure the level of replication by quantifying the level of biotin incorporated in the nascent DNA strands.

A

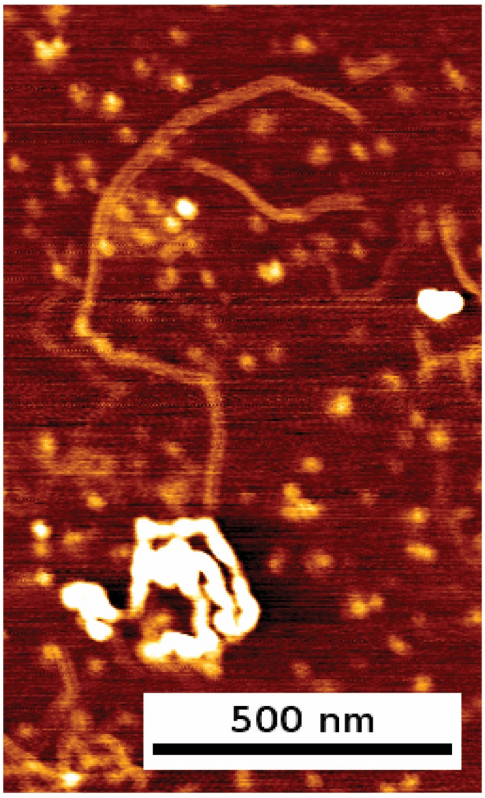

B

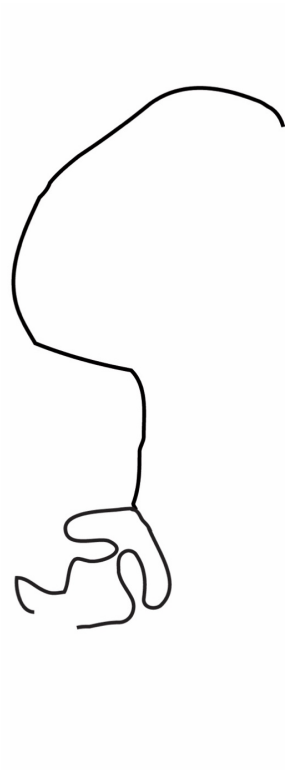

Figure 3.9 Streptavidin specific daughter DNA staining in RI structure

AFM scan showing an example of biotinylated-RI stained with streptavidin, it is evident the peculiar 'Y' shape of the molecule(A) and a schematic representation of the DNA molecule structure(B). Scale bars indicates the colour code associated to the height data of the picture.

3.2 Visualization of DNA replication intermediates by EM

3.2.1 Analysis of ssDNA gaps at the level of the fork structures in the context of DNA replication stalling

As mentioned before, AFM imaging is not suitable to visualize ssDNA gaps. These ssDNA gaps are normally present in physiological RIs structures and their size and number correlate with perturbation of the replication fork progression and its stability[18]. Our group and others, have shown that EM can easily detect ssDNA at the level of replication forks[57,118]. Thus, we exploited the EM ability to visualize and to discriminate between ssDNA and dsDNA to address the consequence of replication stress on the fork structure.

As for many other microscopy techniques, the sample preparation represents a critical step to prevent artifacts to bias our analysis. We especially aim at not introducing false-positive or false-negative molecules in which the DNA thickness would not accurately tell the portion of DNA that is single- or double-stranded. For these reasons one of the most important step of EM sample preparation is the DNA TMP cross-linking procedure. In the *Xenopus* egg extract system, this step is rapidly carried out right after intact replicating nuclei are isolated from the extract. Rapid DNA TMP cross-link is essential to prevent DNA branch migration[153], thereby preserving the DNA structures present at a given time into the nuclei. Moreover, TMP cross-link avoids possible DNA melting that might happen during the subsequent phases of the EM sample preparation.

The accumulation of ssDNA gaps is one of the main consequences of DNA replication fork stalling[45], hence EM represents a powerful tool to study the structural aberrations arising in perturbed DNA replication conditions (***Figure 3.12***). In order to study the effect of replication fork stalling on RIs structures, we set up a system in which genomic DNA replication in *Xenopus* egg extract is challenged using DNA polymerase inhibitors. To better characterize the replication stress response induced by DNA polymerase inhibition

we used two compounds: (1) aphidicolin (APH), a specific inhibitor of the B-family of DNA polymerases[202,203] and, (2) a specific inhibitor of DNA Polymerase α activity, that hereafter we will refer to as MSi1 which was obtained from Luis Toledo (Center for Chromosome Stability, Institute for Cellular and Molecular Medicine, Faculty of Health and Medical Sciences, University of Copenhagen, Copenhagen, Denmark).

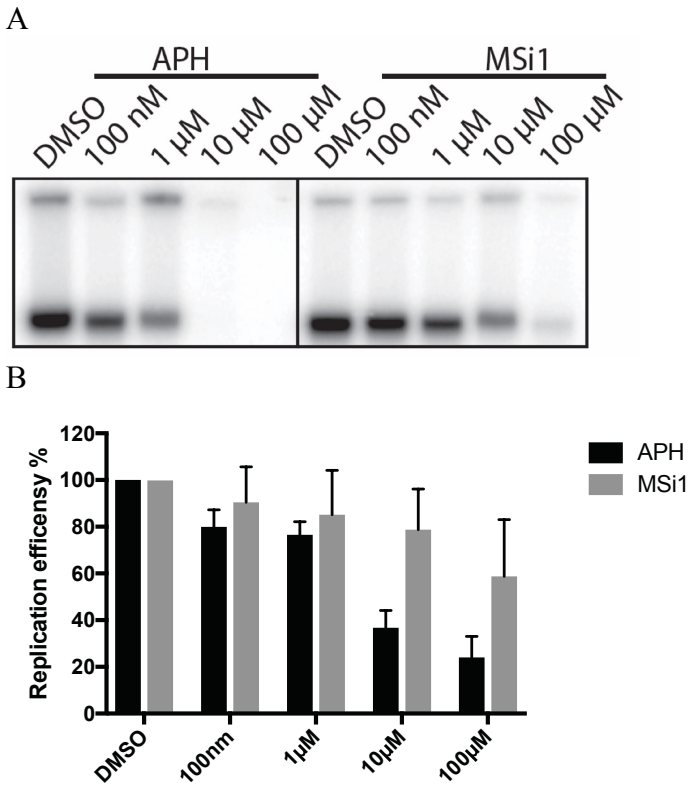

Figure 3.10 DNA polymerase inhibitors effect on bulk DNA replication

DNA Replication assay. Agarose gel autoradiography of total genomic DNA replicated in *Xenopus* extracts supplemented with α-P^{32}-dCPT (A). DMSO or increasing APH or MSi1 concentration were added at time 0 together with demembranated sperm nuclei. In order to evaluate the total amount of DNA replication, samples were stopped after 2 hours after the beginning of the reaction. (B) Relative fold change quantification of three independent experiments. DMSO treated sample is our control (set as 100% of replication efficiency). Error bars represent the SD.

Xenopus laevis egg extracts were supplemented with increasing drugs concentrations at the beginning of DNA replication reaction and DNA replication efficiency was evaluated after 2 hours measuring the overall incorporation of the radiolabelled

nucleotide P^{32}-α-dCTP. In the presence of APH, the total amount of radiolabelled-dCTP decreased in a dose-dependent manner, and DNA synthesis was almost completely inhibited already at 10 μM APH (***Figure 3.10***). MSi1 showed a milder effect on DNA replication compared to APH at equal concentrations (***Figure 3.10***). This result was probably due to the fact that MSi1 specifically inhibits Polα while APH can inhibit all the members of B-family, although to a different extent[204].

Next, we investigated the consequences of these two inhibitors on the recruitment of replication factors to chromatin. The two inhibitors differed in their ability to perturb chromatin binding of replication related proteins: APH caused an accumulation of Polα and Polδ in a dose-dependent manner; while MSi1-treated samples showed an increase in Polα signal and a decrease in Polδ chromatin bound fraction, when compared to the control lane (***Figure 3.11***). Both APH and MSi1 induced accumulation of ATR and Rad51 to chromatin which is consistent with their reported role in the S phase checkpoint and DDR pathway[60].

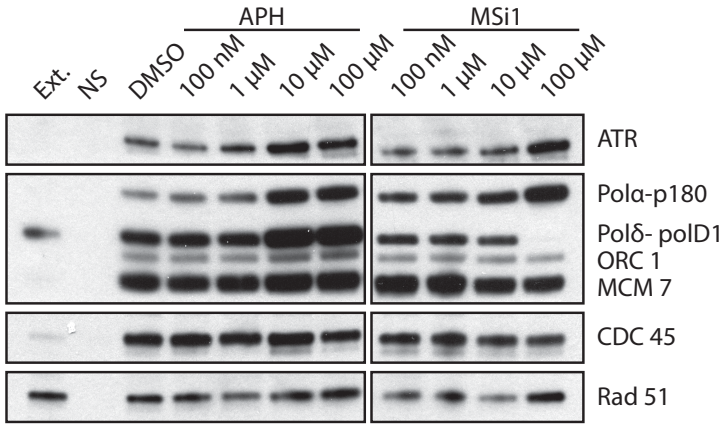

Figure 3.11 DNA polymerases inhibition causes Polα chromatin binding accumulation

Chromatin binding experiment showing the effect of DNA polymerase inhibitors at different concentrations. Drugs were added at time 0 into the egg extract, DNA replication reaction were stopped at 60 min. Ext, extract input. NS, no sperm DNA that provide a control of chromatin fraction. ORC1 was used as loading control of the chromatin fraction.

DNA synthesis inhibition can occur through different modalities depending on the concentration of APH; at relatively low concentrations, APH inhibits new origin firing through a checkpoint-dependent mechanism; while at higher concentrations the direct inhibition of DNA elongation process is predominant[202]. In unchallenged conditions, DNA replication starts approximately 30 min after the addition of sperm DNA to egg extract; during this time sperm chromatin decondenses, nuclei are formed and the DNA replication origins are assembled and fired[153]. Therefore, in order to limit the APH effect on DNA replication initiation and, aiming at impacting mainly on the subsequent elongation phase, we added increasing doses of APH 60 min after the addition of sperm nuclei to the extract. RIs isolated at this time point from the unchallenged *Xenopus* egg extract showed a single short ssDNA gap at the fork junction (***Figure 3.1***).

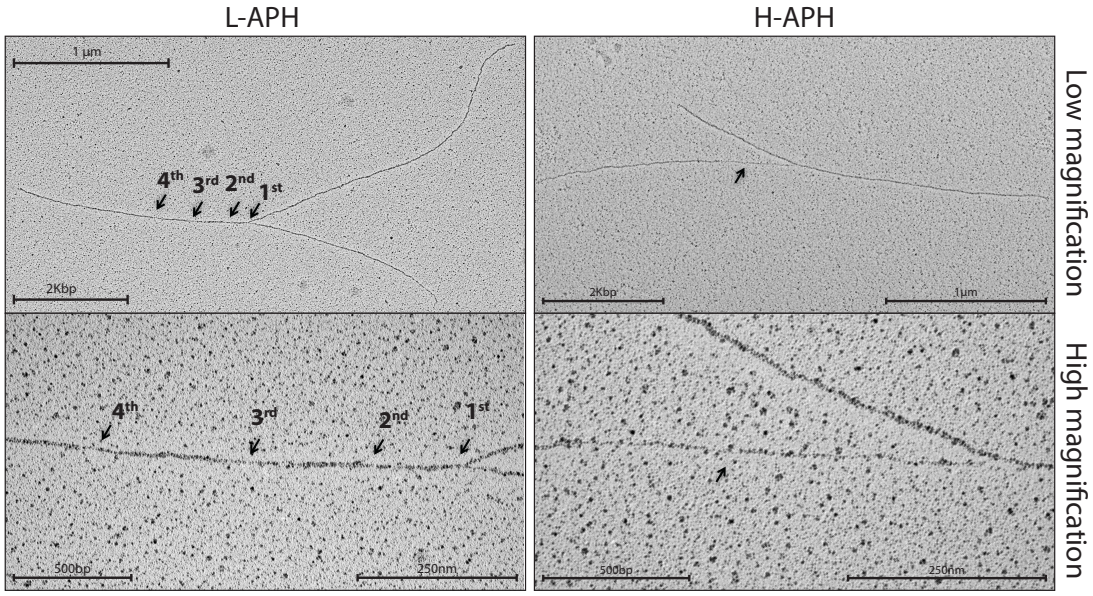

Figure 3.12 ssDNA gaps structure arising in different DNA replication stalling conditions

EM micrographs showing an example of RIs, isolated from extract treated for 1 hour with indicated APH concentration. Black arrowheads point towards ssDNA gaps generated in DNA replication stalling conditions. Ordinal numbers indicate gaps position according to their proximity to the fork junction, i.e. 1st indicates the gap at the fork junction, 2nd indicates the gap behind the 1st and so on.

The ssDNA gap length was around 100 nt (40 nm) on average and usually did not exceed 200 nt (80 nm). On the contrary, RIs isolated from extracts treated with APH accumulated ssDNA close to the fork junction (***Figure 3.13***), the ssDNA gaps visualized were either long stretch of ssDNA at the fork junction or multiple small gaps in proximity of the three-way branch junction depending on the concentration of APH added to the extract (***Figure 3.12***). In particular, long ssDNA stretches were accumulated predominantly when high doses of APH were used (1.5 mM, H-APH), while in the egg extract supplemented with 20 μM of APH (L-APH), RIs harboured multiple short ssDNA gaps. Intriguingly, the ssDNA gaps generated in L-APH condition were similar in length among each other (***Figure 3.14***).

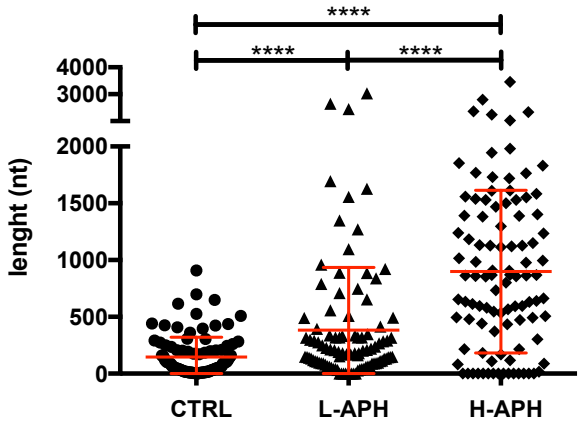

Figure 3.13 APH fork stalling causes ssDNA gaps accumulation at the fork

Graph showing the length of ssDNA gap at the fork junction. RIs were isolated from egg extract treated as indicated: CTR, control extract (DMSO), L-APH or H-APH. Bars indicate the mean ± SD relative to 100 RIs counted in two independent experiments. **** p<0.0001 obtained by multiple comparison Kruskal/Wallis test.

To better understand the involvement of Polα in the generation of these ssDNA gaps we also investigated the effect of specific Polα inhibitor MSi1 on DNA replication fork structures. Addition of 100 μM MSi1 at the beginning of the replication reaction into the extract is sufficient to reduce the replication efficiency of 50% (***Figure 3.10***). In order to

prevent a possible reduction in terms of RIs structure present at a certain given time and to perform experiment in the same conditions used for APH treatments, we added the inhibitor 60 minutes after sperm addition and analysed the structures of the resulting RIs structures 15 or 60 minutes after the drug addition, respectively. Given the strong inhibitory effect on Polδ chromatin binding levels (***Figure 3.11***), a low 10 μM and a high 100 μM concentration were tested. EM experiments revealed that MSi1, like others replication fork stalling agents, causes ssDNA gaps accumulation at the fork junction in a time- and dose-dependent manner (***Figure 3.16***).

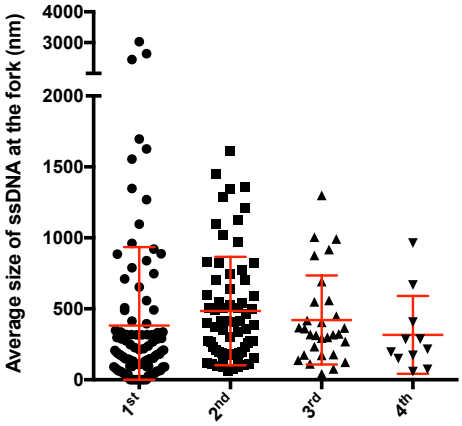

Figure 3.14 ssDNA gaps within the same RIs DNA structure are similar in length

Graph showing the length of ssDNA gap at and behind the fork junction. RIs were isolated from egg extract treated with L-APH condition. Bars indicate the mean ± SD of 100 RIs counted in two independent experiments. Ordinal numbers indicate gap position according to their proximity to the fork junction, i.e. 1st indicates the gap at the fork junction, 2nd indicates the gap next to the 1st and so on.

Remarkably, MSi1, even at 100 μM concentration, did not induce accumulation of long ssDNA stretches but, similarly to L-APH condition, favoured the formation of several small ssDNA gaps at fork junctions. As observed upon APH-treatment, in MSi1 treated extract ssDNA gaps were present only on one of the two daughter strands and never on both (***Figure 3.17***).

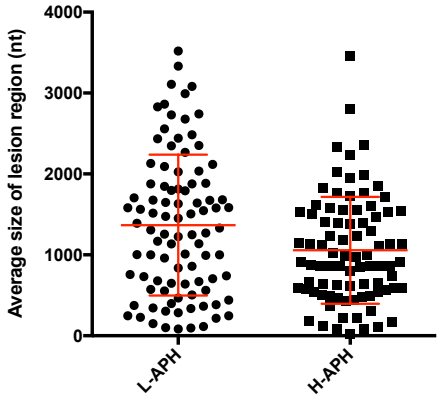

Figure 3.15 DNA lesion regions is usually 1.5 knt in lenght

Graph showing the length of the lesioned region (harbouring a single long or multiple short ssDNA gaps) close to the fork junction. RIs were isolated from extract treated as indicated: L-APH or H-APH. Bars indicate the mean ± SD of 100 RIs counted in two independent experiments.

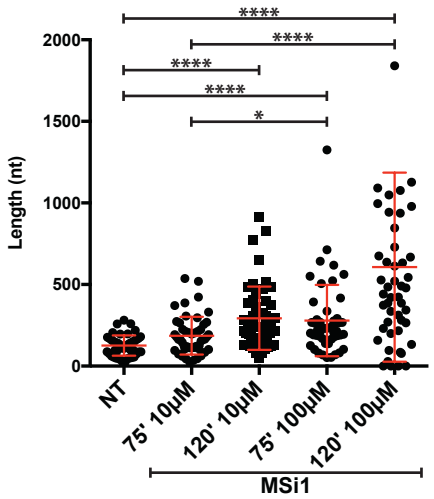

Figure 3.16 Polα inhibition causes ssDNA gaps accumulation at the fork.

Graph showing the length of ssDNA gap at the fork junction. RIs were isolated from extract treated with MSi1 as indicated, NT (not treated extract). Bars indicate the mean ± SD relative to 50 RIs counted in two independent experiments. The p value was obtained by multiple comparison Kruskal/Wallis test, * $p<0.05$ and **** $p<0.0001$.

As the case of L-APH, also MSi1-induced ssDNA gaps had a similar length, independently of their position with respect to the fork junction (***Figure 3.18***). In particular, when the samples were treated with 10 μM MSi1 for either 15 or 60 minutes,

the average size of these lesions was about 200 – 300 nt. Thus, ssDNA gap size increased in a dose- and time-dependent manner (***Figure 3.18***).

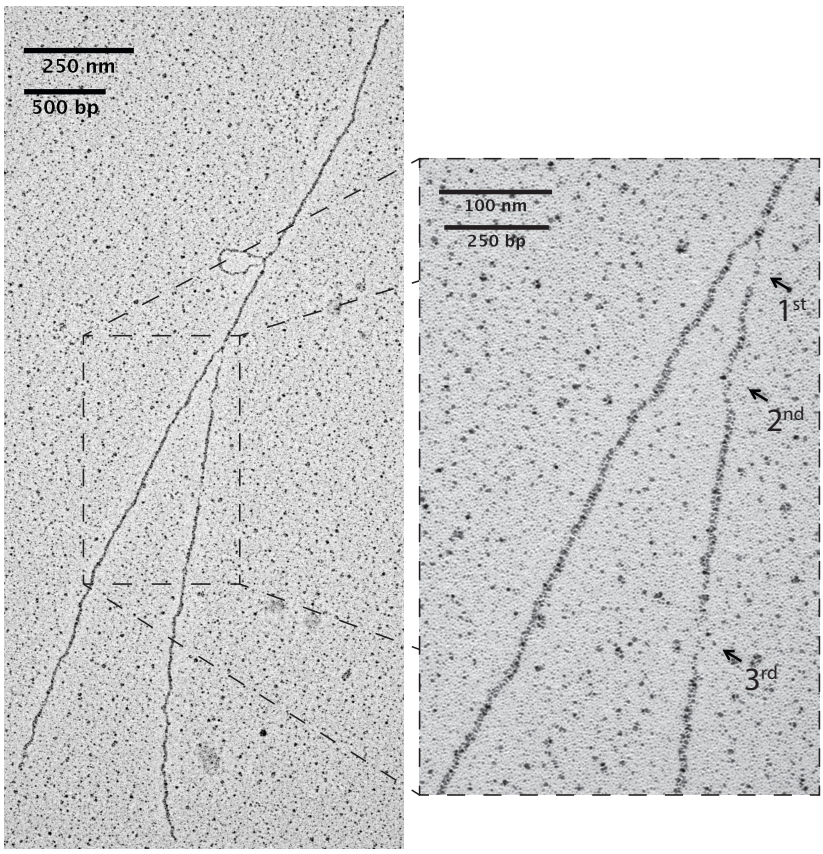

Figure 3.17 MSi1 induces multiple ssDNA gaps accumulation.

EM micrographs showing an example of RI, isolated from extract treated for 15 minutes with 100 μM MSi1. Black arrowheads point ssDNA gaps generated in DNA replication stalling conditions. Ordinal numbers indicate gap positions according to their proximity with the fork junction, i.e. 1st indicates the gap at the fork junction, 2nd indicates the gap next to the 1st and so on.

Accumulation of multiple-ssDNA gaps in mild replication stalling condition (L-APH and MSi1) could be explained by two different mechanisms which are not mutually exclusive. Supposing that gaps were formed on the lagging strand, multiple Okazaki fragments are synthetized at the same time; therefore, Polα inhibition would cause the generation of more than one gap. On the contrary, in the second scenario, the re-priming activity is attempted multiple times. However, in both cases, these processes seem to be restricted to a limited spaced region which did not exceed 2.5 kbp from the fork junction.

This consideration was enforced by the fact that at H-APH concentration only one big ssDNA gap accumulated close to the fork junction and, in this case, its dimension is generally 1.5 kbp in length (***Figure 3.15***).

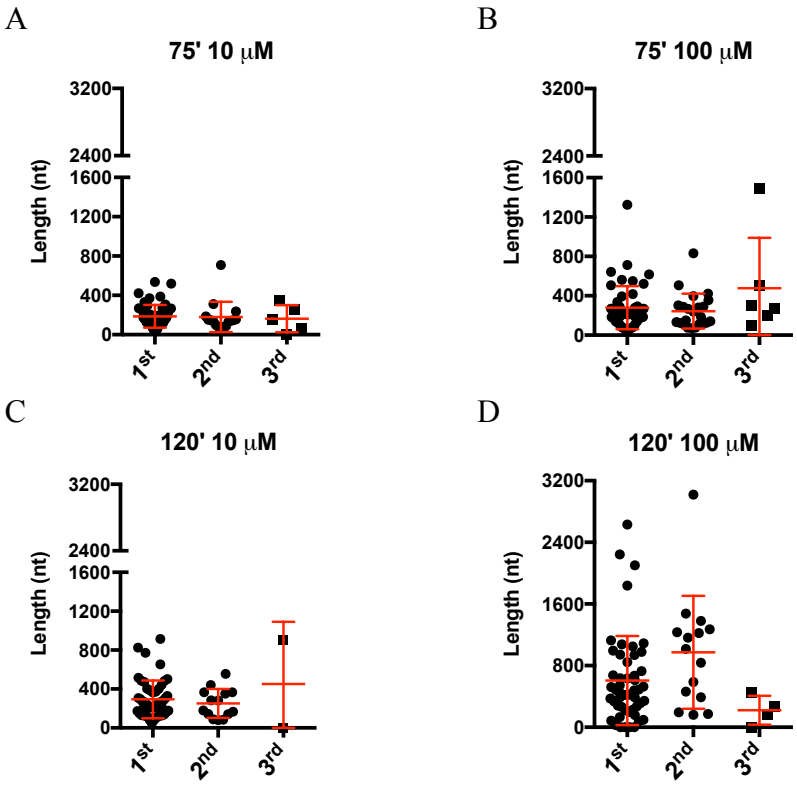

Figure 3.18 Polα inhibition causes multiple ssDNA gaps accumulation

Graph showing the length of ssDNA gap close to the fork junction. RIs were isolated at the indicated time points, 75 min (A and B) and 120 min (C and D). Extract treated at the indicated MSi1 concentration. Bars indicate the mean ± SD relative to 50 RIs counted in two independent experiments. Ordinal numbers indicate gaps position according to their proximity to the fork junction, i.e. 1st indicates the gap at the fork junction, 2nd indicates the gap next to the 1st and so on.

3.2.2 Detection and analysis of RVFs

Another structure caused by replisome stalling is the RVF[128]. We wanted to assess the impact of fork stalling on the number and the structure of RVFs. DNA polymerase inhibition induced by either APH or MSi1 resulted in RVFs accumulation (***Figure 3.19*** and ***Figure 3.20***). Considering the DNA structure of the regressed arms, three types of RVFs were detectable in APH and MSi1 treated extracts (***Figure 3.19***). The first type had

a regressed arm composed by ssDNA only. ssDNA arm in most of these cases was protruding from one of the two daughter strands in the very proximity of the fork junction. The second type of RVF was a cross-shaped structure in which all the DNA branch are constituted by dsDNA. Finally, in the third type the regressed arm was constituted by an initial part of dsDNA, which terminated with a protruding tail of ssDNA.

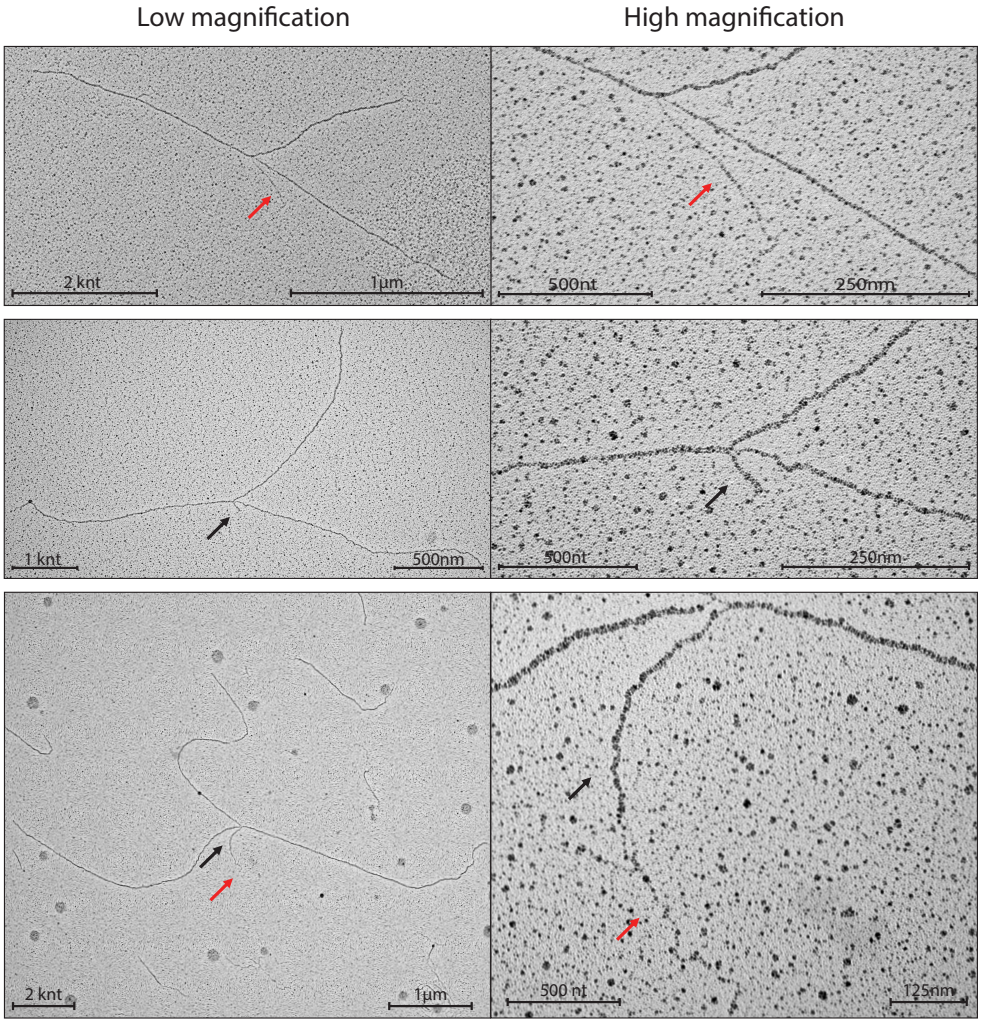

Figure 3.19 DNA polymerase stalling induces RVFs formation

EM micrographs showing an example of a four-way junction RIs, isolated from extract treated for 1 hour with APH. Three different sub-types of regressed arm are showed: ssDNA (upper part of the panel), dsDNA (middle of the panel) and ds/ssDNA (bottom part of the panel). Red arrowheads point towards ssDNA of the regressed arm of the RVFs, black arrowheads indicate the dsDNA part of the reversed branch.

In APH-induced fork stalling condition in *X. laevis* egg extract, ssDNA regressed arms were the most abundant population, representing more than 63% of the total population of RFVs (***Figure 3.20*A**).

DNA polymerase inhibition induced RVFs formation as a general response to fork stalling condition and, in our experiments the percentage of RFVs correlated with the concentration of stalling agent used (***Figure 3.20***). Moreover, RVFs frequency was also dependent on the time of exposure to the replication stalling agent. Indeed, the extracts treated for 15 minutes with MSi1 showed that only the 2% of RIs were RVFs, while in extract in which DNA replication was stalled for 60 minutes this percentage increased up to 6% (***Figure 3.20B***).

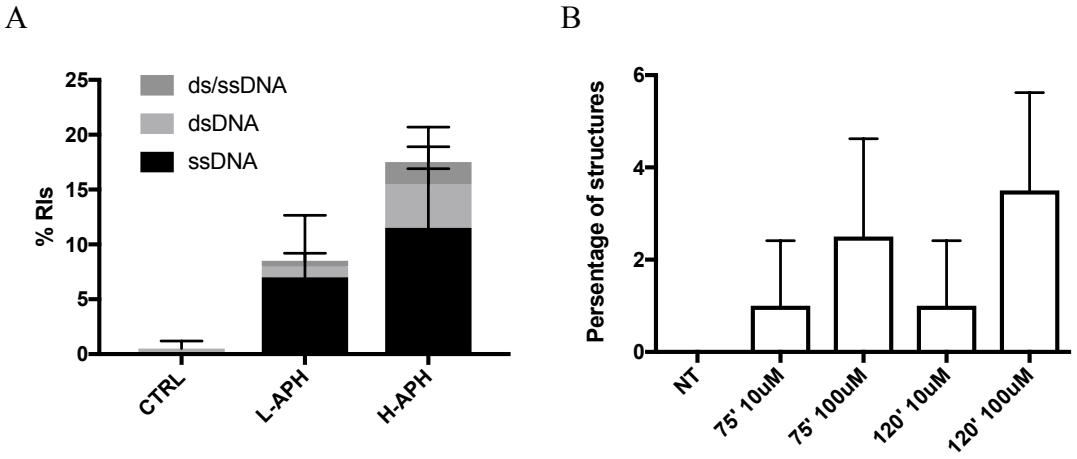

Figure 3.20 RVFs number is time and dose-dependent

(A) Distribution RVFs induced using different APH concentrations. RVFs are subdivided in the three different types: ssDNA, dsDNA or ds/ssDNA. Bars indicate the mean ± SD relative to 100 RIs counted in two independent experiment. (B) Distribution RVFs induced at the indicated time using different MSi1 concentrations. Bars indicate the mean ± SD relative to 50 RIs counted in two independent experiments.

The percentage of RVFs was affected by drugs concentration and time of exposure to them. Instead, the average regressed arm length did not significantly change in the different tested conditions (***Figure 3.21***). However, the regressed arms of APH-induced

RVFs were on average of about 700 nt in length while RVFs isolated from MSi1 treated *X. laevis* egg extract were shorter (on average about 400 nt in length) (***Figure 3.21***).

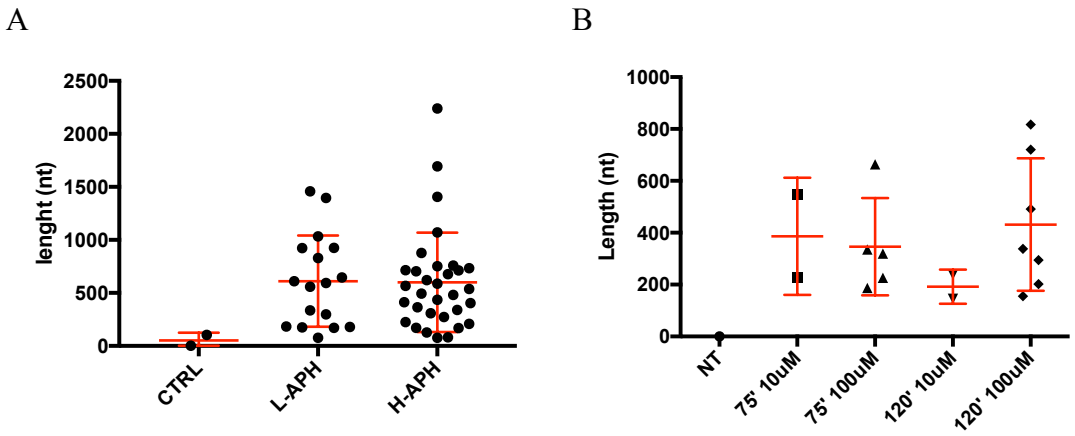

Figure 3.21 Regressed arm length does not change with variations in drug concentration

Graph showing the length of regressed arm. (A) RVFs induced using different APH concentrations. Bars indicate the mean ± SD (n=2). (B) Distribution of RVFs induced at the indicated time using different MSi1 concentrations. Bars indicate the mean ± SD (n=2).

Collectively, these data demonstrate that DNA polymerase inhibition not only induces ssDNA gaps accumulation at the fork junction proximity but it also causes RFVs accumulation. It is noticeable that the average size of the fork gaps correlates with the percentage of RVFs. This may suggest that the ssDNA gap accumulated on one of the two daughter strands can trigger the subsequent RVF formation. This hypothesis is consistent with the fact that more than the 76% of the RVFs showed at least one ssDNA fragment protruding from the regressed arm.

For subsequent experiments we used only APH because it induced a broader range of DNA lesion compared to MSi1 (multiple small ssDNA gaps at L-APH and one big ssDNA gap at H-APH), and it was more potent in inducing RVFs (***Figure 3.20***).

3.3 Smarcal1-mediated RVFs accumulation triggers Mre11-mediated degradation in absence of Rad51 nucleofilament.

3.3.1 Rad51 and Smarcal1 role in RVFs metabolism

In order to gain insights into the molecular mechanisms underlying RVFs formation, *Xenopus* egg extracts were first supplemented with increasing concentrations of APH, added 60 minutes after the start of DNA replication reaction, as previously done for the preparation of EM samples. Then, the effect of different doses of APH on the progression of DNA replication was evaluated by assessing the levels of replicative factors bound to the chromatin by immunoblotting.

At concentrations higher than 10 uM, APH delayed the accumulation of DNA replication factors onto the chromatin (***Figure 3.22***), possibly correlating with a progressive stall of DNA replication forks. Consistently, EM analysis of RIs performed in the same experimental conditions revealed an accumulation of ssDNA gaps at the fork junction in an APH dose-dependent manner (***Figure 3.20A***). This observation also correlated with an enrichment on chromatin of the main single-strand binding proteins, namely RPA and Rad51, with similar dynamics (***Figure 3.22D-E***).

The activation status of ATR-mediated checkpoint, induced by fork stalling, was assessed by immunoblotting mediated detection of the chromatin-bound ATR and of the phosphorylated form of Chk1.

Intriguingly, the maximum intensity of phospho-Chk1 signal was obtained at 1.5 mM APH, whereas EM analysis had previously shown that at this concentration APH induced accumulation of a single big ssDNA gap at the fork junction, while at lower doses it generated multiple smaller gaps (***Figure 3.12***). This observation is in contrast with the hypothesis that the phosphorylation of Chk1 is amplified by multiple ssDNA/dsDNA junctions at the stalled replication fork[45].

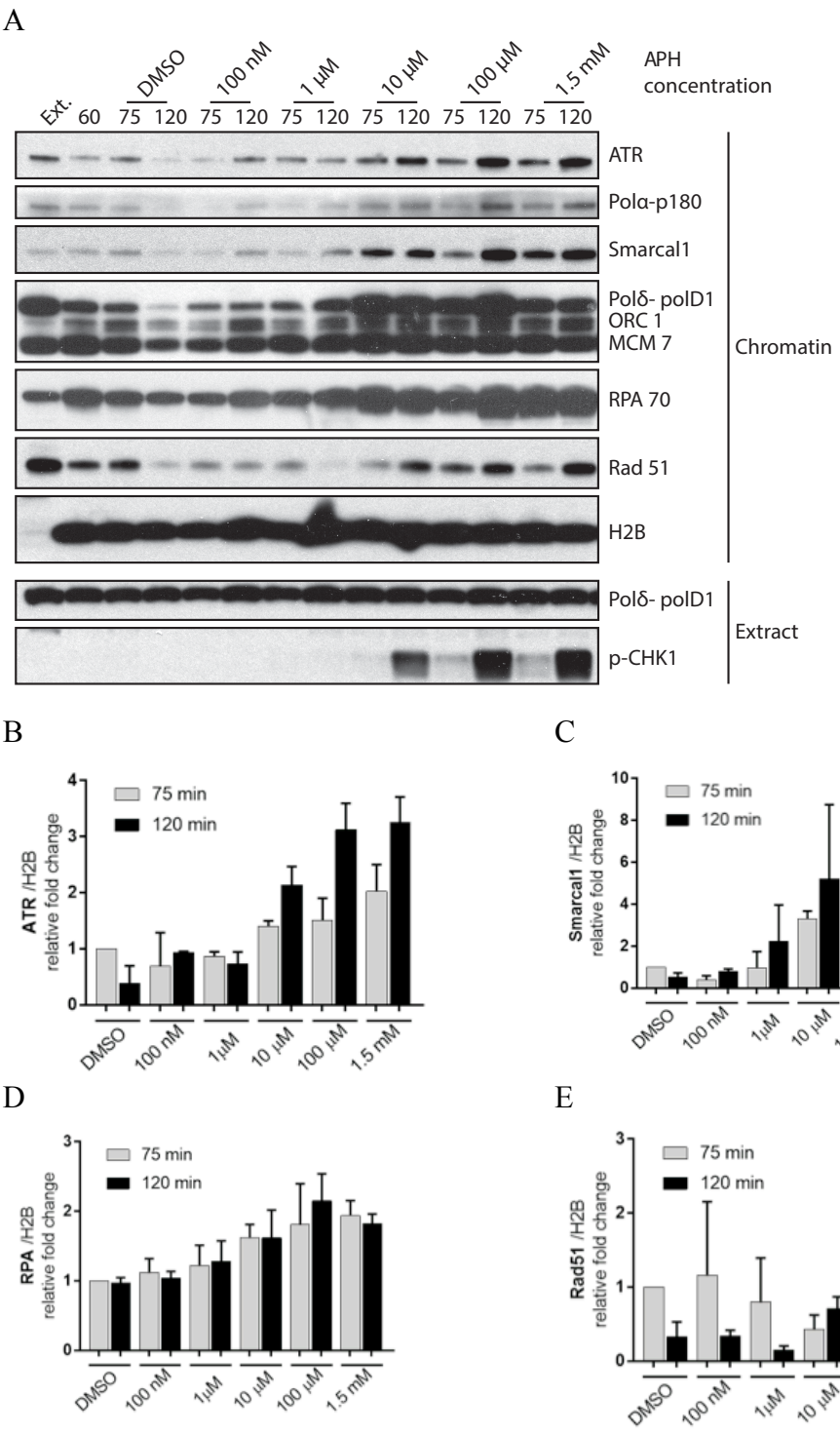

Figure 3.22 APH treatment induces DNA replication polymerases and DDR-related factors accumulation onto chromatin

(A) Chromatin association of indicated protein were assessed in the presence of increasing APH concentration at two different time points, either 15 or 60 minutes after the drug addition. Numbers indicates the time from the DNA sperm addition. 0.5 µl of *Xenopus* extracts were loaded as input lane (Ext). CHk1 phosphorylation was monitored by immunoblotting 1 µl of extract. Total level PolD1 were used as loading control. Histograms represents the quantification of chromatin bound ATR (B), Smarcal1 (C), RPA (D), Rad51 (E), normalized on H2B signal. Bars indicate the mean ± SD (n=3).

Consistent with the hypothesis that APH-induced fork stalling was also ultimately leading to generation of RVFs ***(Figure 3.20A***), we found that Smarcal1, which has been shown to induce the formation of RVFs *in vitro*[147], was enriched onto the chromatin in response to APH treatments (***Figure 3.22C***). The same effect was also observed for Rad51, which has also been reported to be implied in RVFs metabolism[130] (***Figure 3.22***). In order to confirm the contribution of Rad51 and Smarcal1 to RVFs metabolism, we performed EM analysis of DNA intermediates in extracts depleted of Smarcal1 or Rad51 and treated with high concentrations of APH (H-APH).

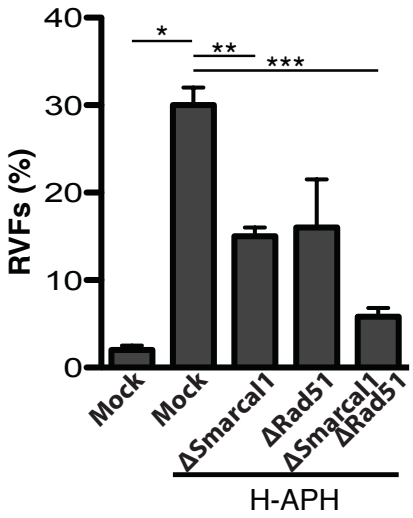

Figure 3.23 EM analysis quantification of Smarcal1/Rad51 contribution to RVFs accumulation

RVF frequency in extracts treated and depleted as indicated. Mean values ± SEM (n= 3) are shown. Mock-depletion was carried out using purified IgG. *, **, *** p <0.01, obtained by unpaired t test between the marked couples. (Picture taken from Kolinjivadi, A. M.; 2017. Ref[192]).

The result of EM analysis revealed that either Smarcal1 or Rad51 depletion was sufficient to significantly reduce the frequency of RVFs, (***Figure 3.23***), suggesting that both these factors are important for RVFs accumulation. Moreover, the simultaneous

depletion of both Smarcal1 and Rad51 further decreased the frequency of RVFs, indicating that the two factors are implied in two different steps of RVFs metabolism.

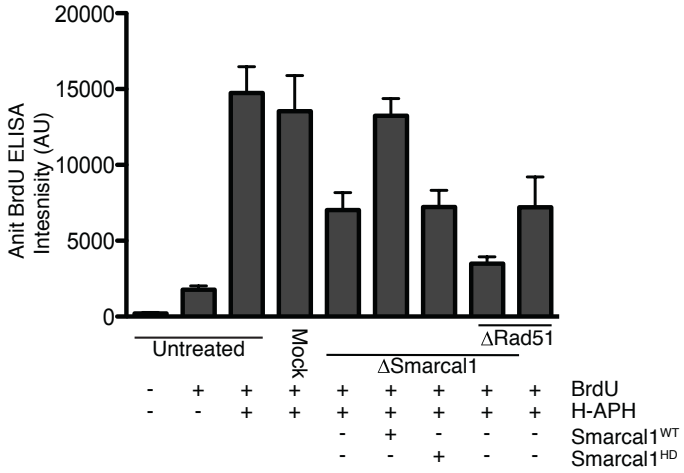

Figure 3.24 ELISA detection of BrdU in nascent ssDNA

ELISA detection of BrdU in nascent ssDNA in nuclei incubated in extracts treated as shown in the figure. Where indicated, extracts were supplemented with 5 ng/**m**L recombinant human Smarcal1^{WT} or catalytically dead Smarcal1^{HD}. Mean intensity values ± SD (n = 3) are shown. (Picture taken from Kolinjivadi, A. M.; 2017. Ref[192])

In order to quantify the relative amount of RVFs and, further confirmed these data, we used a different assay taking advantage of the ability of anti-bromodeoxyuridine (BrdU) antibodies to recognize incorporated BrdU only in the context of ssDNA in non-denaturing conditions[143] (***Figure 3.24***). In particular, we followed the BrdU incorporation in nascent ssDNA by ELISA assay performed on extracts depleted of either Smarcal1 and Rad51 and treated with APH. In the setting of this assay we hypothesized that accumulation of BrdU directly correlated with accumulation of RVFs, as we found a linear relationship between the intensity of BrdU signal and the number of RVFs visualized by EM in the same experimental condition (***Figure 3.23***), and also because the signal was strongly induced by H-APH and significantly inhibited by Smarcal1 depletion (***Figure 3.24***). Moreover, we found that the decrease in BrdU signal in Smarcal1-depleted extracts could be restored by addition of recombinant Smarcal1^{WT}, but not by addition of

its catalytically inactive version[133] Smarcal1^{HD} (***Figure 3.24***). According with the previous results, the co-depletion of Rad51 and Smarcal1 had an additive effect on BrdU incorporation decrement, compared to the single depletions (***Figure 3.24***), indicating that the two proteins act additively to sustain RVF levels.

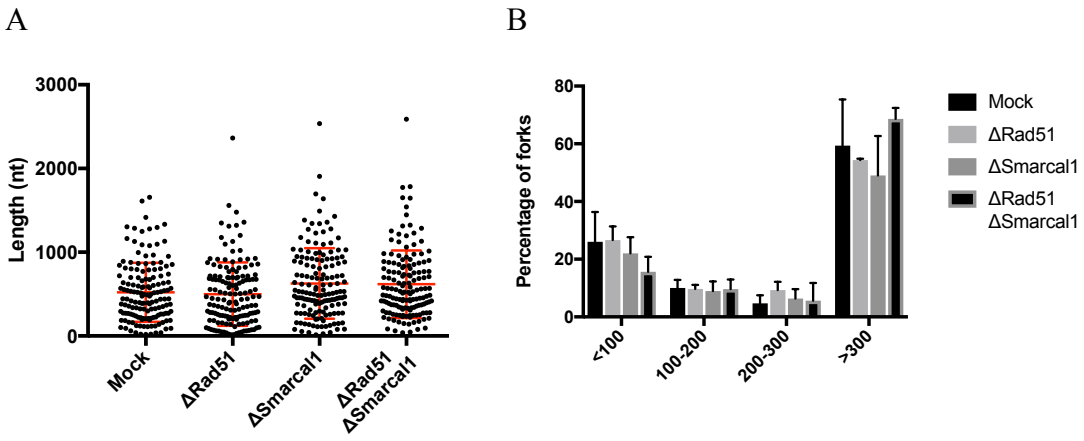

Figure 3.25 Smarcal1 and Rad51 depletion does not impact on ssDNA gaps length at the fork

(A) Graph showing the length of ssDNA gap at the fork junction in extract treated as indicated. Bars indicate the mean ± SD relative to 150 RIs counted in two independent experiment. (B) distribution of fork gaps with different length. Bars indicate the mean ± SD relative to 150 RIs counted in two experiments.

However, neither Smarcal1 depletion nor Rad51 depletion caused any change in the length of the ssDNA gaps accumulated at the fork junction in H-APH conditions (***Figure 3.25***). This suggests that reduction of RVFs number caused by Smarcal1 and Rad51 depletion is not the consequence of the lack of ssDNA.

Intriguingly, RVFs isolated from Smarcal1-depleted extract showed a mild reduction of the regressed arm length compared to the ones obtained from mock-depleted and Rad51-depleted extracts (***Figure 3.26***). This result suggests a direct implication of Smarcal1 in RVFs formation.

Altogether, these results support the idea that Rad51 and Smarcal1 are directly involved in RVFs accumulation as a consequence of replication fork stalling. Since the

simultaneous depletion of these two factors showed an additive effect on RVFs number, we can hypothesize that these two proteins act in two different mechanism that affect RVFs number. Finally, even though the absence of Smarcal1 and Rad51 did not impact on the length of ssDNA gaps accumulated at the fork junction, we found that Smarcal1 depletion caused a reduction of the length of the regressed arm.

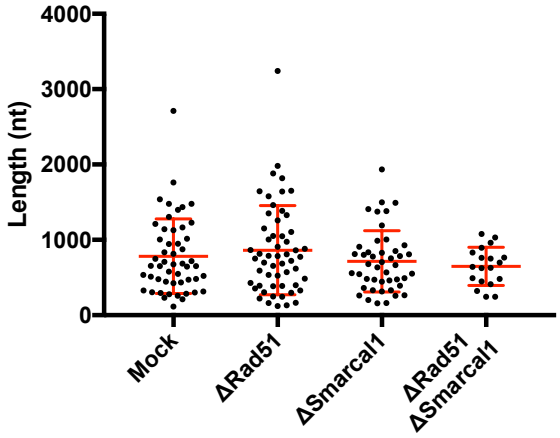

Figure 3.26 Smarcal1-depletion influences the length of regressed branches

Graph showing the length of regressed arms in extract treated as indicated. Bars indicate the mean ± SD (n=2).

3.3.2 Rad51 protects DNA from MRE11 mediated degradation

As we previously reported, the absence of Rad51 in *Xenopus* egg extract induces the accumulation of ssDNA gaps at the fork junction and behind it[118]. Moreover, it has been showed that ssDNA gaps that were found behind the fork were a consequence of Mre11-mediated degradation, as their formation was suppressed by treatment with mirin, a Mre11 inhibitor[118]. Thus, we decided to better characterize the role of Rad51 in protecting DNA from Mre11-mediated degradation. To this purpose, we incubated a fluorescent-labelled DNA substrate with recombinant yeast Mre11, human RPA complex, Rad51^{WT} and Rad51^{T131P}, a mutant identified in Fanconi anemia (FA) patients. Rad51^{T131P} has a reduced ability to form stable Rad51 nucleofilaments[205]. First, we performed a mobility

shift assay of the DNA-protein complex, which allowed us to estimate the molar concentration of proteins required to saturate the ssDNA binding sites of our substrate *in vitro*. In particular, we found that the saturating concentration of Rad51 proteins (4μM) was higher compared to RPA (0.8 μM): this could be explained by the fact that Rad51 ssDNA binding site occupies a very short ssDNA portion (3 nt) [206] while RPA heterotrimer sits on a larger site (30 nt) [207] (***Figure 3.27***).

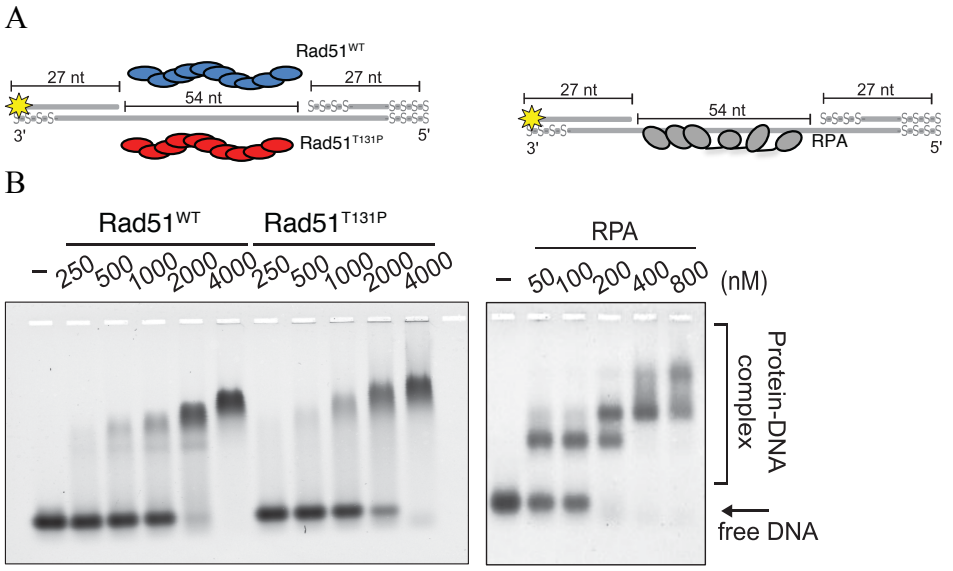

Figure 3.27 Rad51^{wt}, Rad51^{T131P} and RPA binding on gapped DNA template

(A) Schematic representation of Rad51^{WT}, Rad51^{T131P}, or RPA binding to the 5'-fluorescently labelled synthetic gapped DNA substrate containing phosphorothioate bonds (s) shown in the scheme (B) mobility shift assay showing the effect of Rad51^{WT}, Rad51^{T131P}, or RPA pre-incubation synthetic DNA substrate (20 nM) shown in the scheme. (Picture taken from Kolinjivadi, A. M.; 2017. Ref[192]).

The activity of Mre11 was monitored by following the degradation of the DNA substrate by agarose gel electrophoresis in denaturing conditions. The result of this experiment showed that, as expected, a saturating concentration of Rad51^{WT} (4 uM) had a strong protective effect against Mre11-mediated degradation of the DNA (***Figure 3.28***). On the other hand, pre-incubation of the DNA with RPA or Rad51 ^{T131P} did not prevent the substrate degradation, suggesting that a ssDNA binding activity is not sufficient to

antagonize Mre11 activity, but a functional and stable Rad51 nucleofilament is required to carry out this function.

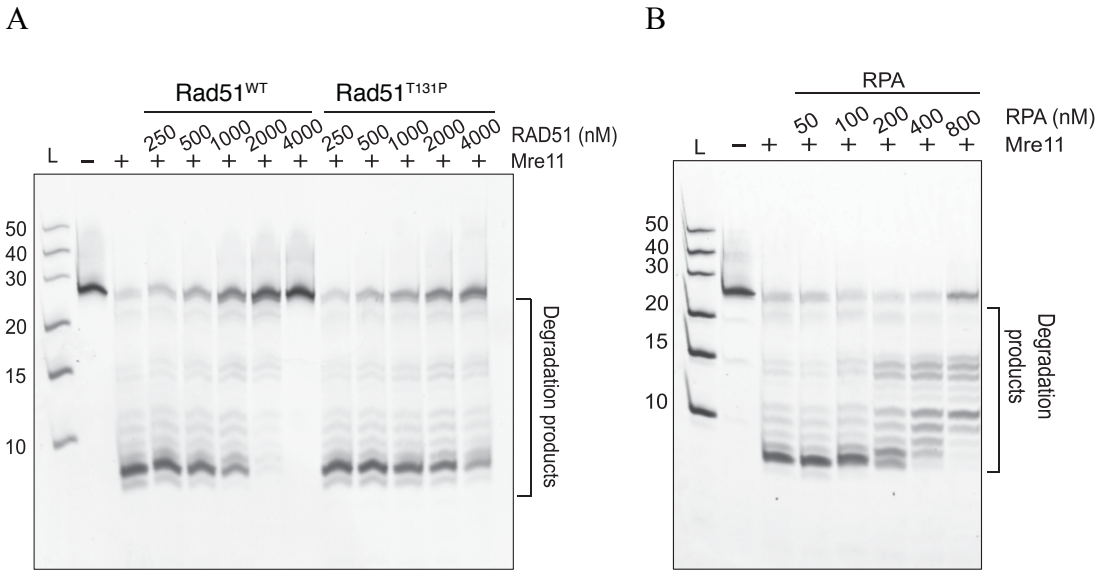

Figure 3.28 Rad51-mediated DNA protection from Mre11 degradation

Denaturing gel showing the effect of Mre11 (30 nm) degradation rates on DNA substrates (20nM) shown in ***Figure 3.27*A** pre-incubated with $Rad51^{WT}$, $Rad51^{T131P}$ (A) and RPA (B) at the indicated concentrations. (Picture taken from Kolinjivadi, A. M.; 2017. Ref[192]).

Since Mre11 and Rad51 are both components of HR-mediated DSBs repair pathway[70], in which Mre11-mediated DSB end resection is required for the recruitment of Rad51 at the damage site, we evaluate the role of Rad51 in antagonizing Mre11-mediated resection on an artificial DNA substrates which recapitulate the structural features of DSBs. To do that, two different fluorescent-labelled DNA substrates were generated, one with a 5' single-stranded overhang and the other one with a 3' single-stranded overhang. Since Mre11 is a 3'-5' exonuclease, we first tested the activity of recombinant Mre11 on the DSB substrate by mobility shift assay. As expected, we observed an extensive degradation of the DNA substrate containing the 5' overhang (***Figure 3.29***) and no Mre11-dependent degradation on other substrates (***Figure 3.29***).

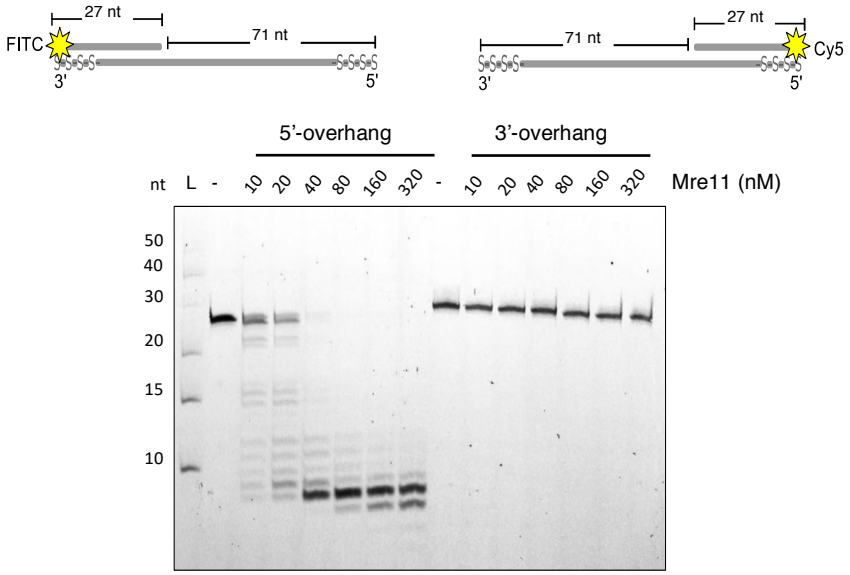

Figure 3.29 Mre11 effect on 3' or 5' overhang DNA templates

Denaturing gel, showing the effect of the indicated amounts of Mre11 protein incubated with the fluorescent labelled DNA substrates containing 5' or 3' overhangs as shown in the scheme. (Picture taken from Kolinjivadi, A. M.; 2017. Ref[192]).

Then, we assessed the ability of Rad51 nucleofilament to protect the 5' overhang substrates from Mre11-mediated degradation. To this end, we pre-incubated the fluorescent-labelled DSB substrates harbouring the 5' overhang with increasing concentrations of $Rad51^{WT}$, $Rad51^{T131P}$ or RPA complex (***Figure 3.30A***) and then we exposed the DNA-protein complexes to Mre11 activity. Similarly to what previously observed, $Rad51^{WT}$ exerted a protection effect against Mre11 mediated degradation of the DNA (***Figure 3.30***), in contrast to RPA or $Rad51^{T131P}$, which did not show any effect (***Figure 3.30***). The result of this experiment suggests that only a stable Rad51 nucleofilament is able to prevent Mre11-mediated degradation also on a DNA template with the structural features of a DSB.

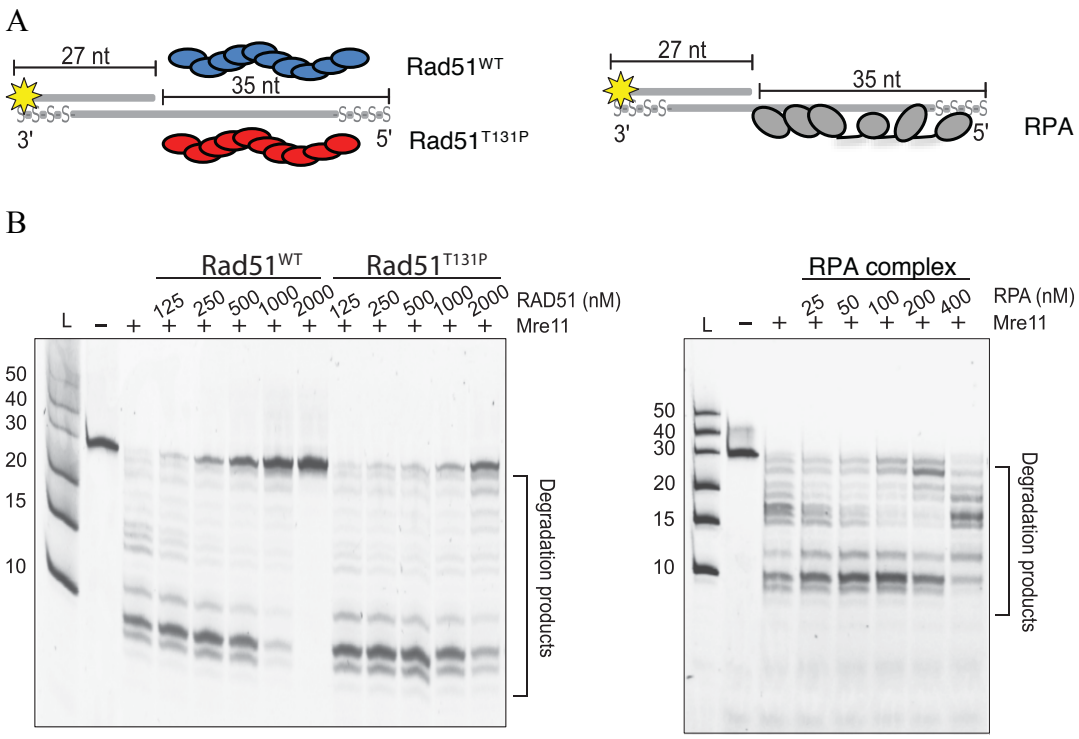

Figure 3.30 Rad51 protection on 3' or 5' overhang DNA from Mre11 nuclease activity

(A) Schematic representation of the DNA protein complexes used for the degradation assay. (B) Denaturing gel showing the effect of Mre11 (30 nm) degradation rates on DNA substrates (20nM) preincubated with $Rad51^{WT}$, $Rad51^{T131P}$ and RPA at the indicated concentrations. (Picture taken from Kolinjivadi, A. M.; 2017. Ref[192]).

3.3.3 Rad51 protects RFVs from Mre11-dependent degradation

As already mentioned, RVFs are a DNA structure generated as a consequence of a replication fork stalling event. From a DNA structural point of view, RVFs are four-way junctions generated from the reannealing of the newly synthetized DNA strands into double-stranded regressed arms. In our EM experiments, we have found that the regressed arms generally expose a ssDNA tail (***Figure 3.19*** and ***Figure 3.20A***), thus recapitulating the same DNA structural features of a DSB.

For this reason, we tested whether Rad51 nucleofilament could also be able to protect a similar four-way junction structure from Mre11-mediated degradation. To do that, we generated a four-way synthetic DNA structure which exposed a 5' overhang (***Figure 3.31A***). As before, we pre-incubated the DNA template with $Rad51^{WT}$, $Rad51^{T131P}$ or

RPA and we exposed them to Mre11. Even in this case, extensive Mre11-mediated DNA degradation was observed when the DNA templates were pre-incubated with RPA or Rad51^{T131P}. Instead, Rad51^{WT} was fully able to prevent Mre11 exonuclease activity (***Figure 3.31B***).

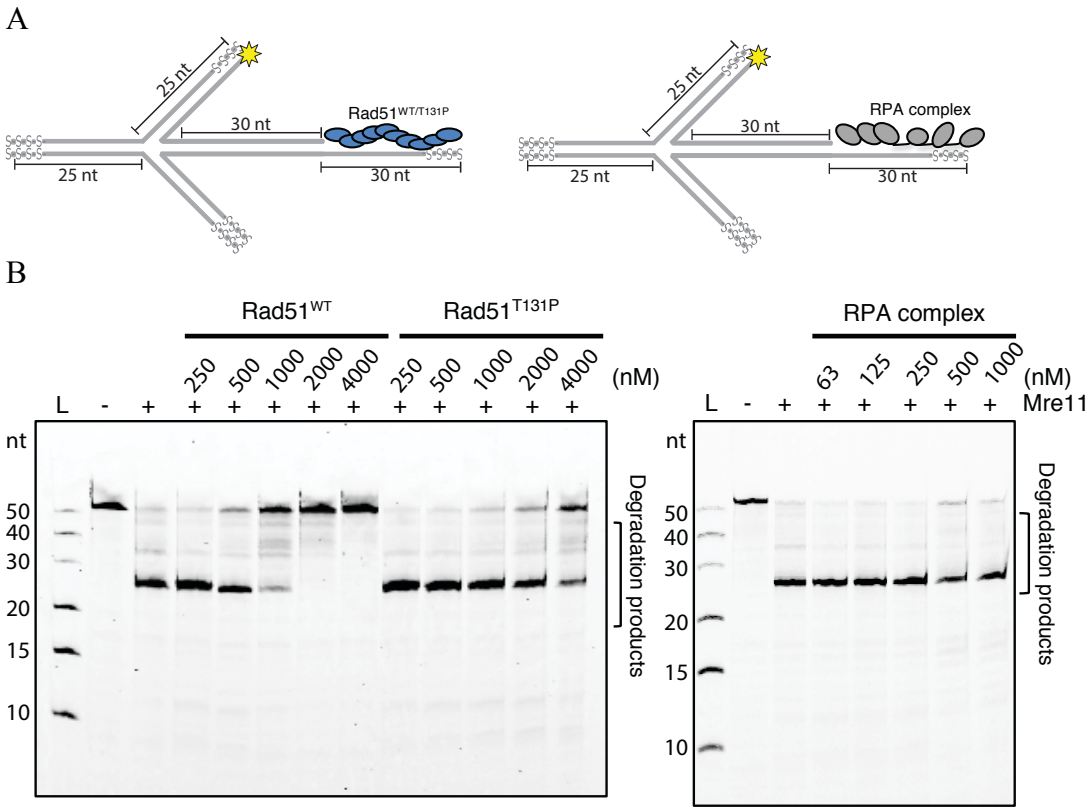

Figure 3.31 Rad51 nucleofilament protects RVFs from Mre11-dediated degradation

(A) Schematic representation of the DNA protein complexes used for the degradation assay. (B) Denaturing polyacrylamide gel showing the effect of Mre11 (30 nm) degradation rates on synthetic RVFs substrates (20nM) preincubated with Rad51^{WT}, Rad51^{T131P} and RPA at the indicated concentrations. (Picture taken from Kolinjivadi, A. M.; 2017. Ref[192]).

The results of this experiment confirmed the role of Rad51 nucleofilament in DNA protection from Mre11-mediated degradation and suggested that the role of Rad51 in RVFs accumulation after fork stalling could occur through antagonizing Mre11 activity.

3.3.4 Smarcal1 role in RVFs metabolism

As discussed before, Smarcal1-depleted extract was deficient in RVFs accumulation after replication stress (***Figure 3.23*** and ***Figure 3.24***). Smarcal1 translocase activity has been proposed to directly catalyse fork reversal *in vitro*[147]. For this reason, we verify whether Smarcal1 is sufficient to directly promote RVFs formation in *X. laevis* egg extract.

To do that, recombinant *Xenopus* Smarcal1 (xSmarcal1) protein was added in different amounts to *Xenopus* egg extract. Intriguingly, increasing concentrations of recombinant xSmarcal1 caused an alteration of the chromatin-bound levels of Rad51, while it did not affect PolD1 or RPA chromatin binding (***Figure 3.32***). The significance of this observation remains to be established.

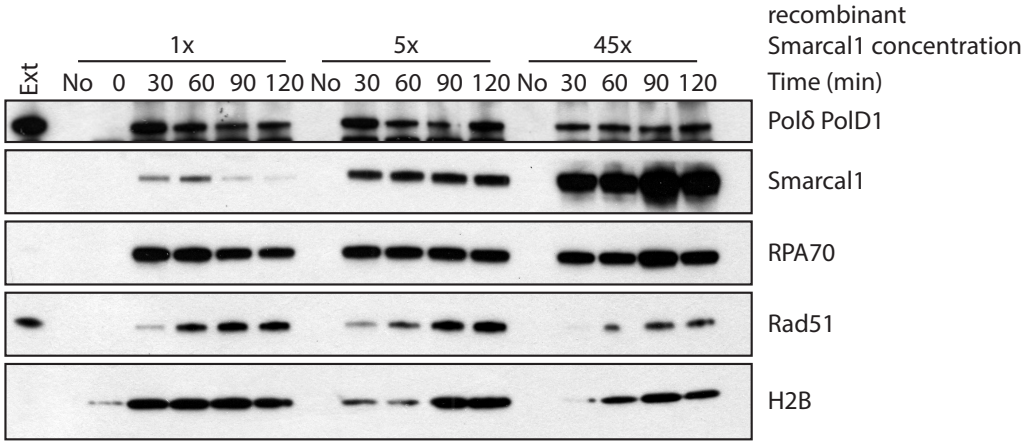

Figure 3.32 Chromatin binding experiment of Smarcal1 overloading onto chromatin

Egg extract was supplemented with three different concentrations of recombinant Smarcal1. Numbers indicates the final Smarcal1 concentration in relative fold change considering the endogenous amount as 1x. Chromatin bound levels were assessed at the indicated minutes from sperm addition. 0.5 μl of *Xenopus* extracts were loaded as input lane (Ext). 'No' indicates control extract supplemented with the indicated amount of recombinant protein but in the absence of sperm DNA.

To test the role of Smarcal1 in RVFs accumulation in *X.* egg extract, we analysed by EM the RIs isolated from extracts incubated with increasing concentration of xSmarcal1.

The results of this analysis showed that xSmarcal1 was sufficient to induce RVFs formation in *Xenopus* extract, both in unchallenged and H-APH treatment conditions (***Figure 3.33***).

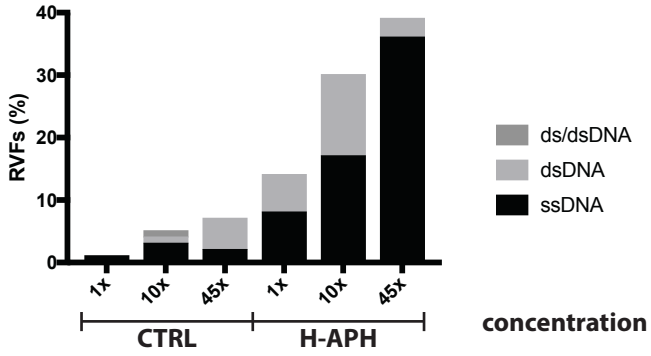

Figure 3.33 EM analysis quantification of the impact of recombinant Smarcal1 addition on to RVFs formation

EM analysis of RVF frequency in extracts treated as indicated. Egg extract was supplemented with three different concentration of recombinant Smarcal1. Numbers indicates the final Smarcal1 concentration in relative fold change considering the endogenous amount as 1x.

Interestingly, we also found that high amounts of Smarcal1 (45x) induced the formation of structures in which reversed branches were present at both side of the replication bubble (***Figure 3.34***). The presence of this particular DNA replication intermediate was found only at high doses of recombinant Smarcal1 and likely reflected the higher frequency of RVFs induced by the massive accumulation of recombinant Smarcal1 on the chromatin.

Even more intriguingly, we showed that Smarcal1 chromatin hyper-loading was able to increase the length of the RVFs regressed arm (***Figure 3.35***) and on the other hand, to decrease the extent of the ssDNA gap accumulated at the fork junction (***Figure 3.36***).

These data suggested that xSmarcal1 is one of the main players of RVFs formation in the *X. laevis* egg extract. As the presence of H-APH significantly stimulates RVFs formation induced by Smarcal1, it is likely that Smarcal1 promotes the conversion of gapped forks into RVFs.

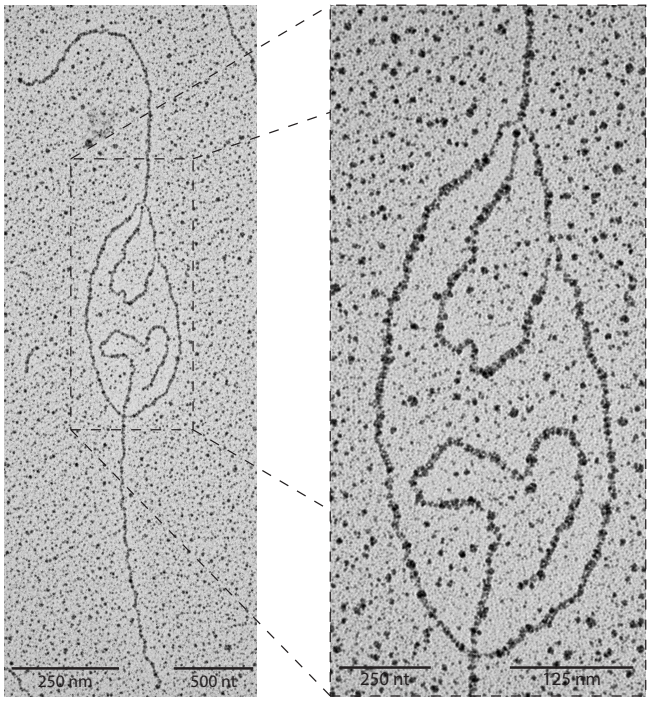

Figure 3.34 Smarcal1 hyper-loading induces the formation of double RVFs in a single replication bubble

EM micrograph showing a replication bubble harbouring two RVFs isolated from *Xenopus* egg extract treated with 45x of Smarcal1. The so-called replication bubble forms when DNA melt and replication initiates forming two replication forks traveling in opposite directions. The inset shows magnification of the replication bubble with two reversed branches. (Picture taken from Kolinjivadi, A. M.; 2017. Ref[192]).

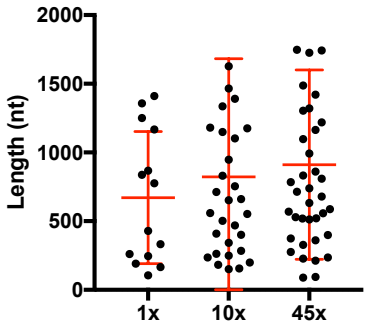

Figure 3.35 Analysis of regressed arm length in egg extract treated with H-APH and supplemented with an excess of Smarcal1

Graph showing the length of regressed arm of RVFs induced upon treatment with H-APH (1.5 mM) and increasing concentrations of recombinant Smarcal1. Bars indicate the mean ± SD

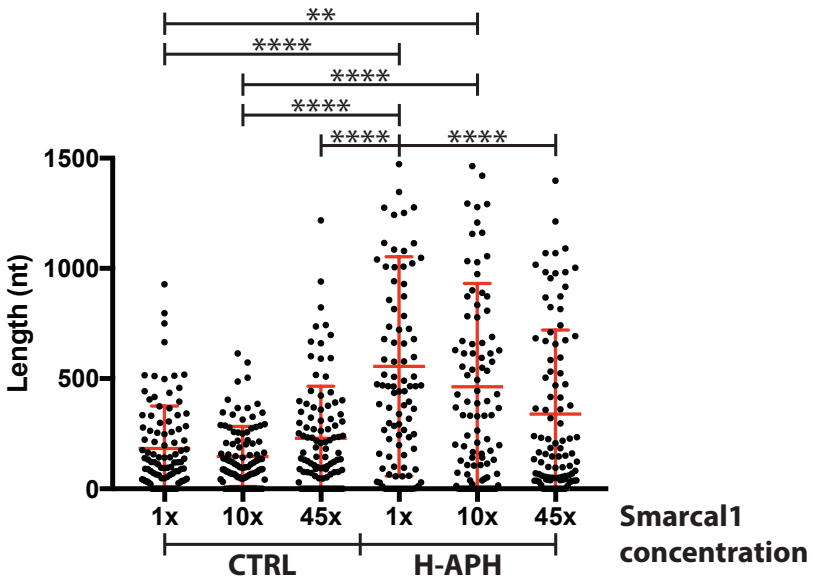

Figure 3.36 Smarcal1 over loading reduces ssDNA gap at the fork junction

(A) Graph showing the length of ssDNA gap at the fork junction. RIs were isolated from extract treated or not with H-APH and, supplemented with increasing Smarcal1 concentration (expressed in relative fold change, 1x represents the endogenous concentration). Bars indicate the mean ± SD relative to 100 RIs counted. (B) Numbers in the table indicate the p value obtained by multiple comparison Kruskal/Wallis test, ** $p<0.01$ and **** $p<0.0001$.

3.3.5 Rad51 overload does not impact on RVFs number

Since previous results have shown that Rad51 depletion causes a reduction in RVFs after replication stress (***Figure 3.23*** and ***Figure 3.24***), we decided to test also the direct effect of Rad51 hyper-loading onto chromatin on the frequency and on the morphology of RVFs formed in *X. laevis* egg extract.

To this end, we first assessed the effect of high doses of recombinant Rad51 on the chromatin binding of common replication related factors (***Figure 3.37***). The result of this experiment showed that hyper-loading of recombinant Rad51 onto chromatin did not alter the protein levels of main replication factors such as DNA polymerase (Polδ and Polα) or the DNA helicase components (Mcm7). Moreover, we found that the binding of

recombinant Rad51 onto the chromatin was not affected by treatment with APH, possibly correlating with the ability of Rad51 to bind both ssDNA and dsDNA.

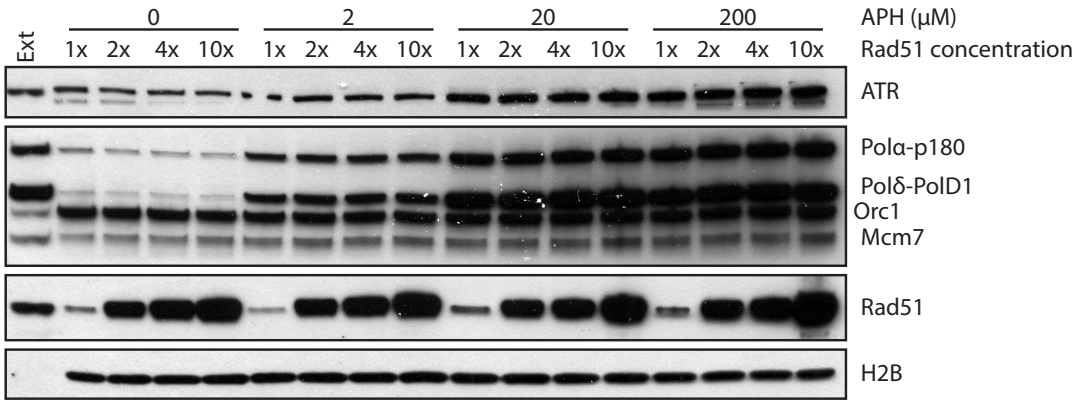

Figure 3.37 Chromatin binding experiment of recombinant Rad51 hyper-loading onto chromatin

Chromatin binding experiment showing egg extract supplemented with increasing concentrations of recombinant Rad51. Numbers indicate the final Rad51 concentration in relative fold change considering the endogenous amount as 1x. Chromatin purification was performed at 60 minutes after sperm nuclei addition into the egg extract. 0.5 μl of *Xenopus* extracts were loaded as input lane (Ext).

Surprisingly, Rad51 hyper-loading did not increase the population of RVFs, even in extracts treated with APH (***Figure 3.38***). This is in contrast with the supposed role of Rad51 in promoting RVFs formation[130].

However, the same EM analysis revealed that, from extract supplemented with high doses of Rad51, it was possible to isolate four-ways structures in which the four arms were two by two equal in length. These structures were highly similar to HJs derived from HR-mediated process rather than RVFs (***Figure 3.39***)[208]. These RIs were unlikely to result from the enzymatic digestion of a RVFs structure as the average length of the DNA branches in these HJ-like structures was generally longer than the average size of regressed arms found in an RVF (***Figure 3.39*** and data not shown). Moreover, in *X. laevis* egg extract the majority of RVFs structures had a ssDNA regressed arm (***Figure 3.20A***), suggesting that these four-ways junctions identified in high Rad51 concentration were possibly derived from a different mechanism rather than the fork reversal. However, at

this stage we could not formally exclude that Rad51 overexpression was inducing protection against degradation of the regressed arm.

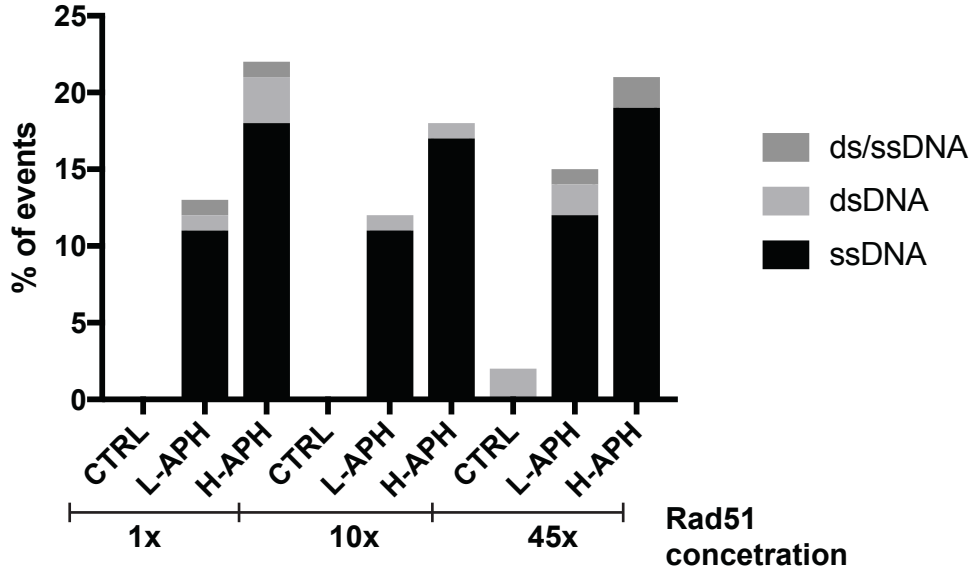

Figure 3.38 EM quantification of RVFs frequency in Rad51 supplemented extract

EM analysis of RVF frequency in extracts treated as indicated. Egg extract was supplemented with three different concentrations of recombinant Rad51. Numbers indicates the final Rad51 concentration in relative fold change considering the endogenous amount as 1x.

Intriguingly, similar HJ-like structures were found in the proximity of the replication fork junction (***Figure 3.39B***), supporting the hypothesis that these structures could arise as a consequence of DNA replication-coupled HR events.

We also found that the relative percentage of HJ-like structures increased accordingly to Rad51 and APH concentration (***Figure 3.40***), possibly reflecting the role of Rad51 in HDR, which could take place also on APH-induced ssDNA gaps lesions.

Moreover, Rad51 supplemented *Xenopus* extract showed reduction of the length of the ssDNA gaps after APH treatment (***Figure 3.41***). In particular, H-APH generates a ssDNA gap at the fork that is longer than the one generated upon L-APH treatment; however, even if this difference is statistically significant, it was abolished when high amount of recombinant Rad51 was loaded on chromatin (***Figure 3.41***).This support the hypothesis

of a role of Rad51 in preventing the degradation of newly synthetized DNA, rather than an involvement of Rad51 in RVFs formation.

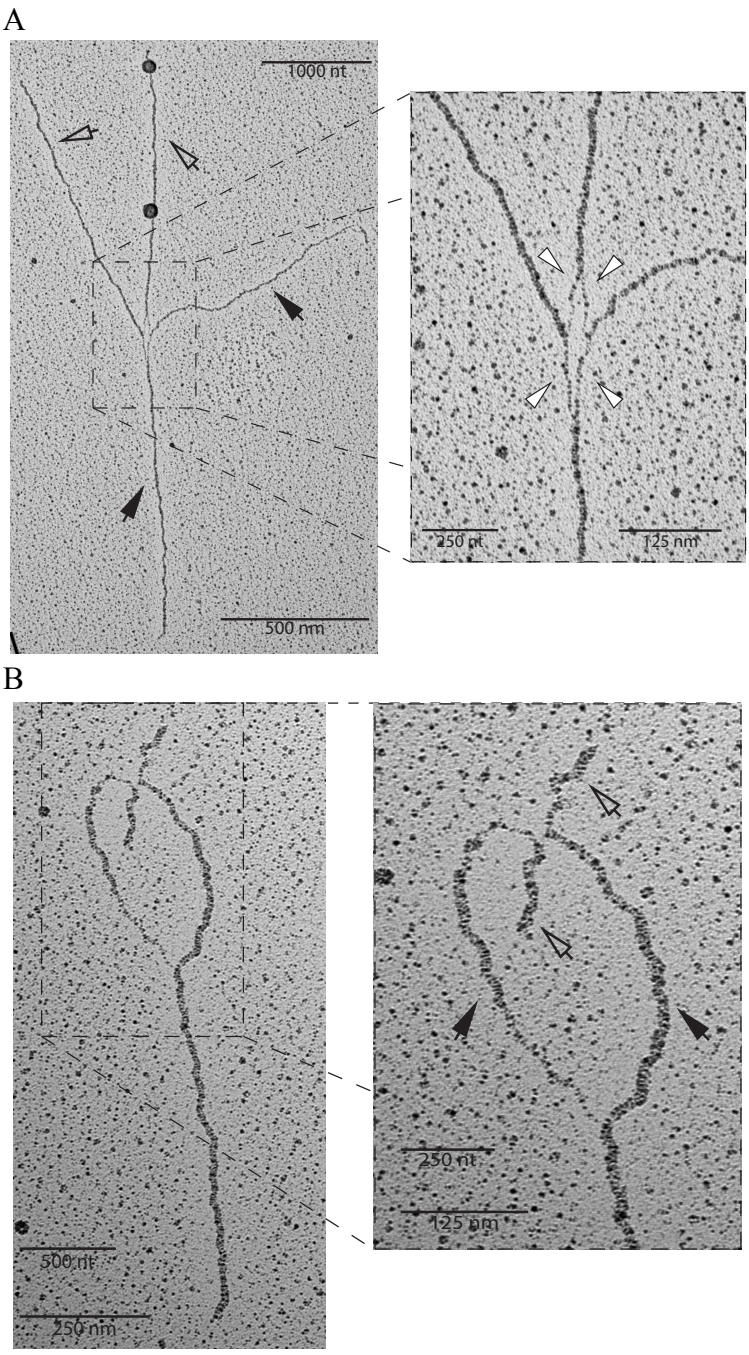

Figure 3.39 Rad51 chromatin hyper-loading induces HJs formation

EM micrographs showing two examples of HJs: similar arrowheads point the DNA strands which are similar in length (to be considered as equals, the difference in length does not exceeds the 10%). (A) Isolated HJ structure. The white arrows point the ssDNA which is generally present at the HJs. (B) HJ structure in close proximity of a replication fork.

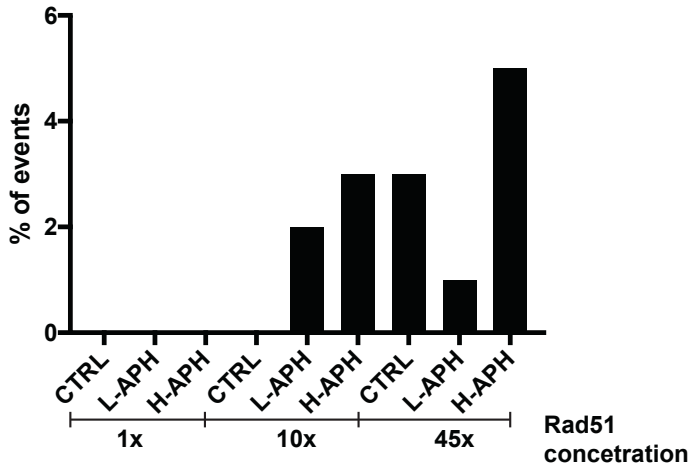

Figure 3.40 EM analysis of HJs frequency upon Rad51 addition

EM analysis of HJs frequency in extracts treated as indicated. Egg extract was supplemented with three different concentrations of recombinant Rad51. Numbers indicates the final Rad51 concentration in relative fold change considering the endogenous amount as 1x.

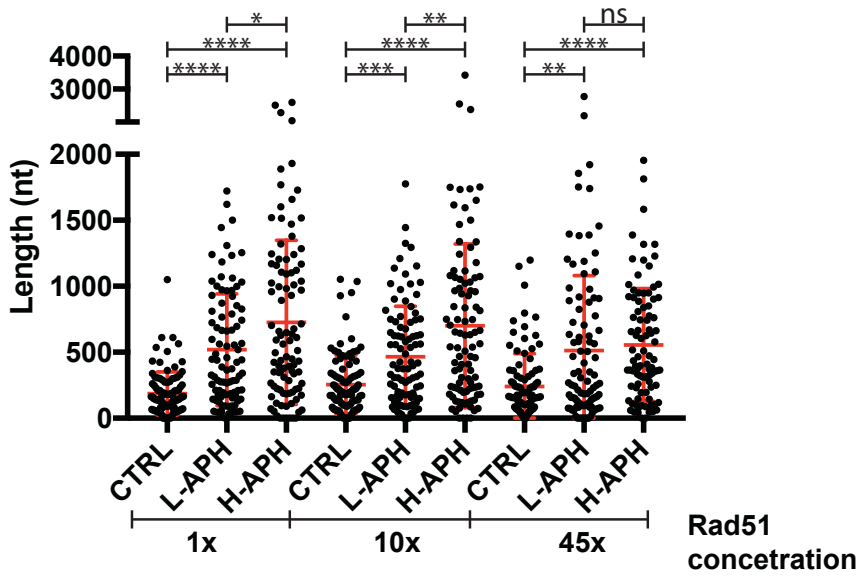

Figure 3.41 EM quantification ssDNA gaps length in Rad51 hyper-loading conditions

(A) Graph showing the length of ssDNA gap at the fork junction. RIs were isolated from extract treated with increasing concentration of APH and supplemented with three different concentrations of recombinant Rad51 (expressed as relative fold change, 1x represent the endogenous Rad51 amount). Bars indicate the mean ± SD relative to 100 RIs counted. * $p<0.05$, ** $p<0.01$, *** $p<0.001$ and **** $p<0.0001$, obtained by unpaired t test between the marked couples.

Taking in consideration the data collected, we can hypothesize that Smarcal1 is directly responsible for the fork regression upon DNA fork stalling, while Rad51 indirectly contributes to stabilize the RVFs levels by preventing their endogenous nuclease-mediated degradation.

3.3.6 Rad51 interacts with Pol-α and Smarcal1 in a chromatin context

Our results indicate that forks with persistent gaps induced by DNA polymerization inhibition obtained with H-APH treatment could be converted by Smarcal1 into RVFs that were susceptible to Mre11-dependent degradation in the absence of Rad51 bound to DNA. Moreover, spontaneous fork junction gaps have also been reported in Rad51-depleted extracts under unchallenged conditions[118], potentially predisposing to RVF formation. Given the fact that both Rad51 and Polα chromatin binding levels were increased in fork stalling conditions (***Figure 3.11***), we hypothesized that Rad51 directly influenced Polα replicative function.

To verify this hypothesis, we immuno-precipitated Rad51 from egg extracts and performed western blot experiments, which highlighted the presence of Polα but not Polδ, (***Figure 3.42***).

Moreover, to test the hypothesis that Rad51 could be one of the factors responsible for Polα chromatin recruitment or stabilization in fork stalling condition, we performed a Rad51 IP in replicating extract. Briefly, 30 minutes after sperm nuclei addition *Xenopus* egg extract was supplemented with either L-APH or DMSO. At 60 minutes from the beginning of the reaction DNA replication was stopped by extract dilution. Total diluted egg extract was lysed and used to perform Rad51 IP.

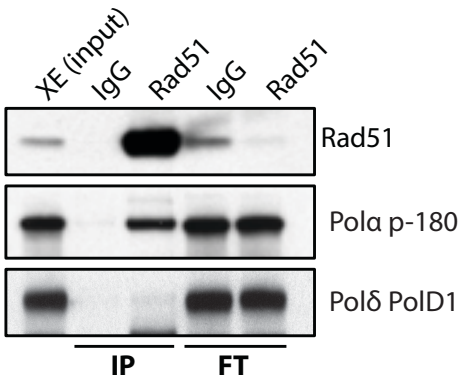

Figure 3.42 Polα and not Polδ co-immunoprecipitates in Rad51 IP

WB of egg extract IPs using the indicated antibodies. Flowthrough (FT) and extract input (XE) are also shown.

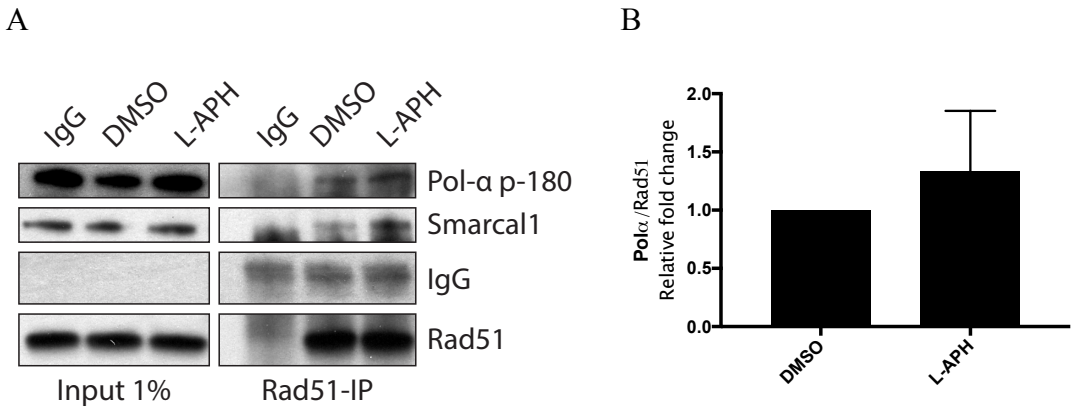

Figure 3.43 DNA replication stress affects Polα and Rad51 interaction

(A) Rad51 IP carried out in total lysate (cytoplasmic material plus nuclei fraction) obtained from replicating egg extract supplemented with sperm nuclei and APH or DMSO, IPs using the indicated antibodies. Total lysate input in the different experimental condition are shown. (B) Histograms represents the quantification of relative signal of Polα normalized on Rad51 signal. Bars indicate the mean ± SD (n=3).

As expected, Polα co-immunoprecipitated with Rad51. More intriguingly the Polα fraction, that was interacting with Rad51, increased in APH fork stalling conditions (***Figure 3.43***). Surprisingly, also a small fraction of Smarcal1 co-immunoprecipitated with Rad51, which may indicate an interaction among these two factors (***Figure 3.43***).

The Polα-Rad51 interaction could shed new light on Rad51 requirement for replication fork resumption after fork stalling condition[120]. Moreover, it could explain why Rad51 depleted extract DNA lesions are similar to the one reported after Polα inhibition (L-APH and MSi1). Finally, Smarcal1-Rad51 interaction could suggest a regulatory role of Rad51 on Smarcal1 activity. Indeed, the inability of Rad51 hyper-chromatin binding to influence the RVFs levels could be explained by a combined mechanism in which, on one hand, Rad51 impedes RVFs formation by promoting Polα-mediated re-priming of ssDNA gap at the stalled fork, while, on the other hand it stabilizes RVFs from Mre11-mediated degradation.

3.3.7 ATR inhibition leads to RVFs accumulation

It has been reported that DNA replication checkpoint deficient yeast cells accumulate reversed forks in DNA replication stalling conditions[59,61]. Moreover, ATR in human cells inhibits Smarcal1 activity to prevent an excess of fork reversal and as a consequence fork collapse[143]. Finally, it has been shown that Rad51 is directly regulated by Chk1[209]. Given the fact that Rad51 and Smarcal1 co-immunoprecipitated (***Figure 3.43***), and that previous studies have shown that both Rad51 and Smarcal1 are regulated by checkpoint, we decided to study the effect of ATR inhibition [210] (ATRi) on RIs in *Xenopus* egg extract.

Then, we assessed the consequence of ATRi on DNA RIs structures. Similar to Smarcal1 hyper-loading experiments described above, ATR inhibition in *Xenopus* egg extract resulted in an increase of RVFs frequency compared to the mock-treated samples. Intriguingly, the percentage of RVFs was almost doubled in both L-APH and H-APH conditions (***Figure 3.45***). These observations are consistent with an ATR-dependent inhibition of Smarcal1 function. Moreover, ATR inhibition resulted in ssDNA gap length shortening similar to the one obtained in extract where Smarcal1 was hyper-loaded onto

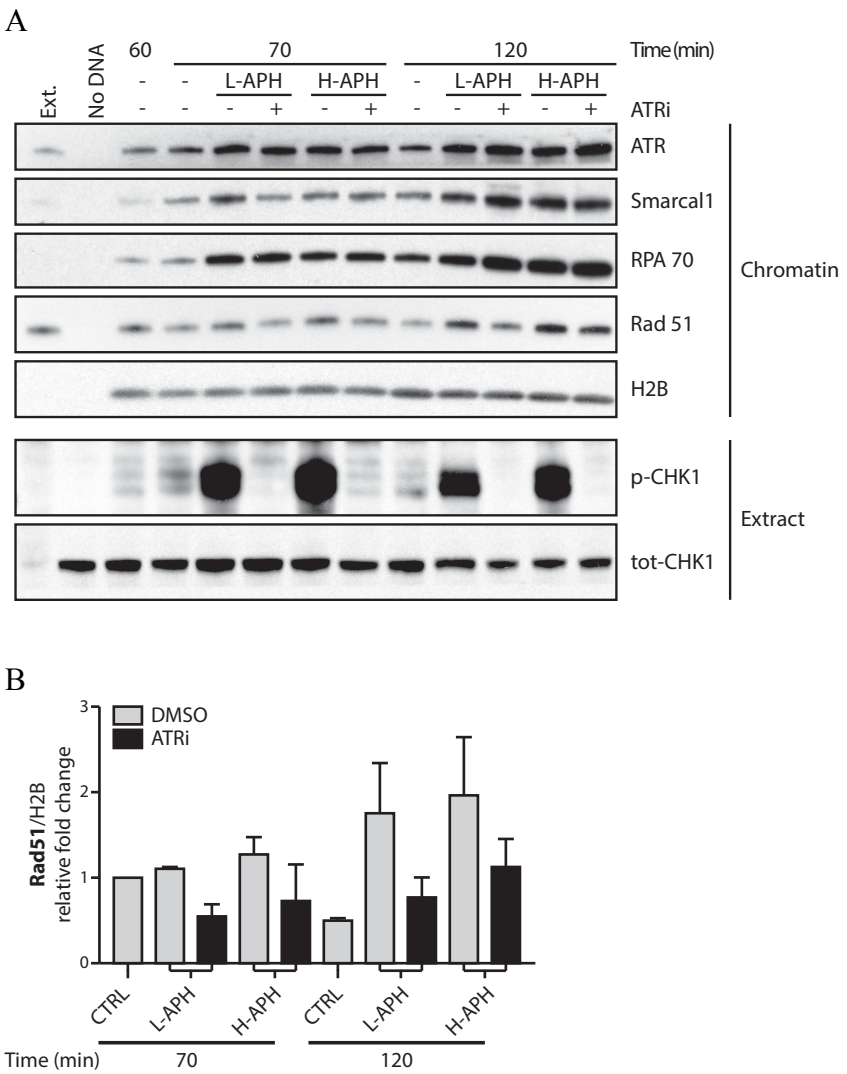

Figure 3.44 ATR inhibition affects Rad51 Chromatin binding

(A) Chromatin fractionation experiment obtained from egg extract supplemented with or without ATRi and with different APH concentrations. ATRi and APH were added simultaneously at 60 minutes after sperm nuclei addition into the extract. The time in minutes (60, 70 and 120) at which replication reactions were stopped is indicated in the figure. 0.5 μl of *Xenopus* extracts were loaded as input lane (Ext). 'No DNA' indicates the internal control of chromatin purification procedure that is obtained by omitting sperm nuclei addition. CHk1 phosphorylation (serine 344) immunoblotting was carried out by loading 1 μl of the reaction at the indicated time points. Total level of Chk1 were used as loading control. (B) Histogram represents the relative levels of chromatin-bound Rad51 normalized on H2B signal. Bars indicate the mean ± SD (n=3).

the chromatin (***Figure 3.36*** and ***Figure 3.46***). The significance of this finding remains to be established.

At the protein level ATR inhibition resulted in a decreased of Rad51 chromatin binding level compare especially in APH treated extract (***Figure 3.44***). However, Smarcal1 chromatin bonding was not altered in ATRi treated extract.

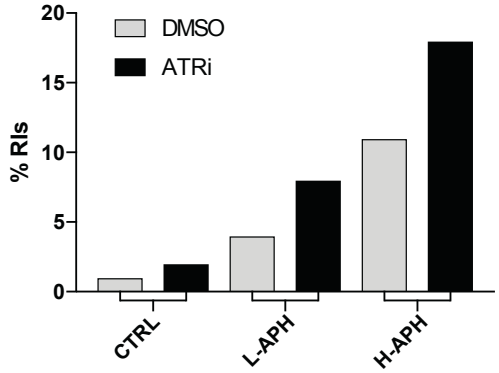

Figure 3.45 ATRi induces accumulation of RVFs

EM analysis of RVF frequency in extracts treated as indicated. Egg extract was supplemented with or without APH (L, low and H, high) and ATRi as indicated in the figure at 60 minutes after starting the reactions. RIs were purified at 120 minutes.

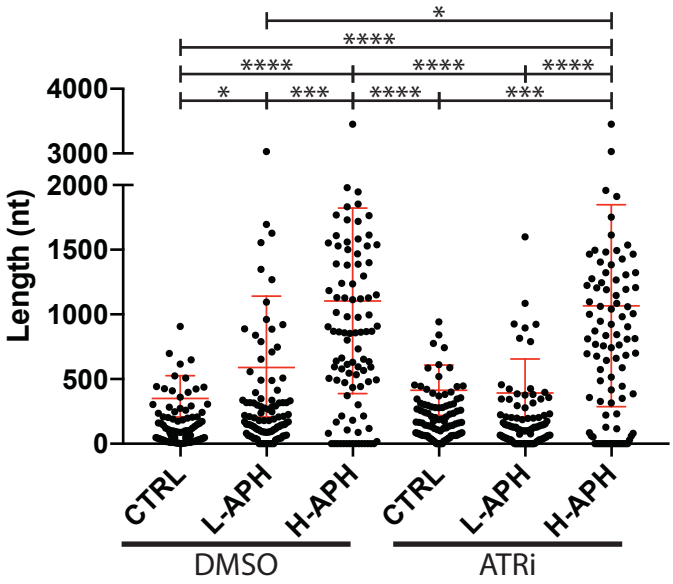

Figure 3.46 ATRi leads to the reduction of ssDNA gaps length at the fork junction

(A) Graph showing the length of ssDNA gap at the fork junction. RIs were isolated from egg extract in the presence or absence of increasing concentrations of APH and ATRi (as indicated in the figure). Bars indicate the mean ± SD relative to 100 RIs counted. (B) Numbers in the table indicate the p value obtained by multiple comparison Kruskal/Wallis test, * $p<0.05$, *** $p<0.001$ and **** $p<0.0001$.

4 Discussion

4.1 Advantages and limits of AFM and EM in RIs visualization

Genome instability is one of the hallmarks of cancer cells. One of the most accepted models proposes that oncogenes driving cell proliferation induce DNA replication stress, which, in turn, generates genomic instability and promotes tumorigenesis.[27-29].

One of the most delicate moment for genome integrity is DNA replication. Genome stability can be threatened by replication stress events. Each cell in the human body faces tens of thousands of DNA lesion per day[65] and when the DNA replication machinery encounters an obstacle, the DNA replication checkpoint can be activated. ATR is recruited at the stalled replication fork and phosphorylates several substrates, including the checkpoint kinase Chk1 and the ssDNA binding protein RPA. However, the exact DNA structure that can activate the ATR signalling cascade is controversial for two main reasons. First, different damaging agents lead to ATR activation, albeit producing different kinds and levels of replication stress. Second, the well-accepted model of polymerase-helicase uncoupling has been challenged by direct visualization of stalled RIs by EM, which did not support extensive symmetric uncoupling of DNA at stalled forks.

In this thesis we characterized the consequences of DNA polymerases inhibition on RIs structures. In order to study DNA replication forks structures at the single molecule level, we adopted EM- and AFM-based imaging techniques.

Both these imaging techniques are able to resolve DNA structures at nanometric resolution. However, they strongly differ in terms of sample preparation and visualization conditions[211]. In particular, AFM samples preparation is fast and simple, DNA imaging can be achieved directly spotting DNA and proteins on mica support, without the need of staining or fixation. Freshly cleaved mica, naturally offers a surface flat at nanometric level. Moreover, it is electrostatically charged allowing an easy and fast absorption of biological macromolecules. AFM images are built as a consequence of the direct physical

interaction between a probe tip and the samples. This allows the visualization of samples in different fluidic medium (air or buffers). These features make AFM suitable to study DNA protein complexes structures.

In this thesis, we setup a method to visualize DNA structures of RIs by AFM imaging (***Figure 3.2***). Moreover, we tried to discriminate the newly-synthetized DNA from the parental strand in RI structures exploiting the ability of the *X. laevis* egg extract to incorporate biotin-dUTP into the nascent DNA strands (***Figure 3.7***). To validate our ability to visualize biotin-dUTP we used PCR-based approach. We generated four PCR products with differential content of biotin-dUTP (***Figure 3.3***) and we stained them using recombinant streptavidin. As expected, streptavidin bound differentially to the different biotinylated-DNA samples (***Figure 3.4***). We used the average volume of single streptavidin-DNA complexes to discriminate among the different PCR products. The volume data showed a linear correlation between volumetric hindrance of the streptavidin-DNA complex and the biotin content into DNA molecules (***Figure 3.5***). These results provided the proof-of-principle that streptavidin staining of biotinylated-DNA and AFM could be applied to monitor nascent DNA synthesis. However, when biotin-dUTP was used in *Xenopus* egg extract, streptavidin staining of biotinylated-RI structures resulted in aggregate formation. This result is likely the consequence of the ability of a single streptavidin tetramer to bind four biotin adducts at the same time (***Figure 3.8***). Nonetheless, using this approach, it was also possible to identify some RIs in which the biotin-dUTP could be recognized at the level of a classical Y structure (***Figure 3.9***), although they represented a minority of the stained molecules.

To efficiently visualize nascent DNA by AFM, further improvements and adjustments of the methodology will be required. The formation of biotinylated-DNA/streptavidin aggregates can be solved by using monomeric streptavidin or monovalent streptavidin, which binds one molecule at a time. Moreover, reducing biotin-dUTP concentration in the DNA replication reaction mix would allow a better visualization of the DNA strands.

The new methodology described here could be important to gain fundamental insights in the molecular mechanism behind DNA replication and DNA repair. The labelling of the newly synthesized DNA would formally identify all RIs, even those without a classical Y-shape. For instance, the specific staining of newly synthetized DNA would give the formal proof that RVFs are generated by the annealing of the daughter DNA strands. In addition, this technique could help us to unambiguously identify some peculiar DNA structures. For instance, it could help us to formally demonstrate that Rad51 can induce HJs originating from a pathway different than that of the fork reversal (***Figure 3.39*** and ***Figure 4.1B***). Furthermore, DNA polymerases activity could be identified based on differential affinity for biotin-dUTP[212]. Exploiting these DNA polymerase proprieties, it would be possible to discriminate the leading from the lagging DNA strand.

Despite the easy specimen preparation, AFM imaging is time consuming if a big portion of the sample stage has to be scanned, as the case of RIs visualization. Moreover, the classical protocol for DNA imaging does not allow visualization of ssDNA. The visualization of DNA molecules by AFM is done in semi-dry conditions, so the mica surface is always subjected to the environmental humidity and in these conditions, ssDNA tend to form secondary structures[181].

In contrast to AFM, EM-based DNA imaging requires a long and delicate sample preparation. However, EM allows a relatively fast scanning of the sample surface. On the other hand, the classical preparation for the DNA imaging requires the DNA spreading in a buffer containing denaturing agents (see section 2.13.1). In denaturing conditions, proteins tend to generate aggregates probably due to electrostatic attractions. Thus, the denaturing buffer favours the DNA spreading but it does not allow an easy visualization of protein-DNA complexes. As a consequence, biotin-dUTP detection with streptavidin cannot be easily performed as with AFM.

4.2 DNA lesion and significant for genome stability

Our group and others, have shown that EM is an accurate methodology to monitor ssDNA at the level of replication forks[56,57,118]. A small ssDNA gap is often present at the replication fork junction (***Figure 3.1*** and ***Figure 4.1A***) and, from our analysis, it is evident that the its length is directly correlated with the level of replication stress (***Figure 3.12*** and ***Figure 3.13***). However, different from previous hypothesis, functional uncoupling between DNA polymerases and the helicase machinery leads to the accumulation of asymmetric ssDNA affecting only one strand of the fork[45]. ssDNA, rapidly coated by RPA, eventually leads to the S phase checkpoint activation (***Figure 3.22***). Complete inhibition of replication related DNA polymerase in H-APH treatment creates a big ssDNA gap and not a symmetric gap, indicating that the CMG helicase is also arrested by H-APH and that the CMG does not progress when polymerase activity is stalled. The presence of an asymmetric ssDNA gag instead suggests that inhibition of Polymerases synthesizing the lagging strand are affected leading to formation of gaps mainly on lagging strands at stalled forks, whereas inhibition of leading strand polymerases also arrests CMG progression. In line with this hypothesis, MSi1 or APH, generated mainly two or three ssDNA gaps a low doses whereas they generated a large ssDNA gap at higher doses when Pol alpha is completely inhibited[204] (***Figure 3.12***, ***Figure 3.17*** and ***Figure 4.1***). These data could be explained by two different models: (a) a maximum of three Okazaki fragments are synthetized at a given time; (b) re-priming is attempted multiple times. Moreover, the length of all the ssDNA gaps generated in Polα inhibition was increased accordingly to the time of treatment (***Figure 3.18C-D***). The ssDNA gaps enlargement could be explained by two different mechanisms: (a) the direct inhibition of the DNA polymerase activity and (b) a nuclease-mediated process.

Intriguingly, the DNA region in which the ssDNA gaps were present, in both L-APH and H-APH conditions, were usually 1.5 kbp in length, measured from the fork junction

(***Figure 3.15***). This could be the consequence of a control mechanism which avoids the formation of excessive amount of ssDNA, which could be subjected to nuclease activity, spontaneous hydrolysis, and enzyme-induced deamination, often resulting in base substitutions or processing into DSBs [213].

Significantly, fork stalling conditions cause an increase in RIs showing a reversed branch. In particular, we were able to identify three different types of reversed branch constituted by only ssDNA, only dsDNA or by both ds- and ssDNA (***Figure 3.19***). These structures were differentially represented in the egg extract, and the RVFs population with a ssDNA tail was more than the 76% of the total (***Figure 3.20***). Notably, the different treatments did not influence the reversed branch length (***Figure 3.21***). Moreover, the average size of the regressed arm was similar to the average ssDNA gaps size accumulated at the fork junction (***Figure 3.13***, ***Figure 3.16*** and ***Figure 3.21***). These results further support the hypothesis that ssDNA at the fork triggers fork remodelling into RVFs.

4.3 Smarcal1 and Rad51 as players of the replication fork remodelling process

Here, using *Xenopus* egg extract we showed also that Polα, Smarcal1 and Rad51 chromatin binding levels are increased as a consequence of DNA polymerases inhibition (***Figure 3.11*** and ***Figure 3.22***). Moreover, we found that Rad51 interacts with both Smarcal1 and Polα in a chromatin context upon replication fork stalling condition (***Figure 3.42***). Rad51-Polα interaction could explain why Rad51 deficiency leads to spontaneous ssDNA gaps accumulation[118]. Consistently, we found that direct Polα inhibition (L-APH and MSi1) generates multiple ssDNA gaps (***Figure 3.12*** and ***Figure 3.17***). These findings might also explain the Rad51 requirement for stalled fork restart[32,120]. The ssDNA gaps generated in Polα inhibition conditions had a similar length

to the one reported for Okazaki fragments[214] (***Figure 3.14*** and ***Figure 3.18***). Thus, ssDNA accumulation might happen on lagging strands, although we cannot exclude that ssDNA can be generated also on stalled leading strands. In this context, Rad51-mediated re-priming could help DNA synthesis resumption downstream of the stalled fork. Then, polymerase could partially fill the fork junction gap, leading to the formation of internal gaps behind forks, which could be further enlarged by the action of Mre11 in the absence of Rad51-mediated protection[118]. Consistent with this hypothesis, Rad51 hyper-loading onto the chromatin reduces the ssDNA gap at the fork junction (***Figure 3.41***). Moreover, in DNA replication challenging condition, Rad51 stimulates the formation of HJ structures close to the fork junction (***Figure 3.39B***). These results provide fundamental molecular insights into the Rad51-dependent fork protection mechanisms, revealing surprising links between the proteins associated to the HR and the DNA replication pathways.

If the fork stalling condition is persistent and DNA lesions are not efficiently repaired, ssDNA gaps can become a substrate of Smarcal1, which, in turn, promotes the RVFs formation. We showed that Smarcal1 is one of the main fork remodellers. Indeed, Smarcal1 depletion in *Xenopus* egg extract decreased the level of RVFs of about the 50% (***Figure 3.23*** and ***Figure 3.24***). Other proteins with helicase and translocase activity, such as Rad54[131], ZRANB3[133], HLTF[134], FBH1[135], RECQ5[136], and FANCM[137], have been proposed to participate to the fork reversal redundantly with Smarcal1 and might play a role in promoting RVFs formation in Smarcal1 independent fashion. We showed that Smarcal1 hyper-chromatin binding is sufficient to induce RVFs that, during fork stalling, were not only increased in number, but they also displayed a longer reversed branch (***Figure 3.33*** and ***Figure 3.35***). Smarcal1 might be inducing fork reversal starting from ssDNA gaps formed on the leading or on the lagging strand when RPA molecules are abundant or in limiting amounts, respectevely[147]. ssDNA length at the fork junction directly correlates with the levels of RVFs (***Figure 3.13***, ***Figure 3.16*** and ***Figure 3.20***).

We showed that direct Polα inhibition is sufficient to induce RVFs formation, similarly to what happens in absence of the Primase gene[57] or Polα-stabilizing factors such as Tipin-Timeless[215].

According to similar findings[130], we observed a reduction in RVFs levels when Rad51 was depleted. Moreover, the depletion of both Rad51 and Smarcal1 further reduced the RVFs number (***Figure 3.23*** and ***Figure 3.24***). Thus, this suggests that the two proteins either have both an active role in inducing fork reversal, or they are implicated in different processes that regulate RVFs levels. Intriguingly, Rad51 hyper-loading onto chromatin did not influence the percentage of RVFs (***Figure 3.39***), but in an opposite fashion it reduced the ssDNA gaps at the RIs (***Figure 3.41***).

Previous work from our lab has correlated newly synthetized DNA degradation with Rad51 absence. Here, we provided biochemical evidence that Rad51 nucleofilaments directly protect ssDNA from Mre11-mediated resection. We showed that a stable Rad51 nucleofilament is essential to prevent Mre11-mediated degradation. Indeed, neither RPA nor Rad51^{T131P}, unable to form stable Rad51 nucleofilaments[205], prevented DNA resection (***Figure 3.28***, ***Figure 3.30*** and ***Figure 3.31***). The Rad51^{T131P} mutation was identified in Fanconi Anaemia (FA) cells[205], suggesting that protection of nascent DNA is important to prevent genome instability associated with FA. We assessed the function of Rad51 nucleofilament-mediated DNA protection on different DNA substrates. In particular, we showed how unprotected RVFs can function as entry point for Mre11, which starts the degradation of newly synthetized DNA. Mre11 might only initiate DNA degradation at RVFs, which could then be completed by nucleases such as ExoI, DNA2, and others in combination with WRN or BLM helicases[70].

Collectively, our data suggest that while Smarcal1 is directly responsible for the RVFs formation, Rad51 is responsible for the RVFs protection from Mre11-mediated degradation. Thus, it indirectly contributes to sustain the RVFs levels.

Here, we assessed also the effect of the inhibition of the checkpoint on RVFs levels. It has been reported that Smarcal1 is a substrate of ATR[145]. In particular, ATR-mediated phosphorylation of Smarcal1 is responsible for its inhibition[143]. Indeed, similarly to Smarcal1 hyper-chromatin binding, ATR inhibition resulted in an increased level of RVFs, even if to a lower extent (***Figure 3.34*** and ***Figure 3.45***). Considering that Smarcal1 is inhibited by checkpoint activation, it is likely that this process is more represented in genomic regions, such as centromeres, in which ATR activation is suppressed[155].

Moreover, we reported that, upon ATR inhibition, Rad51 chromatin binding levels are compromised (***Figure 3.44***). Altogether, our results suggested that ATR could control the RVFs metabolism by a two ways mechanism. On one hand, ATR promotes Rad51 binding to the chromatin. As a consequence, ATR inhibition impairs Polα-mediated re-priming, and Rad51-mediated fork protection against nuclease attacks. On the other hand, ATR inhibition can result in Smarcal1 hyper-activation, similarly to Smarcal1 chromatin hyper-loading conditions.

Understanding this response may be of key relevance for clinical applications, such as diagnosis and treatment of diseases caused by defective responses to replication stress, like cancer. Specific combinations of selective ATR pathway inhibitors could provide a rapid mechanism of cancer cell killing due to, at least in part, aberrant processing of stalled replication forks.

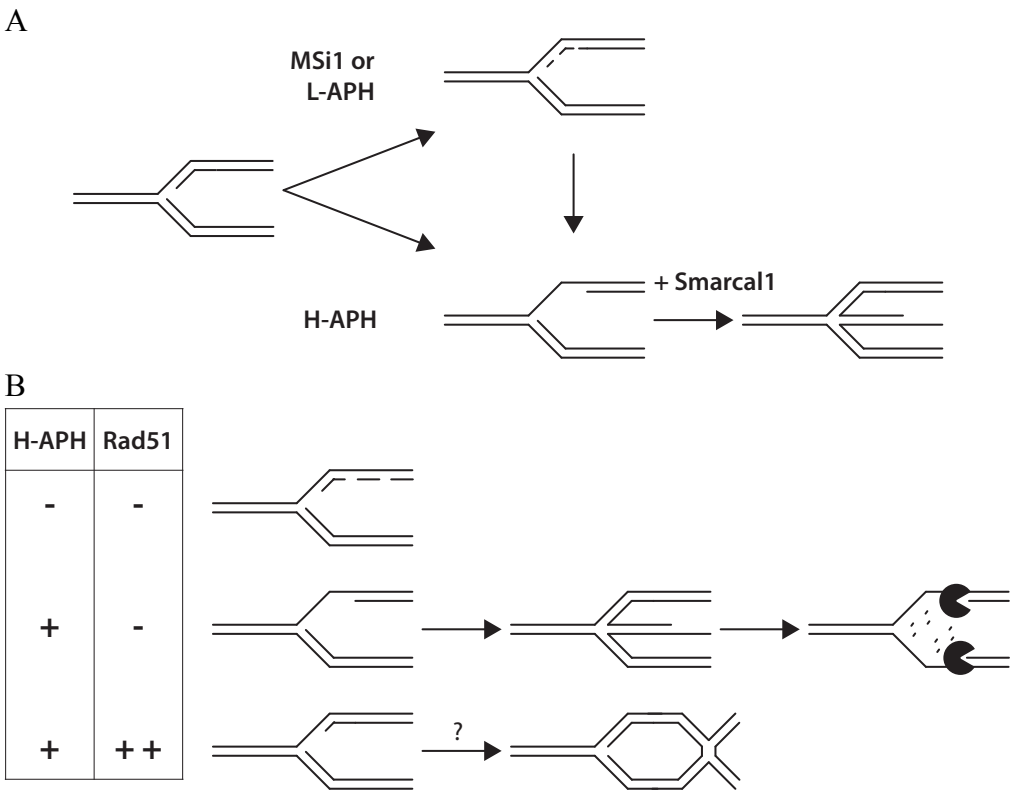

Figure 4.1 Model showing the effect of DNA polymerase inhibition and Rad51 depletion

(A) DNA polymerase inhibition leads to ssDNA accumulation al the fork junction both mild treatment (L-APH and MSi1) or in severe treatment (H-APH). Smarcal1 will eventually convert the ssDNA accumulated at the fork junction in RVFs. (B) Rad51 depletion leads to ssDNA accumulation at the fork junction and behind it (upper part). The combination of Rad51-deficient conditions and replication stress leads to RVFs formation that are degraded by endogenous nucleases because Rad51 absence (middle part). The overexpression of Rad51, in replication stress condition, inhibit an excess of ssDNA accumulation at the level of the replication fork. However, Rad51 excess induces HJ formation, HJs are may accumulated troughs recombination pathway (lower part).

5 References

1 Bell, S. P. & Dutta, A. DNA replication in eukaryotic cells. *Annual review of biochemistry* **71**, 333-374, doi:10.1146/annurev.biochem.71.110601.135425 (2002).

2 Hübscher, U. in *DNA Replication: Methods and Protocols* (eds Sonya Vengrova & Jacob Z. Dalgaard) 19-33 (Humana Press, 2009).

3 Masai, H., Matsumoto, S., You, Z., Yoshizawa-Sugata, N. & Oda, M. Eukaryotic chromosome DNA replication: where, when, and how? *Annual review of biochemistry* **79**, 89-130, doi:10.1146/annurev.biochem.052308.103205 (2010).

4 Mechali, M. Eukaryotic DNA replication origins: many choices for appropriate answers. *Nature reviews. Molecular cell biology* **11**, 728-738, doi:10.1038/nrm2976 (2010).

5 Abdurashidova, G. *et al.* Start sites of bidirectional DNA synthesis at the human lamin B2 origin. *Science* **287**, 2023-2026, doi:DOI 10.1126/science.287.5460.2023 (2000).

6 Giacca, M. *et al.* Fine mapping of a replication origin of human DNA. *Proceedings of the National Academy of Sciences of the United States of America* **91**, 7119-7123 (1994).

7 Cooper, G. M. in *The Cell: A Molecular Approach* (ed Sunderland (MA)) Ch. 4, (Sinauer Associates, 2000).

8 Ligasova, A., Raska, I. & Koberna, K. Organization of human replicon: singles or zipping couples? *J Struct Biol* **165**, 204-213, doi:10.1016/j.jsb.2008.11.004 (2009).

9 Hizume, K., Yagura, M. & Araki, H. Concerted interaction between origin recognition complex (ORC), nucleosomes and replication origin DNA ensures stable ORC-origin binding. *Genes Cells* **18**, 764-779, doi:10.1111/gtc.12073 (2013).

10 Fragkos, M., Ganier, O., Coulombe, P. & Mechali, M. DNA replication origin activation in space and time. *Nature reviews. Molecular cell biology* **16**, 360-374, doi:10.1038/nrm4002 (2015).

11 Moyer, S. E., Lewis, P. W. & Botchan, M. R. Isolation of the Cdc45/Mcm2-7/GINS (CMG) complex, a candidate for the eukaryotic DNA replication fork helicase. *Proceedings of the National Academy of Sciences of the United States of America* **103**, 10236-10241, doi:10.1073/pnas.0602400103 (2006).

12 Bochman, M. L. & Schwacha, A. The Mcm complex: unwinding the mechanism of a replicative helicase. *Microbiol Mol Biol Rev* **73**, 652-683, doi:10.1128/MMBR.00019-09 (2009).

13 Simon, A. C., Sannino, V., Costanzo, V. & Pellegrini, L. Structure of human Cdc45 and implications for CMG helicase function. *Nature communications* **7**, 11638, doi:10.1038/ncomms11638 (2016).

14 Duzdevich, D. *et al.* The dynamics of eukaryotic replication initiation: origin specificity, licensing, and firing at the single-molecule level. *Mol Cell* **58**, 483-494, doi:10.1016/j.molcel.2015.03.017 (2015).

15 Sawa, M. & Masai, H. Drug design with Cdc7 kinase: a potential novel cancer therapy target. *Drug design, development and therapy* **2**, 255-264 (2008).

16 Walter, J. & Newport, J. Initiation of eukaryotic DNA replication: origin unwinding and sequential chromatin association of Cdc45, RPA, and DNA polymerase alpha. *Mol Cell* **5**, 617-627, doi:10.1016/S1097-2765(00)80241-5 (2000).

17 Aguilera, A. & Garcia-Muse, T. Causes of genome instability. *Annual review of genetics* **47**, 1-32, doi:10.1146/annurev-genet-111212-133232 (2013).

18 Zeman, M. K. & Cimprich, K. A. Causes and consequences of replication stress. *Nat Cell Biol* **16**, 2-9, doi:10.1038/ncb2897 (2014).

19 Blow, J. J., Gillespie, P. J., Francis, D. & Jackson, D. A. Replication origins in Xenopus egg extract Are 5-15 kilobases apart and are activated in clusters that fire at different times. *The Journal of cell biology* **152**, 15-25 (2001).

20 Perera, R. L. *et al.* Mechanism for priming DNA synthesis by yeast DNA polymerase alpha. *Elife* **2**, e00482, doi:10.7554/eLife.00482 (2013).

21 Zheng, L. & Shen, B. Okazaki fragment maturation: nucleases take centre stage. *J Mol Cell Biol* **3**, 23-30, doi:10.1093/jmcb/mjq048 (2011).

22 Fukui, T. *et al.* Distinct roles of DNA polymerases delta and epsilon at the replication fork in Xenopus egg extracts. *Genes to Cells* **9**, 179-191, doi:10.1111/j.1365-2443.2004.00716.x (2004).

23 Liu, B., Hu, J., Wang, J. & Kong, D. Direct Visualization of RNA-DNA Primer Removal from Okazaki Fragments Provides Support for Flap Cleavage and Exonucleolytic Pathways in Eukaryotic Cells. *The Journal of biological chemistry* **292**, 4777-4788, doi:10.1074/jbc.M116.758599 (2017).

24 Fachinetti, D. *et al.* Replication Termination at Eukaryotic Chromosomes Is Mediated by Top2 and Occurs at Genomic Loci Containing Pausing Elements. *Molecular Cell* **39**, 595-605, doi:10.1016/j.molcel.2010.07.024 (2010).

25 Dewar, J. M., Budzowska, M. & Walter, J. C. The mechanism of DNA replication termination in vertebrates. *Nature* **525**, 345-350, doi:10.1038/nature14887 (2015).

26 Dewar, J. M. & Walter, J. C. Mechanisms of DNA replication termination. *Nature reviews. Molecular cell biology* **18**, 507-516, doi:10.1038/nrm.2017.42 (2017).

27 Macheret, M. & Halazonetis, T. D. DNA replication stress as a hallmark of cancer. *Annu Rev Pathol* **10**, 425-448, doi:10.1146/annurev-pathol-012414-040424 (2015).

28 Hanahan, D. & Weinberg, R. A. Hallmarks of cancer: the next generation. *Cell* **144**, 646-674, doi:10.1016/j.cell.2011.02.013 (2011).

29 Hanahan, D. & Weinberg, R. A. The hallmarks of cancer. *Cell* **100**, 57-70 (2000).

30 Magdalou, I., Lopez, B. S., Pasero, P. & Lambert, S. A. The causes of replication stress and their consequences on genome stability and cell fate. *Seminars in cell & developmental biology* **30**, 154-164, doi:10.1016/j.semcdb.2014.04.035 (2014).

31 Anglana, M., Apiou, F., Bensimon, A. & Debatisse, M. Dynamics of DNA replication in mammalian somatic cells: nucleotide pool modulates origin choice and interorigin spacing. *Cell* **114**, 385-394 (2003).

32 Petermann, E., Orta, M. L., Issaeva, N., Schultz, N. & Helleday, T. Hydroxyurea-stalled replication forks become progressively inactivated and require two different RAD51-mediated pathways for restart and repair. *Mol Cell* **37**, 492-502, doi:10.1016/j.molcel.2010.01.021 (2010).

33 Chabosseau, P. *et al.* Pyrimidine pool imbalance induced by BLM helicase deficiency contributes to genetic instability in Bloom syndrome. *Nature communications* **2**, 368, doi:10.1038/ncomms1363 (2011).

34 Woodward, A. M. *et al.* Excess Mcm2-7 license dormant origins of replication that can be used under conditions of replicative stress. *Journal of Cell Biology* **173**, 673-683, doi:DOI 10.1083/jcb.200602108 (2006).

35 Ge, X. Q., Jackson, D. A. & Blow, J. J. Dormant origins licensed by excess Mcm2-7 are required for human cells to survive replicative stress. *Genes & development* **21**, 3331-3341, doi:10.1101/gad.457807 (2007).

36 Durkin, S. G. & Glover, T. W. Chromosome fragile sites. *Annual review of genetics* **41**, 169-192, doi:10.1146/annurev.genet.41.042007.165900 (2007).

37 Schwartz, M., Zlotorynski, E. & Kerem, B. The molecular basis of common and rare fragile sites. *Cancer Lett* **232**, 13-26, doi:10.1016/j.canlet.2005.07.039 (2006).

38 Achar, Y. J. & Foiani, M. in *Adv Exp Med Biol* Vol. 1042 Ch. 20, 455-487 (2017).

39 Brambati, A., Colosio, A., Zardoni, L., Galanti, L. & Liberi, G. Replication and transcription on a collision course: eukaryotic regulation mechanisms and implications for DNA stability. *Front Genet* **6**, 166, doi:10.3389/fgene.2015.00166 (2015).

40 Errico, A. & Costanzo, V. Mechanisms of replication fork protection: a safeguard for genome stability. *Critical reviews in biochemistry and molecular biology* **47**, 222-235, doi:10.3109/10409238.2012.655374 (2012).

41 Abraham, R. T. Cell cycle checkpoint signaling through the ATM and ATR kinases. *Genes & development* **15**, 2177-2196, doi:10.1101/gad.914401 (2001).

42 Rodrigue, A. *et al.* Interplay between human DNA repair proteins at a unique double-strand break in vivo. *The EMBO journal* **25**, 222-231, doi:10.1038/sj.emboj.7600914 (2006).

43 Panier, S. & Boulton, S. J. Double-strand break repair: 53BP1 comes into focus. *Nature reviews. Molecular cell biology* **15**, 7-18, doi:10.1038/nrm3719 (2014).

44 Villa, M., Bonetti, D., Carraro, M. & Longhese, M. P. Rad9/53BP1 protects stalled replication forks from degradation in Mec1/ATR-defective cells. *EMBO Rep* **19**, 351-367, doi:10.15252/embr.201744910 (2018).

45 Byun, T. S., Pacek, M., Yee, M. C., Walter, J. C. & Cimprich, K. A. Functional uncoupling of MCM helicase and DNA polymerase activities activates the ATR-dependent checkpoint. *Genes & development* **19**, 1040-1052, doi:10.1101/gad.1301205 (2005).

46 Acevedo, J., Yan, S. & Michael, W. M. Direct Binding to Replication Protein A (RPA)-coated Single-stranded DNA Allows Recruitment of the ATR Activator TopBP1 to Sites of DNA Damage. *The Journal of biological chemistry* **291**, 13124-13131, doi:10.1074/jbc.M116.729194 (2016).

47 Haahr, P. *et al.* Activation of the ATR kinase by the RPA-binding protein ETAA1. *Nat Cell Biol* **18**, 1196-1207, doi:10.1038/ncb3422 (2016).

48 Bass, T. E. *et al.* ETAA1 acts at stalled replication forks to maintain genome integrity. *Nat Cell Biol* **18**, 1185-1195, doi:10.1038/ncb3415 (2016).

49 MacDougall, C. A., Byun, T. S., Van, C., Yee, M. C. & Cimprich, K. A. The structural determinants of checkpoint activation. *Genes & development* **21**, 898-903, doi:10.1101/gad.1522607 (2007).

50 Michael, W. M., Ott, R., Fanning, E. & Newport, J. Activation of the DNA replication checkpoint through RNA synthesis by primase. *Science* **289**, 2133-2137 (2000).

51 Lee, J. & Dunphy, W. G. Rad17 Plays a Central Role in Establishment of the Interaction between TopBP1 and the Rad9-Hus1-Rad1 Complex at Stalled Replication Forks. *Molecular Biology of the Cell* **21**, 926-935, doi:10.1091/mbc.E09-11-0958 (2010).

52 Zhao, H. & Piwnica-Worms, H. ATR-mediated checkpoint pathways regulate phosphorylation and activation of human Chk1. *Molecular and cellular biology* **21**, 4129-4139, doi:10.1128/MCB.21.13.4129-4139.2001 (2001).

53 Kumagai, A. & Dunphy, W. G. Claspin, a novel protein required for the activation of Chk1 during a DNA replication checkpoint response in Xenopus egg extracts. *Mol Cell* **6**, 839-849 (2000).

54 Errico, A. *et al.* Tipin/Tim1/And1 protein complex promotes Pol alpha chromatin binding and sister chromatid cohesion. *The EMBO journal* **28**, 3681-3692, doi:10.1038/emboj.2009.304 (2009).

55 Simon, A. C. *et al.* A Ctf4 trimer couples the CMG helicase to DNA polymerase alpha in the eukaryotic replisome. *Nature* **510**, 293-297, doi:10.1038/nature13234 (2014).

56 Abe, T. *et al.* AND-1 fork protection function prevents fork resection and is essential for proliferation. *Nature communications* **9**, 3091, doi:10.1038/s41467-018-05586-7 (2018).

57 Fumasoni, M., Zwicky, K., Vanoli, F., Lopes, M. & Branzei, D. Error-free DNA damage tolerance and sister chromatid proximity during DNA replication rely on the Polalpha/Primase/Ctf4 Complex. *Mol Cell* **57**, 812-823, doi:10.1016/j.molcel.2014.12.038 (2015).

58 Lucca, C. *et al.* Checkpoint-mediated control of replisome-fork association and signalling in response to replication pausing. *Oncogene* **23**, 1206-1213, doi:10.1038/sj.onc.1207199 (2004).

59 Sogo, J. M., Lopes, M. & Foiani, M. Fork reversal and ssDNA accumulation at stalled replication forks owing to checkpoint defects. *Science* **297**, 599-602, doi:DOI 10.1126/science.1074023 (2002).

60 Branzei, D. & Foiani, M. The DNA damage response during DNA replication. *Curr Opin Cell Biol* **17**, 568-575, doi:10.1016/j.ceb.2005.09.003 (2005).

61 Lopes, M. *et al.* The DNA replication checkpoint response stabilizes stalled replication forks. *Nature* **412**, 557-561, doi:10.1038/35087613 (2001).

62 Lopes, M., Foiani, M. & Sogo, J. M. Multiple mechanisms control chromosome integrity after replication fork uncoupling and restart at irreparable UV lesions. *Mol Cell* **21**, 15-27, doi:10.1016/j.molcel.2005.11.015 (2006).

63 Hashimoto, Y. & Costanzo, V. in *DNA Recombination: Methods and Protocols* (ed Hideo Tsubouchi) 437-445 (Humana Press, 2011).

64 Errico, A., Costanzo, V. & Hunt, T. Tipin is required for stalled replication forks to resume DNA replication after removal of aphidicolin in Xenopus egg extracts. *Proceedings of the National Academy of Sciences of the United States of America* **104**, 14929-14934, doi:10.1073/pnas.0706347104 (2007).

65 Lindahl, T. & Barnes, D. E. Repair of endogenous DNA damage. *Cold Spring Harb Symp Quant Biol* **65**, 127-133, doi:10.1101/sqb.2000.65.127 (2000).

66 Jackson, S. P. & Bartek, J. The DNA-damage response in human biology and disease. *Nature* **461**, 1071-1078, doi:10.1038/nature08467 (2009).

67 Xu, Y. & Her, C. Inhibition of Topoisomerase (DNA) I (TOP1): DNA Damage Repair and Anticancer Therapy. *Biomolecules* **5**, 1652-1670, doi:10.3390/biom5031652 (2015).

68 de Campos-Nebel, M., Larripa, I. & Gonzalez-Cid, M. Topoisomerase II-mediated DNA damage is differently repaired during the cell cycle by non-homologous end joining and homologous recombination. *PLoS One* **5**, e12541, doi:10.1371/journal.pone.0012541 (2010).

69 Mahaney, B. L., Meek, K. & Lees-Miller, S. P. Repair of ionizing radiation-induced DNA double-strand breaks by non-homologous end-joining. *The Biochemical journal* **417**, 639-650, doi:10.1042/BJ20080413 (2009).

70 Ranjha, L., Howard, S. M. & Cejka, P. Main steps in DNA double-strand break repair: an introduction to homologous recombination and related processes. *Chromosoma* **127**, 187-214, doi:10.1007/s00412-017-0658-1 (2018).

71 Pastwa, E. & Blasiak, J. Non-homologous DNA end joining. *Acta Biochim Pol* **50**, 891-908, doi:035004891 (2003).

72 Liu, T. & Huang, J. DNA End Resection: Facts and Mechanisms. *Genomics Proteomics Bioinformatics* **14**, 126-130, doi:10.1016/j.gpb.2016.05.002 (2016).

73 Seki, M., Marini, F. & Wood, R. D. POLQ (Pol theta), a DNA polymerase and DNA-dependent ATPase in human cells. *Nucleic acids research* **31**, 6117-6126, doi:10.1093/nar/gkg814 (2003).

74 Wang, H. & Xu, X. Microhomology-mediated end joining: new players join the team. *Cell Biosci* **7**, 6, doi:10.1186/s13578-017-0136-8 (2017).

75 Wright, W. D., Shah, S. S. & Heyer, W. D. Homologous recombination and the repair of DNA double-strand breaks. *The Journal of biological chemistry* **293**, 10524-10535, doi:10.1074/jbc.TM118.000372 (2018).

76 Ferretti, L. P., Lafranchi, L. & Sartori, A. A. Controlling DNA-end resection: a new task for CDKs. *Front Genet* **4**, 99, doi:10.3389/fgene.2013.00099 (2013).

77 Costanzo, V. & Gautier, J. in *Methods in molecular biology (Clifton, N.J.)* Vol. 241 255-267 (2004).

78 Costanzo, V., Robertson, K. & Gautier, J. in *Methods in molecular biology (Clifton, N.J.)* Vol. 280 213-227 (2004).

79 Costanzo, V. *et al.* Reconstitution of an ATM-dependent checkpoint that inhibits chromosomal DNA replication following DNA damage. *Mol Cell* **6**, 649-659 (2000).

80 Ma, C. J., Gibb, B., Kwon, Y., Sung, P. & Greene, E. C. Protein dynamics of human RPA and RAD51 on ssDNA during assembly and disassembly of the RAD51 filament. *Nucleic acids research* **45**, 749-761, doi:10.1093/nar/gkw1125 (2017).

81 Taylor, M. R. G. *et al.* A Polar and Nucleotide-Dependent Mechanism of Action for RAD51 Paralogs in RAD51 Filament Remodeling. *Mol Cell* **64**, 926-939, doi:10.1016/j.molcel.2016.10.020 (2016).

82 Compton, S. A., Ozgur, S. & Griffith, J. D. Ring-shaped Rad51 paralog protein complexes bind Holliday junctions and replication forks as visualized by electron microscopy. *The Journal of biological chemistry* **285**, 13349-13356, doi:10.1074/jbc.M109.074286 (2010).

83 Taylor, M. R. G. *et al.* Rad51 Paralogs Remodel Pre-synaptic Rad51 Filaments to Stimulate Homologous Recombination. *Cell* **162**, 271-286, doi:10.1016/j.cell.2015.06.015 (2015).

84 Badie, S. *et al.* RAD51C facilitates checkpoint signaling by promoting CHK2 phosphorylation. *The Journal of cell biology* **185**, 587-600, doi:10.1083/jcb.200811079 (2009).

85 Somyajit, K., Saxena, S., Babu, S., Mishra, A. & Nagaraju, G. Mammalian RAD51 paralogs protect nascent DNA at stalled forks and mediate replication restart. *Nucleic acids research* **43**, 9835-9855, doi:10.1093/nar/gkv880 (2015).

86 Tarsounas, M., Davies, D. & West, S. C. BRCA2-dependent and independent formation of RAD51 nuclear foci. *Oncogene* **22**, 1115-1123, doi:10.1038/sj.onc.1206263 (2003).

87 Patel, K. J. *et al.* Involvement of Brca2 in DNA repair. *Mol Cell* **1**, 347-357 (1998).

88 Godin, S. K., Sullivan, M. R. & Bernstein, K. A. Novel insights into RAD51 activity and regulation during homologous recombination and DNA replication. *Biochem Cell Biol* **94**, 407-418, doi:10.1139/bcb-2016-0012 (2016).

89 Schlacher, K. *et al.* Double-strand break repair-independent role for BRCA2 in blocking stalled replication fork degradation by MRE11. *Cell* **145**, 529-542, doi:10.1016/j.cell.2011.03.041 (2011).

90 Jasin, M. Homologous repair of DNA damage and tumorigenesis: the BRCA connection. *Oncogene* **21**, 8981-8993, doi:10.1038/sj.onc.1206176 (2002).

91 Schlacher, K., Wu, H. & Jasin, M. A distinct replication fork protection pathway connects Fanconi anemia tumor suppressors to RAD51-BRCA1/2. *Cancer Cell* **22**, 106-116, doi:10.1016/j.ccr.2012.05.015 (2012).

92 Krejci, L., Altmannova, V., Spirek, M. & Zhao, X. Homologous recombination and its regulation. *Nucleic acids research* **40**, 5795-5818, doi:10.1093/nar/gks270 (2012).

93 Suwaki, N., Klare, K. & Tarsounas, M. RAD51 paralogs: roles in DNA damage signalling, recombinational repair and tumorigenesis. *Seminars in cell & developmental biology* **22**, 898-905, doi:10.1016/j.semcdb.2011.07.019 (2011).

94 Li, X., Stith, C. M., Burgers, P. M. & Heyer, W. D. PCNA Is Required for Initiation of Recombination-Associated DNA Synthesis by DNA Polymerase delta. *Molecular Cell* **36**, 704-713, doi:10.1016/j.molcel.2009.09.036 (2009).

95 Wilson, M. A. *et al.* Pif1 helicase and Poldelta promote recombination-coupled DNA synthesis via bubble migration. *Nature* **502**, 393-396, doi:10.1038/nature12585 (2013).

96 Dolle, C. & Ziegler, M. ADP-ribosylation of DNA moving into focus. *The FEBS journal* **284**, 3999-4001, doi:10.1111/febs.14326 (2017).

97 Hanzlikova, H. *et al.* The Importance of Poly(ADP-Ribose) Polymerase as a Sensor of Unligated Okazaki Fragments during DNA Replication. *Mol Cell*, doi:10.1016/j.molcel.2018.06.004 (2018).

98 Feng, X. & Koh, D. W. Roles of poly(ADP-ribose) glycohydrolase in DNA damage and apoptosis. *International review of cell and molecular biology* **304**, 227-281, doi:10.1016/B978-0-12-407696-9.00005-1 (2013).

99 Megnin-Chanet, F., Bollet, M. A. & Hall, J. Targeting poly(ADP-ribose) polymerase activity for cancer therapy. *Cellular and molecular life sciences : CMLS* **67**, 3649-3662, doi:10.1007/s00018-010-0490-8 (2010).

100 Talhaoui, I. *et al.* Poly(ADP-ribose) polymerases covalently modify strand break termini in DNA fragments in vitro. *Nucleic acids research* **44**, 9279-9295, doi:10.1093/nar/gkw675 (2016).

101 Rouleau, M., Patel, A., Hendzel, M. J., Kaufmann, S. H. & Poirier, G. G. PARP inhibition: PARP1 and beyond. *Nat Rev Cancer* **10**, 293-301, doi:10.1038/nrc2812 (2010).

102 Yazinski, S. A. *et al.* ATR inhibition disrupts rewired homologous recombination and fork protection pathways in PARP inhibitor-resistant BRCA-deficient cancer cells. *Genes & development* **31**, 318-332, doi:10.1101/gad.290957.116 (2017).

103 Sirbu, B. M. *et al.* Analysis of protein dynamics at active, stalled, and collapsed replication forks. *Genes & development* **25**, 1320-1327, doi:10.1101/gad.2053211 (2011).

104 Aze, A., Zhou, J. C., Costa, A. & Costanzo, V. DNA replication and homologous recombination factors: acting together to maintain genome stability. *Chromosoma* **122**, 401-413, doi:10.1007/s00412-013-0411-3 (2013).

105 Sonoda, E. *et al.* Rad51-deficient vertebrate cells accumulate chromosomal breaks prior to cell death. *The EMBO journal* **17**, 598-608, doi:10.1093/emboj/17.2.598 (1998).

106 Venkitaraman, A. R. Cancer susceptibility and the functions of BRCA1 and BRCA2. *Cell* **108**, 171-182 (2002).

107 Luo, G. *et al.* Disruption of mRad50 causes embryonic stem cell lethality, abnormal embryonic development, and sensitivity to ionizing radiation. *Proceedings of the National Academy of Sciences of the United States of America* **96**, 7376-7381 (1999).

108 Zhu, J., Petersen, S., Tessarollo, L. & Nussenzweig, A. Targeted disruption of the Nijmegen breakage syndrome gene NBS1 leads to early embryonic lethality in mice. *Curr Biol* **11**, 105-109 (2001).

109 Zhao, S. *et al.* Functional link between ataxia-telangiectasia and Nijmegen breakage syndrome gene products. *Nature* **405**, 473-477 (2000).

110 Yamaguchi-Iwai, Y. *et al.* Mre11 is essential for the maintenance of chromosomal DNA in vertebrate cells. *Embo Journal* **18**, 6619-6629, doi:DOI 10.1093/emboj/18.23.6619 (1999).

111 Tashiro, S. *et al.* S phase specific formation of the human Rad51 protein nuclear foci in lymphocytes. *Oncogene* **12**, 2165-2170 (1996).

112 Raderschall, E., Golub, E. I. & Haaf, T. Nuclear foci of mammalian recombination proteins are located at single-stranded DNA regions formed after DNA damage. *Proceedings of the National Academy of Sciences of the United States of America* **96**, 1921-1926, doi:DOI 10.1073/pnas.96.5.1921 (1999).

113 Mizuta, R. *et al.* RAB22 and RAB163/mouse BRCA2: Proteins that specifically interact with the RAD51 protein. *Proceedings of the National Academy of Sciences of the United States of America* **94**, 6927-6932, doi:DOI 10.1073/pnas.94.13.6927 (1997).

114 Scully, R. *et al.* Dynamic changes of BRCA1 subnuclear location and phosphorylation state are initiated by DNA damage. *Cell* **90**, 425-435 (1997).

115 Daboussi, F. *et al.* A homologous recombination defect affects replication-fork progression in mammalian cells. *Journal of cell science* **121**, 162-166, doi:10.1242/jcs.010330 (2008).

116 Branzei, D. & Szakal, B. Building up and breaking down: mechanisms controlling recombination during replication. *Critical reviews in biochemistry and molecular biology* **52**, 381-394, doi:10.1080/10409238.2017.1304355 (2017).

117 Su, X., Bernal, J. A. & Venkitaraman, A. R. Cell-cycle coordination between DNA replication and recombination revealed by a vertebrate N-end rule degron-Rad51. *Nature structural & molecular biology* **15**, 1049-1058, doi:10.1038/nsmb.1490 (2008).

118 Hashimoto, Y., Ray Chaudhuri, A., Lopes, M. & Costanzo, V. Rad51 protects nascent DNA from Mre11-dependent degradation and promotes continuous DNA synthesis. *Nature structural & molecular biology* **17**, 1305-1311, doi:10.1038/nsmb.1927 (2010).

119 Tashiro, S., Walter, J., Shinohara, A., Kamada, N. & Cremer, T. Rad51 accumulation at sites of DNA damage and in postreplicative chromatin. *Journal of Cell Biology* **150**, 283-291, doi:DOI 10.1083/jcb.150.2.283 (2000).

120 Hashimoto, Y., Puddu, F. & Costanzo, V. RAD51- and MRE11-dependent reassembly of uncoupled CMG helicase complex at collapsed replication forks. *Nature structural & molecular biology* **19**, 17-24, doi:10.1038/nsmb.2177 (2011).

121 Lemacon, D. *et al.* MRE11 and EXO1 nucleases degrade reversed forks and elicit MUS81-dependent fork rescue in BRCA2-deficient cells. *Nature communications* **8**, 860, doi:10.1038/s41467-017-01180-5 (2017).

122 Costes, A. & Lambert, S. A. Homologous recombination as a replication fork escort: fork-protection and recovery. *Biomolecules* **3**, 39-71, doi:10.3390/biom3010039 (2012).

123 Bhat, K. P. & Cortez, D. RPA and RAD51: fork reversal, fork protection, and genome stability. *Nature structural & molecular biology* **25**, 446-453, doi:10.1038/s41594-018-0075-z (2018).

124 Lord, C. J. & Ashworth, A. RAD51, BRCA2 and DNA repair: a partial resolution. *Nature structural & molecular biology* **14**, 461-462, doi:10.1038/nsmb0607-461 (2007).

125 Lomonosov, M., Anand, S., Sangrithi, M., Davies, R. & Venkitaraman, A. R. Stabilization of stalled DNA replication forks by the BRCA2 breast cancer susceptibility protein. *Genes & development* **17**, 3017-3022, doi:10.1101/gad.279003 (2003).

126 Mijic, S. *et al.* Replication fork reversal triggers fork degradation in BRCA2-defective cells. *Nature communications* **8**, 859, doi:10.1038/s41467-017-01164-5 (2017).

127 Kolinjivadi, A. M. *et al.* Moonlighting at replication forks - a new life for homologous recombination proteins BRCA1, BRCA2 and RAD51. *FEBS Lett* **591**, 1083-1100, doi:10.1002/1873-3468.12556 (2017).

128 Neelsen, K. J. & Lopes, M. Replication fork reversal in eukaryotes: from dead end to dynamic response. *Nature reviews. Molecular cell biology* **16**, 207-220, doi:10.1038/nrm3935 (2015).

129 Hu, J. *et al.* The intra-S phase checkpoint targets Dna2 to prevent stalled replication forks from reversing. *Cell* **149**, 1221-1232, doi:10.1016/j.cell.2012.04.030 (2012).

130 Zellweger, R. *et al.* Rad51-mediated replication fork reversal is a global response to genotoxic treatments in human cells. *The Journal of cell biology* **208**, 563-579, doi:10.1083/jcb.201406099 (2015).

131 Bugreev, D. V., Rossi, M. J. & Mazin, A. V. Cooperation of RAD51 and RAD54 in regression of a model replication fork. *Nucleic acids research* **39**, 2153-2164, doi:10.1093/nar/gkq1139 (2011).

132 Betous, R. *et al.* SMARCAL1 catalyzes fork regression and Holliday junction migration to maintain genome stability during DNA replication. *Genes & development* **26**, 151-162, doi:10.1101/gad.178459.111 (2012).

133 Ciccia, A. *et al.* Polyubiquitinated PCNA recruits the ZRANB3 translocase to maintain genomic integrity after replication stress. *Mol Cell* **47**, 396-409, doi:10.1016/j.molcel.2012.05.024 (2012).

134 Kile, A. C. *et al.* HLTF's Ancient HIRAN Domain Binds 3' DNA Ends to Drive Replication Fork Reversal. *Mol Cell* **58**, 1090-1100, doi:10.1016/j.molcel.2015.05.013 (2015).

135 Fugger, K. *et al.* FBH1 Catalyzes Regression of Stalled Replication Forks. *Cell reports*, doi:10.1016/j.celrep.2015.02.028 (2015).

136 Kanagaraj, R., Saydam, N., Garcia, P. L., Zheng, L. & Janscak, P. Human RECQ5beta helicase promotes strand exchange on synthetic DNA structures resembling a stalled replication fork. *Nucleic acids research* **34**, 5217-5231, doi:10.1093/nar/gkl677 (2006).

137 Gari, K., Decaillet, C., Delannoy, M., Wu, L. & Constantinou, A. Remodeling of DNA replication structures by the branch point translocase FANCM. *Proceedings of the National Academy of Sciences of the United States of America* **105**, 16107-16112, doi:10.1073/pnas.0804777105 (2008).

138 Berti, M. *et al.* Human RECQ1 promotes restart of replication forks reversed by DNA topoisomerase I inhibition. *Nature structural & molecular biology* **20**, 347-354, doi:10.1038/nsmb.2501 (2013).

139 Pepe, A. & West, S. C. MUS81-EME2 promotes replication fork restart. *Cell reports* **7**, 1048-1055, doi:10.1016/j.celrep.2014.04.007 (2014).

140 Thangavel, S. *et al.* DNA2 drives processing and restart of reversed replication forks in human cells. *The Journal of cell biology* **208**, 545-562, doi:10.1083/jcb.201406100 (2015).

141 Pasero, P. & Vindigni, A. Nucleases Acting at Stalled Forks: How to Reboot the Replication Program with a Few Shortcuts. *Annual review of genetics* **51**, 477-499, doi:10.1146/annurev-genet-120116-024745 (2017).

142 Sidorova, J. A game of substrates: replication fork remodeling and its roles in genome stability and chemo-resistance. *Cell Stress* **1**, 115-133, doi:10.15698/cst2017.12.114 (2017).

143 Couch, F. B. *et al.* ATR phosphorylates SMARCAL1 to prevent replication fork collapse. *Genes & development* **27**, 1610-1623, doi:10.1101/gad.214080.113 (2013).

144 Leslie, M. A fresh start for stalled forks. *Journal of Cell Biology* **208**, 495-495, doi:DOI 10.1083/jcb.2085if (2015).

145 Postow, L., Woo, E. M., Chait, B. T. & Funabiki, H. Identification of SMARCAL1 as a component of the DNA damage response. *The Journal of biological chemistry* **284**, 35951-35961, doi:10.1074/jbc.M109.048330 (2009).

146 Boerkoel, C. F. *et al.* Mutant chromatin remodeling protein SMARCAL1 causes Schimke immuno-osseous dysplasia. *Nature genetics* **30**, 215-220, doi:10.1038/ng821 (2002).

147 Betous, R. *et al.* Substrate-selective repair and restart of replication forks by DNA translocases. *Cell reports* **3**, 1958-1969, doi:10.1016/j.celrep.2013.05.002 (2013).

148 Ciccia, A. *et al.* The SIOD disorder protein SMARCAL1 is an RPA-interacting protein involved in replication fork restart. *Genes & development* **23**, 2415-2425, doi:10.1101/gad.1832309 (2009).

149 Betous, R., Glick, G. G., Zhao, R. & Cortez, D. Identification and characterization of SMARCAL1 protein complexes. *PLoS One* **8**, e63149, doi:10.1371/journal.pone.0063149 (2013).

150 Nam, E. A. & Cortez, D. ATR signalling: more than meeting at the fork. *The Biochemical journal* **436**, 527-536, doi:10.1042/BJ20102162 (2011).

151 Shi, W. *et al.* The role of RPA2 phosphorylation in homologous recombination in response to replication arrest. *Carcinogenesis* **31**, 994-1002, doi:10.1093/carcin/bgq035 (2010).

152 Gillespie, P. J., Gambus, A. & Blow, J. J. Preparation and use of Xenopus egg extracts to study DNA replication and chromatin associated proteins. *Methods* **57**, 203-213, doi:10.1016/j.ymeth.2012.03.029 (2012).

153 Sannino, V., Pezzimenti, F., Bertora, S. & Costanzo, V. in *Methods in enzymology* (Academic Press, 2017).

154 Brun, R. B. Studies on fertilization in Xenopus laevis. *Biol Reprod* **11**, 513-518 (1974).

155 Aze, A., Sannino, V., Soffientini, P., Bachi, A. & Costanzo, V. Centromeric DNA replication reconstitution reveals DNA loops and ATR checkpoint suppression. *Nat Cell Biol* **18**, 684-691, doi:10.1038/ncb3344 (2016).

156 Blow, J. J. & James, P. J. C. in *Cold Spring Harbor Monograph Archive; Volume 31 (1996): DNA Replication in Eukaryotic Cells* (1996).

157 Blow, J. J. & Laskey, R. A. Initiation of DNA replication in nuclei and purified DNA by a cell-free extract of Xenopus eggs. *Cell* **47**, 577-587, doi:10.1016/0092-8674(86)90622-7 (1986).

158 Wroble, B. N. & Sible, J. C. Chk2/Cds1 protein kinase blocks apoptosis during early development of Xenopus laevis. *Developmental dynamics : an official publication of the American Association of Anatomists* **233**, 1359-1365, doi:10.1002/dvdy.20449 (2005).

159 Hyrien, O., Maric, C. & Mechali, M. Transition in specification of embryonic metazoan DNA replication origins. *Science* **270**, 994-997 (1995).

160 Kasas, S. *et al.* Escherichia coli RNA polymerase activity observed using atomic force microscopy. *Biochemistry* **36**, 461-468, doi:10.1021/bi9624402 (1997).

161 Qian, R. L. *et al.* Visualization of chromatin folding patterns in chicken erythrocytes by atomic force microscopy (AFM). *Cell research* **7**, 143-150, doi:10.1038/cr.1997.15 (1997).

162 Lyubchenko, Y. L., Gall, A. A. & Shlyakhtenko, L. S. in *DNA-Protein Interactions: Principles and Protocols* (ed Tom Moss) 569-578 (Humana Press, 2001).

163 Quénetù, D. in *Atomic Force Microscopy Investigations into Biology - From Cell to Protein* (eds K. Dimitriadis Emilios & Dalal Yamini) Ch. 9, (InTech, 2012).

164 Sedlackova, H., Cechova, B., Mlcouskova, J. & Krejci, L. RECQ4 selectively recognizes Holliday junctions. *DNA Repair (Amst)* **30**, 80-89, doi:10.1016/j.dnarep.2015.02.020 (2015).

165 Van, C., Yan, S., Michael, W. M., Waga, S. & Cimprich, K. A. Continued primer synthesis at stalled replication forks contributes to checkpoint activation. *The Journal of cell biology* **189**, 233-246, doi:10.1083/jcb.200909105 (2010).

166 Newport, J. Nuclear reconstitution in vitro: stages of assembly around protein-free DNA. *Cell* **48**, 205-217 (1987).

167 Lohka, M. & Masui, Y. Formation in vitro of sperm pronuclei and mitotic chromosomes induced by amphibian ooplasmic components. *Science* **220**, 719-721, doi:10.1126/science.6601299 (1983).

168 Menut, S., Lemaitre, J. M., Hair, A. & Méchali, M. in *A comparative Methods Approach to the Study of Oocytes and Embryos* Ch. 11, (Oxford University Press, 1999).

169 Endean, D. J. & Smithies, O. Replication of plasmid DNA in fertilized Xenopus eggs is sensitive to both the topology and size of the injected template. *Chromosoma* **97**, 307-314, doi:10.1007/bf00371971 (1989).

170 Binnig, G., Quate, C. F. & Gerber, C. Atomic force microscope. *Physical review letters* **56**, 930-933, doi:10.1103/PhysRevLett.56.930 (1986).

171 van Helleputte, H. R. J. R., Haddeman, T. B. J., Verheijen, M. J. & Baalbergen, J.-J. Comparative study of 3D measurement techniques (SPM, SEM, TEM) for submicron structures. *Microelectronic Engineering* **27**, 547-550, doi:10.1016/0167-9317(94)00164-p (1995).

172 Russell, P. & Batchelor, D. SEM and AFM: Complementary Techniques for Surface Investigations. *MICROSCOPY AND ANALYSIS*, doi:10.1.1.503.5387 (2001).

173 Yokokawa, M. *et al.* Fast-scanning atomic force microscopy reveals the molecular mechanism of DNA cleavage by ApaI endonuclease. *IEE Proc Nanobiotechnol* **153**, 60-66, doi:10.1049/ip-nbt:20050018 (2006).

174 Yamamoto, D. *et al.* High-speed atomic force microscopy techniques for observing dynamic biomolecular processes. *Methods in enzymology* **475**, 541-564, doi:10.1016/S0076-6879(10)75020-5 (2010).

175 Crampton, N. *et al.* Fast-scan atomic force microscopy reveals that the type III restriction enzyme EcoP15I is capable of DNA translocation and looping. *Proceedings of the National Academy of Sciences* **104**, 12755 (2007).

176 Kizaki, S., Suzuki, Y., Takenaka, T., Endo, M. & Sugiyama, H. AFM analysis of changes in nucleosome wrapping induced by DNA epigenetic modification. *Biomaterials Science* **2**, 1399-1403, doi:10.1039/c4bm00113c (2014).

177 Fuentes-Perez, M. E., Dillingham, M. S. & Moreno-Herrero, F. AFM volumetric methods for the characterization of proteins and nucleic acids. *Methods* **60**, 113-121, doi:10.1016/j.ymeth.2013.02.005 (2013).

178 Dupres, V., Verbelen, C. & Dufrene, Y. F. Probing molecular recognition sites on biosurfaces using AFM. *Biomaterials* **28**, 2393-2402, doi:10.1016/j.biomaterials.2006.11.011 (2007).

179 Lyubchenko, Y. L. & Shlyakhtenko, L. S. AFM for analysis of structure and dynamics of DNA and protein-DNA complexes. *Methods* **47**, 206-213, doi:10.1016/j.ymeth.2008.09.002 (2009).

180 Zheng, J., Li, Z., Wu, A. & Zhou, H. AFM studies of DNA structures on mica in the presence of alkaline earth metal ions. *Biophys Chem* **104**, 37-43, doi:10.1016/S0301-4622(02)00335-6 (2003).

181 Hamon, L. *et al.* High-resolution AFM imaging of single-stranded DNA-binding (SSB) protein--DNA complexes. *Nucleic acids research* **35**, e58, doi:10.1093/nar/gkm147 (2007).

182 Bock, C.-T., Franz, S., Zentgraf, H. & Sommerville, J. in *Reviews in Cell Biology and Molecular Medicine Major Reference Works* (2006).

183 Lopes, M. in *DNA Replication: Methods and Protocols* (eds Sonya Vengrova & Z. Jacob Dalgaard) 605-631 (Humana Press, 2009).

184 Follonier, C., Oehler, J., Herrador, R. & Lopes, M. Friedreich's ataxia-associated GAA repeats induce replication-fork reversal and unusual molecular junctions. *Nature structural & molecular biology* **20**, 486-494, doi:10.1038/nsmb.2520 (2013).

185 Mejlvang, J. *et al.* New histone supply regulates replication fork speed and PCNA unloading. *The Journal of cell biology* **204**, 29-43, doi:10.1083/jcb.201305017 (2014).

186 Neelsen, K. J., Zanini, I. M., Herrador, R. & Lopes, M. Oncogenes induce genotoxic stress by mitotic processing of unusual replication intermediates. *The Journal of cell biology* **200**, 699-708, doi:10.1083/jcb.201212058 (2013).

187 Pena-Diaz, J. *et al.* Noncanonical mismatch repair as a source of genomic instability in human cells. *Mol Cell* **47**, 669-680, doi:10.1016/j.molcel.2012.07.006 (2012).

188 Fouche, N., Ozgur, S., Roy, D. & Griffith, J. D. Replication fork regression in repetitive DNAs. *Nucleic acids research* **34**, 6044-6050, doi:10.1093/nar/gkl757 (2006).

189 Compton, S. A., Tolun, G., Kamath-Loeb, A. S., Loeb, L. A. & Griffith, J. D. The Werner syndrome protein binds replication fork and holliday junction DNAs as an oligomer. *The Journal of biological chemistry* **283**, 24478-24483, doi:10.1074/jbc.M803370200 (2008).

190 Villarreal, S. A. & Stewart, P. L. CryoEM and image sorting for flexible protein/DNA complexes. *J Struct Biol* **187**, 76-83, doi:10.1016/j.jsb.2013.12.002 (2014).

191 Miller, O. L., Jr. & Beatty, B. R. Portrait of a gene. *J Cell Physiol* **74**, Suppl 1:225+, doi:10.1002/jcp.1040740424 (1969).

192 Kolinjivadi, A. M. *et al.* Smarcal1-Mediated Fork Reversal Triggers Mre11-Dependent Degradation of Nascent DNA in the Absence of Brca2 and Stable Rad51 Nucleofilaments. *Mol Cell* **67**, 867-881 e867, doi:10.1016/j.molcel.2017.07.001 (2017).

193 Marini, V. & Krejci, L. Unwinding of synthetic replication and recombination substrates by Srs2. *DNA Repair (Amst)* **11**, 789-798, doi:10.1016/j.dnarep.2012.05.007 (2012).

194 Rowles, A. *et al.* Interaction between the Origin Recognition Complex and the Replication Licensing Systemin Xenopus. *Cell* **87**, 287-296, doi:10.1016/s0092-8674(00)81346-x (1996).

195 Vollenweider, H. J., Sogo, J. M. & Koller, T. A routine method for protein-free spreading of double- and single-stranded nucleic acid molecules. *Proceedings of the National Academy of Sciences of the United States of America* **72**, 83-87 (1975).

196 Neish, C. S., Martin, I. L., Henderson, R. M. & Edwardson, J. M. Direct visualization of ligand-protein interactions using atomic force microscopy. *Br J Pharmacol* **135**, 1943-1950, doi:10.1038/sj.bjp.0704660 (2002).

197 Gonzalez, M. *et al.* Interaction of biotin with streptavidin. Thermostability and conformational changes upon binding. *The Journal of biological chemistry* **272**, 11288-11294 (1997).

198 Paul, N. & Yee, J. PCR incorporation of modified dNTPs: the substrate properties of biotinylated dNTPs. *Biotechniques* **48**, 333-334, doi:10.2144/000113405 (2010).

199 Anderson, J. P., Angerer, B. & Loeb, L. A. Incorporation of reporter-labeled nucleotides by DNA polymerases. *Biotechniques* **38**, 257-264, doi:10.2144/05382RR02 (2005).

200 Roche, P. J. in *In Situ Hybridization Protocols* (eds Ian A. Darby & Tim D. Hewitson) 9-16 (Humana Press, 2006).

201 Demonte, D., Dundas, C. M. & Park, S. Expression and purification of soluble monomeric streptavidin in Escherichia coli. *Appl Microbiol Biotechnol* **98**, 6285-6295, doi:10.1007/s00253-014-5682-y (2014).

202 Luciani, M. G., Oehlmann, M. & Blow, J. J. Characterization of a novel ATR-dependent, Chk1-independent, intra-S-phase checkpoint that suppresses initiation of replication in Xenopus. *Journal of cell science* **117**, 6019-6030, doi:10.1242/jcs.01400 (2004).

203 Rowles, A., Tada, S. & Blow, J. J. Changes in association of the Xenopus origin recognition complex with chromatin on licensing of replication origins. *Journal of cell science* **112 (Pt 12)**, 2011-2018 (1999).

204 Seki, S., Hosogi, N. & Oda, T. Differential sensitivity to aphidicolin of replicative DNA synthesis and ultraviolet-induced unscheduled DNA synthesis in vivo in mammalian cells. *Acta medica Okayama* **38**, 227-237, doi:10.18926/AMO/30354 (1984).

205 Wang, A. T. *et al.* A Dominant Mutation in Human RAD51 Reveals Its Function in DNA Interstrand Crosslink Repair Independent of Homologous Recombination. *Mol Cell* **59**, 478-490, doi:10.1016/j.molcel.2015.07.009 (2015).

206 Qiu, Y. *et al.* Srs2 prevents Rad51 filament formation by repetitive motion on DNA. *Nature communications* **4**, 2281, doi:10.1038/ncomms3281 (2013).

207 Kim, C., Paulus, B. F. & Wold, M. S. Interactions of human replication protein A with oligonucleotides. *Biochemistry* **33**, 14197-14206 (1994).

208 Giannattasio, M. *et al.* Visualization of recombination-mediated damage bypass by template switching. *Nature structural & molecular biology* **21**, 884-892, doi:10.1038/nsmb.2888 (2014).

209 Sorensen, C. S. *et al.* The cell-cycle checkpoint kinase Chk1 is required for mammalian homologous recombination repair. *Nat Cell Biol* **7**, 195-201, doi:10.1038/ncb1212 (2005).

210 Charrier, J. D. *et al.* Discovery of potent and selective inhibitors of ataxia telangiectasia mutated and Rad3 related (ATR) protein kinase as potential anticancer agents. *Journal of medicinal chemistry* **54**, 2320-2330, doi:10.1021/jm101488z (2011).

211 Daban, J. R. Electron microscopy and atomic force microscopy studies of chromatin and metaphase chromosome structure. *Micron* **42**, 733-750, doi:10.1016/j.micron.2011.05.002 (2011).

212 Hottin, A. & Marx, A. Structural Insights into the Processing of Nucleobase-Modified Nucleotides by DNA Polymerases. *Acc Chem Res* **49**, 418-427, doi:10.1021/acs.accounts.5b00544 (2016).

213 Tubbs, A. & Nussenzweig, A. Endogenous DNA Damage as a Source of Genomic Instability in Cancer. *Cell* **168**, 644-656, doi:10.1016/j.cell.2017.01.002 (2017).

214 Ogawa, T. & Okazaki, T. Discontinuous DNA replication. *Annual review of biochemistry* **49**, 421-457, doi:10.1146/annurev.bi.49.070180.002225 (1980).

215 Errico, A., Aze, A. & Costanzo, V. Mta2 promotes Tipin-dependent maintenance of replication fork integrity. *Cell Cycle* **13**, 2120-2128, doi:10.4161/cc.29157 (2014).